NATIONAL TECHNICAL UNIVERSITY OF ATHENS
Laboratory of Steam Boilers and Thermal Plants
Department of Thermal Engineering of School of Mechanical Engineering

DIPLOMA THESIS

Flexible models for the design and dynamic operation of single and dual pressure Organic Rankine Cycle systems: application to an LNG carrier

Of the Student

PLAGIANOS GEORGIOS PANAGIOTIS

SUPERVISOR:

Karellas Sotirios, Associate Professor
School of Mechanical Engineering, NTUA

CO-SUPERVISORS:

Lazzaretto Andrea, Associate Professor
School of Industrial Engineering, University of Padova
Sergio Rech, Ph.D.
School of Industrial Engineering, University of Padova

Athens, September,2016

Θα ήθελα να ευχαριστήσω την οικογένειά μου, που ήταν πάντα δίπλα μου όλα αυτά τα χρόνια

Abstract

In large scale naval field, the propulsion system is usually electrical, in order to allow a free placement of the internal combustion engines (ICE), more flexible coupling with the power transmission and noise reduction. What is more, ships usually travel in steady speed, meaning that their load is steady and therefore their waste heat is steady. On that basis organic Rankine cycles (ORCs) are a promising technology to utilize the available waste heat in order to increase the efficiency and reduce fuel consumption. The design of the system must be as to maximize the power production and not to alter the working point of the ICEs. What is more its stability and safety must be guaranteed.

Simulation models are a convenient tool to both design and simulate the behavior of a system. After the design models are created, the design point can be determined for various fluids with a simple change of inputs. Also dynamic simulations are a cheap, fast and reliable way to evaluate systems stability and performance in dynamic conditions and allow the definition of the control strategy.

In this thesis flexible design point models of ORCs have been created in order to optimize the power output and determine the working fluid with the best performance. In addition to this, the basic parameters of the heat exchangers have been calculated and also performance parameters of other components. These data are used in order to create a dynamic model to simulate the cycles' dynamic response and develop a control strategy. The application of the models is done in a LNG carrier

Three different ORC layout are considered in this study. Single-stage, two-stages both subcritical, and two stages with the high pressure stage to be supercritical. The power output respectively for the best scenario in each layout are: 383,61 kW, 625,61 kW and 720,16 kW respectively. The control strategy proposed is the control of the superheating and subcooling temperature difference for the subcritical evaporators and condensers and entropy in the supercritical turbine's inlet. The results show that the systems reach steady state conditions within 150 seconds after the end of the inputs' variation.

Περίληψη

Στα πλοία μεγάλου μεγέθους, το σύστημα πρόωσης είναι συνήθως ηλεκτρικό, προς ελεύθερη τοποθέτηση των μηχανών εσωτερικής καύσης (ΜΕΚ), έχοντας πιο ευέλικτη σύνδεση με το σύστημα μετάδοσης κίνησης και μειώνοντας τον θόρυβο παράλληλα. Τα πλοία ταξιδεύουν συνήθως με σταθερή ταχύτητα, κατ' επέκταση και σταθερό φορτίο και σταθερά ποσά απορρυπτόμενης θερμότητας. Το περιβάλλον αυτό καθιστά την εγκατάσταση Οργανικών Κύκλων Rankine (ORC) μια πολλά υποσχόμενη τεχνολογία για αξιοποίηση της θερμότητας αυτής, με στόχο την αύξηση του βαθμού απόδοσης και την μείωση της κατανάλωσης καυσίμου. Ο σχεδιασμός του συστήματος πρέπει να γίνει έτσι ώστε να μεγιστοποιείται η παραγωγή ισχύος, δίχως να μεταβάλλεται το σημείο λειτουργίας των ΜΕΚ. Επιπλέον πρέπει να έχει εγγυημένη σταθερότητά και ασφάλεια.

Τα προσομοιωτικά μοντέλα είναι μία μέθοδος σχεδιασμού συστημάτων και προσομοίωσης της συμπεριφοράς τους. Με την κατασκευή μοντέλων σχεδιασμού μπορεί να βρεθεί το βέλτιστο σημείο σχεδιασμού του συστήματος για ευρείς συνθήκες λειτουργίας, για διάφορα οργανικά μέσα, αλλάζοντας μόνο τις μεταβλητές εισόδου του μοντέλου. Επίσης, τα δυναμικά μοντέλα προσομοίωσης αποτελούν έναν φθηνό, γρήγορο και αξιόπιστο τρόπο να εκτιμηθεί η σταθερότητα και η συμπεριφορά του συστήματος σε δυναμικές συνθήκες λειτουργίας, επιτρέποντας ταυτόχρονα και τον σχεδιασμό κατάλληλου συστήματος ελέγχου.

Η παρούσα διπλωματική αφορά την κατασκευή ευέλικτων μοντέλων σχεδιασμού και προσομοίωσης ORC. Τα μοντέλα σχεδιασμού υπολογίζουν το σημείο σχεδίασης του κύκλου που βελτιστοποιεί την παραγωγή ισχύος, για διάφορα οργανικά μέσα. Επιπλέον διαστασιολογούν βασικά εξαρτήματα του κύκλου όπως οι εναλλάκτες θερμότητας. Η διαστασιολόγηση είναι αναγκαία για την δημιουργία των δυναμικών μοντέλων, που προσομοιώνουν την μεταβατική λειτουργία του συστήματος σε αλλαγή των εξωτερικών παραμέτρων. Αυτό επιτρέπει την ανάπτυξη ενός συστήματος ελέγχου που θα κρατάει την λειτουργία σε ασφαλείς συνθήκες. Η εφαρμογή των μοντέλων έγινε σε ένα LNG carrier.

Τρεις διαφορετικοί κύκλοι μελετώνται στην παρούσα εργασία. Μία υποκρίσιμη πίεση ατμοποίησης, δύο υποκρίσιμες πιέσεις ατμοποίησης και δύο πιέσεις ατμοποίησης εκ των οποίων η μία είναι υπερκρίσιμη. Η παραγωγή ισχύος είναι 383,61 kW, 625,61 kW και 720,16 kW αντίστοιχα. Η στρατηγική του συστήματος ελέγχου είναι να κρατάει σταθερή την υπόψυξη, την υπερθέρμανση για τους υποκρίσιμους ατμοποιητες και την εντροπία εισόδου στον υπερκρίσιμο στρόβιλο. Προς επίτευξη του μεταβάλει τις στροφές των αντλιών και την παροχή του κρύου ρεύματος στον συμπυκνωτή. Τα αποτελέσματα δείχνουν πως το σύστημα αυτό είναι επαρκές και πως τα συστήματα ισορροπούν 150 δευτερόλεπτα μετά την σταθεροποίηση των μεταβολών των παραμέτρων εισόδου.

Table of contents

Nomenclature

A	Surface [m^2]
B_c	Baffle spacing [m]
C_p	Specific heat at constant pressure [J/kg K]
d_{in}	Tubes' inner diameter [m]
d_{out}	Tubes' outer diameter [m]
D_s	Shell's inner diameter [m]
D	Density [kg/m^3]
h	Specific enthalpy [J/kg]
K_t	Stodola coefficient [m^2]
L	Tube length [m]
$\dot{m}$	Mass flow rate [kg/s]
Nu	Nusselt number
Nt	Number of tubes
P	Pressure [kPa]
p_t	Pinch between tubes [m]
pp	Pinch point [K]
Pr	Prandle number
Re	Reynolds number
Q	Heat transfer rate [W]
s	Specific entropy [J/kg K]
T	Temperature [K]
u	fluid velocity [m/s]
U	Overall heat transfer coefficient [kW/m^2K]
$\dot{V}$	Volumetric flow rate [m^3/s]
ICE	Internal Combustion Engines
LNG	Liquefied Natural Gas
W	Power [kW]
wf	Working fluid
ΔT_{sup}	Superheating temp. difference
ΔT_{sub}	Subcooling temp. difference

Greek letters

μ	dynamic viscosity [Ns/m^2]
α	Convection coefficient [kW/m^2K]
η	Efficiency
ϕ	Heat recovery factor

Abbreviations, apexes and subscripts

hot	hot source stream
cold	cold source stream
cond	condenser
evap	evaporator
pre	preheater
sub	subcooling
sup	superheating
dp	design point
odp	off design point
in	inlet
out	outlet
is	isentropic
opt	optimum

HP high evaporation pressure

LP low evaporation pressure

turb turbine

Introduction

Heat engines are machines that operate between two temperatures to generate mechanical work. They absorb high temperature heat from a medium and after producing mechanical power they reject heat at different temperature levels. The process of waste heat utilization uses this heat to produce additional power and reject the rest of the heat at lower temperature. The Organic Rankine Cycle (ORC) is a system able to operate with a low temperature heat source. Water-steam Rankine cycles are unable to produce power with high efficiency if the hot source temperature is low, while ORC can achieve good efficiency. Typical efficiencies are in the range of 5% to 23% depending on the heat source characteristics and working fluid.

The correct choice of the ORC design point is of critical importance, as it determines the overall efficiency of the system both at design and off-design point conditions. Additionally, a high priority matter is to guarantee a safe and efficient operations of the system at off-design conditions. Dynamic models predict transient and equilibrium behavior of the system under different external constraints, so helping in the creation of safe operating conditions and good control strategies prior to the creation of the system.

Attention must be paid to the selection of the organic fluid that will be used as a working medium because it has a major impact both on thermal and overall system efficiency. As Karellas et. al. [3] show, for the same conditions of low temperature waste heat recovery different working fluids have up to 7% difference in the system performance. Although the number of working fluids is high, there are some studies which give indications of the characteristics that an organic fluid should have according to each particular case, such as the critical point temperature as suggested by Vivian et. al. [4].

An interesting field of ORC application is waste heat recovery. Ships have large amounts of waste heat due to the usage of internal combustion engines (ICE) as Spouse et. al. [5] shows. Shu et. al. [6] also reviewed the waste heat recovery on two-stroke IC engine aboard ships and indicate that ORC is the best system to recover heat at this low grade. Soffiato et. al. [7] indicate the possible hot streams that can be utilized by an ORC in an LNG carrier and have studied this particular occasion. Also it should be noticed the ships travel most of the time at a constant speed, which makes it convenient to install an ORC. In naval applications safety is of great importance and if a system is to be applied it must have proven its reliability and safety.

Dynamic models are a convenient way to check the models performance at partial loads and to design a control strategy. Wei et. al. [8] made a comparison study between different kind of models and concludes that different kinds have big differences both in accuracy and computational time. Vaja [13] presents a simple and flexible way to model an ORC system by connecting discrete components. His

approach is being followed in this thesis due to the simplicity that has. Quoilin et al. [10] designed a dynamic model of an ORC and used it in order to develop a control strategy, showing the usefulness of dynamic models.

The aim of this thesis is to create general and flexible models in order to determine the design point of three different ORC systems and develop flexible dynamic models in order to simulate and control them. The three different ORC cycles that considered in this study are: one pressure level, two subcritical pressure levels and two pressure levels, one of which is subcritical and the other supercritical. The models are also applied to a LNG carrier. The goal is to exploit waste heat energy from the ship ICE through an ORC waste heat recovery system. To this end, design point models are applied to calculate the optimum design point of the cycle for different fluids. Also basic characteristics of the system components are calculated, as length and number of tubes in shell-n-tube heat exchangers. In addition to this, dynamic Off-design models are applied at variable loads of the ship engine and a control strategy is presented to validate the stability and safety of the system, which is a high priority matter in naval applications.

1. Literature review

In this chapter review in the literature is done. There are presented important publications that have contributed in the scientific fields that affect the current study. The review is focus in ORC architecture for waste heat recovery, in the choice of different working fluids, the coupling of ORCs with ICE and the dynamic models. Unfortunately, the literature in dynamic modeling of ORCs is not considered sufficient. The modeling approaches proposed by authors are limited and they are not explained fully enough as to be understood and applied. This is because the dynamic modelling of ORCs is a still growing field and there is no global model to predict the behavior of all systems.

1.1 Review on ORC architecture for waste heat recovery

ORC is a commonly accepted way to convert low temperature heat sources into power. Their design allows them to operate without human presence and their maintenance needs are low. As a result, several units are in operation currently and ORC is a field that keeps growing. Except the simple cycle, more architectures are proposed in the literature, giving more possible designs in order to recover waste heat and transform it into power. Lecompte [22] made a review in the different kinds of ORC.

As a reference, he considered the most common one, the subcritical ORC (SCORC or basic ORC). Its layout is shown on the next figure. It is consisted by a pump, an evaporator, an expander and a condenser. The pump forces the working fluid into the evaporator where it evaporates and exits as vapor, usually superheated. Then it expands through the expander, producing the useful mechanical work, which is commonly transformed into electricity by a generator. After this it enters in the condenser as a superheated vapor, changes phase and exits as liquid. Then it is pressurized again by the pump, closing the cycle.

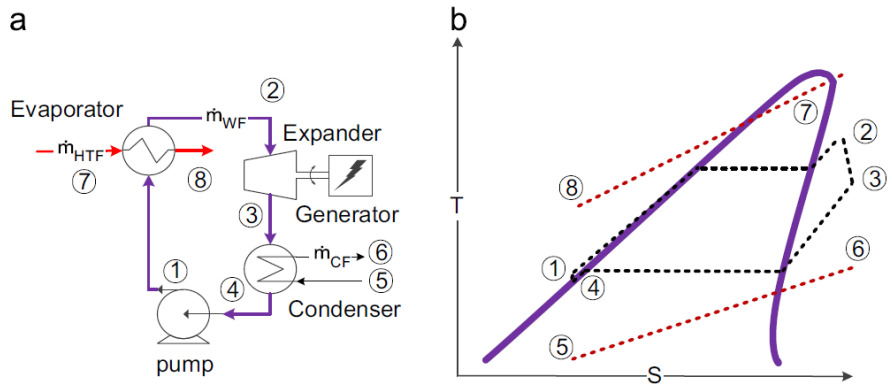

Fig 1.1 Subcritical ORC [22]

Several author propose the use of a recuperator (RC) after the expander. This is done in order to transfer heat from the superheated expanded vapor to the subcooled liquid after the pump. Because of this, dry fluids have better potential when a recuperator is used. This may lead to a big increase in thermal efficiency. But if there is no limitation in the outlet temperature of the hot source this will not result in higher power output, while having the cost of an additional component. A typical case that recuperation is used is when exploiting heat from flue gases, due to the limitations in their output temperature as acid dew point must not be reached.

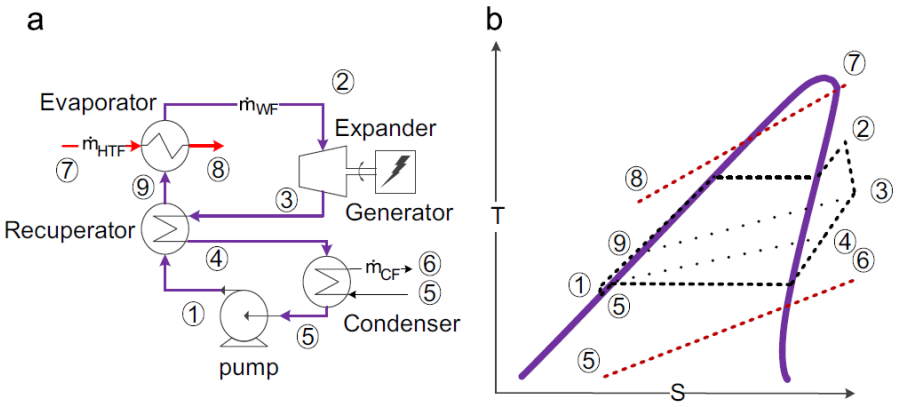

Fig 1.2 ORC with recuperator [22]

Another alternation of the basic ORC is the regenerative ORC (RG). This is usually done by a turbine's bleeding as it is done in steam Rankine cycles. In this way the thermal efficiency is increased and the irreversibility of the cycle is decreased. But as stated in cases of waste heat recovery there is no need to increase the thermal efficiency without increasing the power output on the same time, unless there is a problem like the ADP of flew gases.

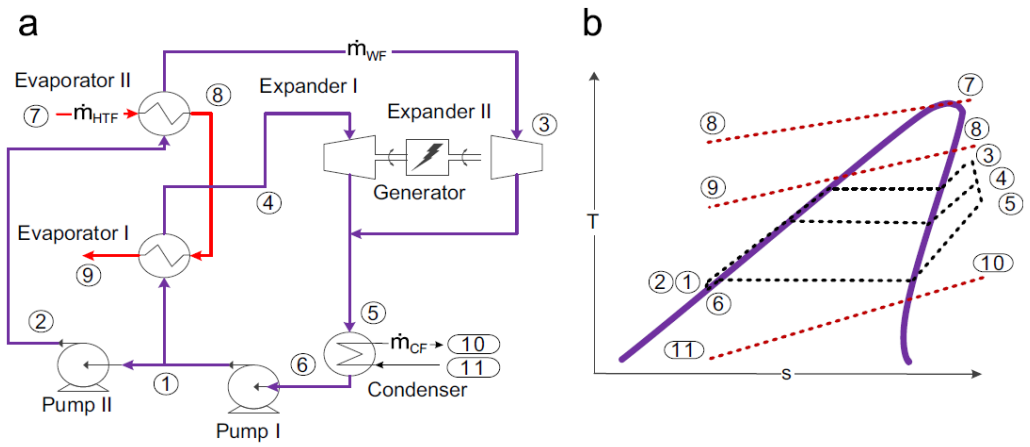

Fig 1.3 ORC with turbine bleeding [22]

A different approach is the organic flash cycle (OFC). In this case the liquid does not change phase in the evaporator towards becoming vapor. Instead, after the preheating of subcooled liquid, the liquid is throttled down to a lower pressure flash tank. In the tank the saturated liquid is separated from the saturated vapor. The vapor is leaded to the expander to expand. The liquid depending on the case can be leaded to the condenser or can be throttled again in order to provide more vapor, of lower pressure, which will be expanded afterwards. The OFC has in general good heat recovery as no phase change is happening during the heat transfer but has lower thermal efficiency due to the irreversibility that is caused by the throttle. Attention must be paid to the fluid selection because if the fluid that is used is wet, then in the end of the expansion there will be two phase mixture. This may cause problem to the expander due to the existence of droplets.

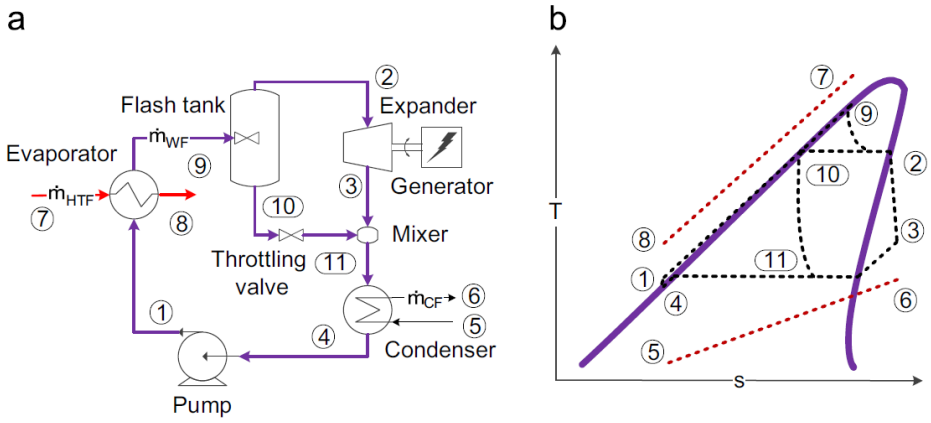

Fig 1.4 OFC cycle [22]

The trilateral (triangular) cycle (TLC) in T-s diagram resembles a OFC. It also does not evaporate the fluid during the heat exchange. Its main characteristic is that the expansion begins from the liquid phase without any flash and ends in the two phase region. In this way the heat recovery is very good as in OFC and also the irreversibility of the flash is avoided. Again the thermal efficiency is lower but the overall efficiency may be better than the one of the basic ORC due to the good heat recovery. The main problem in this case is the expander, because the expansion is done inside the two phase region and the efficiency is low.

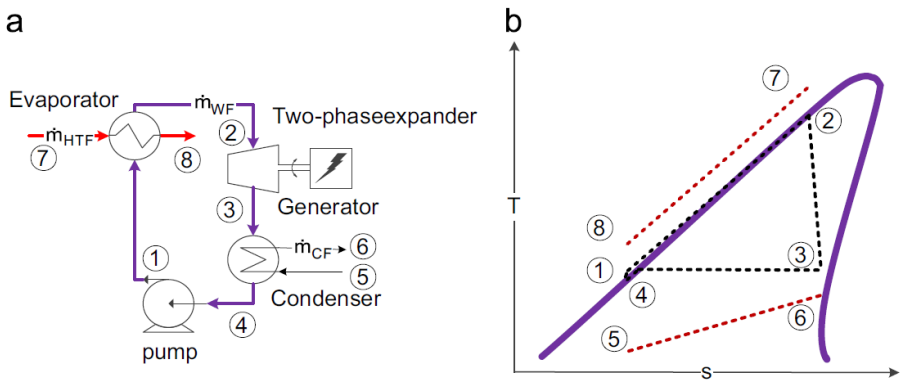

Fig 1.5 TLC [22]

In the literature, instead of the usage of pure organic fluid, is proposed the usage of mixtures of fluids. This involves the use of zeotropic mixtures. In this way the phase change is not done any more under constant temperate. The result of this is the decrease of the irreversibility of the cycle and therefor the increase in the exergy efficiency. Although there is some improvement in comparison with the basic ORC, it is around 3% the difference, so the writer proposes thermos-economic investigation to be done before choosing to design a ORC using a zeotropic mixture of fluids.

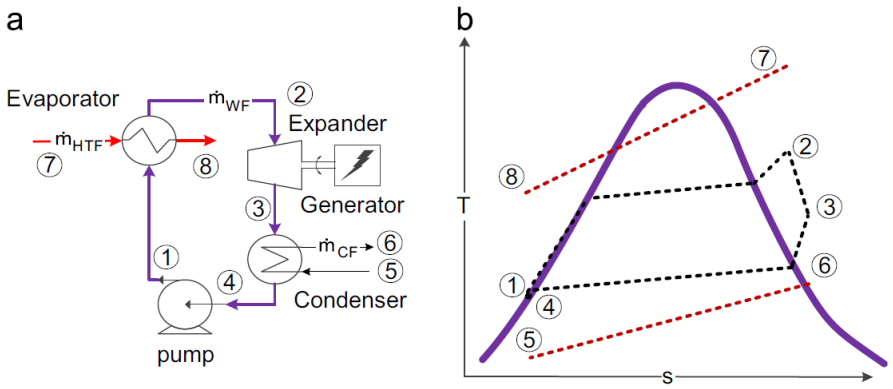

Fig 1.6 ORC with zeotropic mixtures [22]

Following the same evolution path as the one of steam Rankine cycle, transcritical (supercritical) ORCs are now possible to be designed with good efficiency and no undesirable problems. By reaching supercritical pressure the heating is be done without phase change, leading to better heat recovery. Usually it has less thermal efficiency but due to very good heat transfer it may result in bigger power output. Of course the selection of working fluids is limited to the ones which have critical temperature lower to the one of the heat source. Also depending on the fluid the heat exchange in the condenser may be done in supercritical conditions or in the two phase region, resulting different design of the condenser. In the layout there is no change of the component there is no change in comparison with the basic ORC.

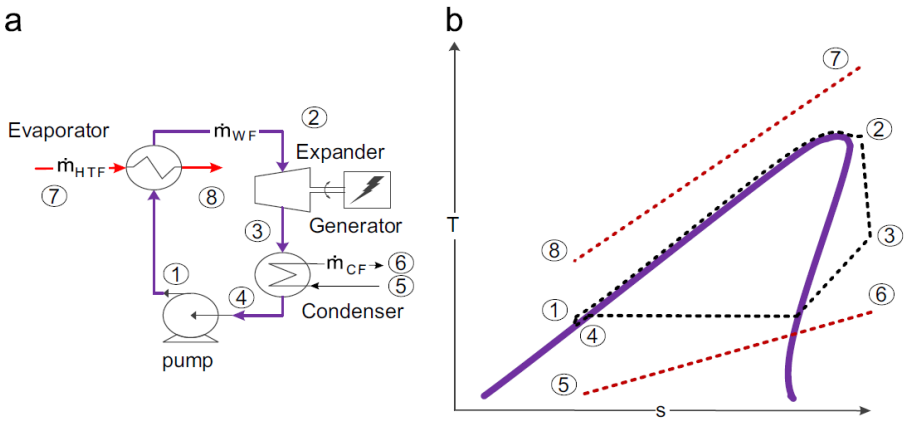

Fig 1.7 Supercritical ORC [22]

Instead of having only one evaporation level, more pressure levels can be more effective as they have the possibility to decrease the heat's sure temperature more. more pinch point temperature differences are introduced to the cycle, but they are between different streams and so higher heat recovery is possible. Losses in two pressure level evaporator can be as low as 26% of the total irreversibility while in basic ORC are from 30% to 77%. The pressure levels of the evaporators must be chosen carefully and some methodologies for choosing them are proposed in the literature. As the pressure levels increase the cycle turn to be similar to the theoretical Lorentz cycle. On the one hand this might sound very promising, on the other the total UA required is bigger, meaning biggest components, and the complexity of the system is increased as more pumps and expanders are introduced too. The layout changes too.

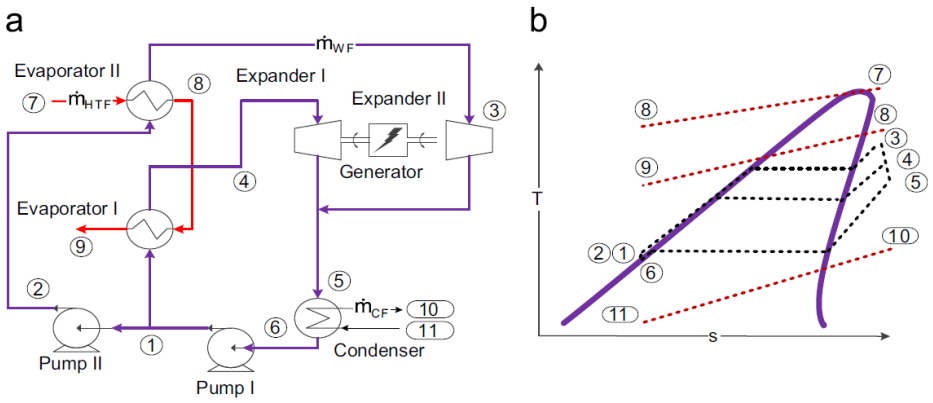

Fig 1.8 Multi evaporation level ORC [22]

1.2 Review on the working fluids

The organic Rankine cycle, as is indicated by the name, is a Rankine cycle which uses an organic medium instead of water in order to produce energy. Although it is said organic, the medium doesn't necessarily have to be an organic one in order for the cycle to obtain the name. For example, CO_2 and ammonia can be used in an ORC. Due to the vast difference in the applications that organic fluids are used and the big differences that their properties have, attention must be paid to the selection of the cycle's fluid. According to Velez [15] some of the parameters that are usually exanimated are:

Environmental: All refrigerants have an impact on the ozone layer and global warming. These impacts are measured by Ozone Depletion Potential (ODP) which is defined and limited by Montreal Protocol and Global Warming Potential (GWP) which is by Kyoto Protocol. These International Agreements have been made in order to promote the usage of more environmental friendly chemical substances among other.

Security: As chemical substances the refrigerants can be toxic and flammable. These factors make a leakage dangerous and must be taken into account when designing a system. ASHRAE has developed a classification system especially for refrigerants in order to indicate the danger level that their usage has. This is shown on Fig. 2.9:

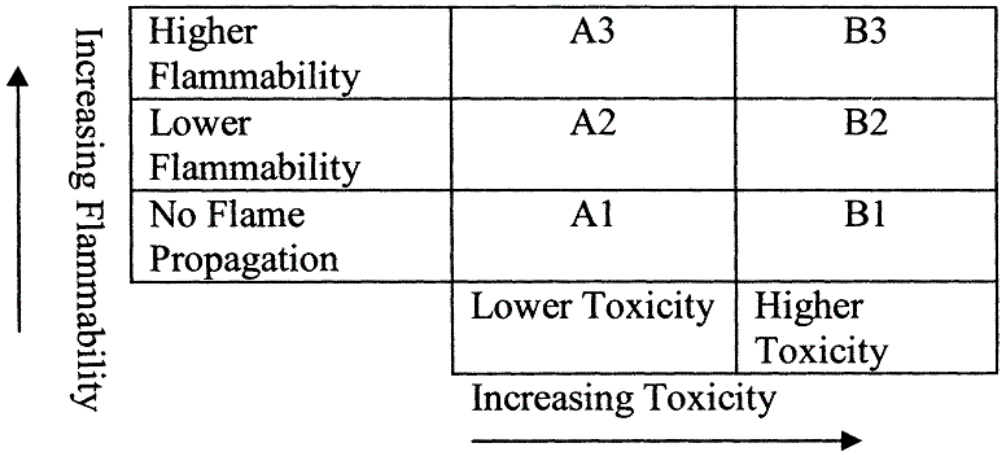

Fig 1.9 ASHRAE classification system

Stability: heat source's temperature restricts the usage of some fluids. These is because if they are exposed to temperatures above a certain point and on the chemical structure is altered and the cycle is affected as a result. Also the danger might be increased in case of leakage.

Pressure: high pressure is required in order for the cycle to operate. As the pressure increases the cycle's efficiency increases in some cases, but complexity and resistance of the equipment are increased also, leading to increased installation cost.

Availability and low cost: for obvious reasons fluids with high availability and low cost are preferable to the ones that are not.

Latent heat and molecular weight: high molecular weight and latent heat results in more energy absorbed from the hot source and also contributes towards the reduction of the size of system's components as less mass and volume flow rates are required.

Low freezing point: freezing point must be low enough to assure the lack of freezing condition during cycle's operation.

Saturation curve: every fluid has a unique saturation curve which leads to a unique slope in the saturated vapor area in a T-s diagram. If the slope is vertical, then the fluid is called isentropic. If it is negative or positive, it is called wet or dry respectively. Dry fluids cannot end the expansion inside the two phase area and that is an advantage compered to wet fluids as water, which needs superheating. The next figure clarifies the differences between these fluids.

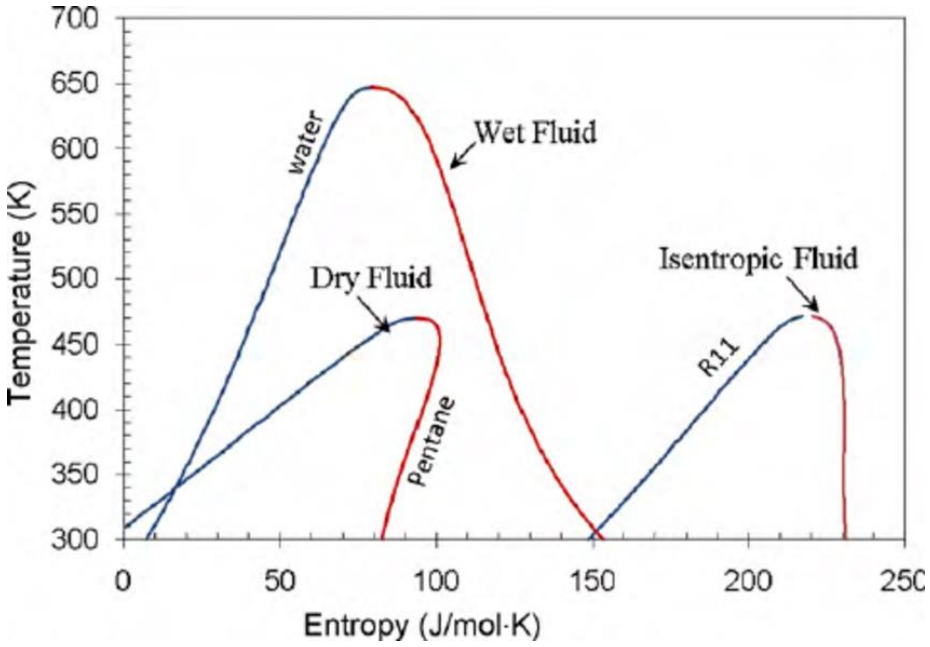

Fig. 1.10 Possible saturation curves

In general, the selection of the proper fluid for the ORC is not easy due to the many different criteria in which this choice is based. The peculiar situation of the ships and the regulations that they have make this choice very crucial. Soffiato [7] chose to study the following liquids for an ORC-WHR process on board a ship: R-134a, R-125, R-236fa, R-245ca, R-245fa, R-227ea. Larsen [16] in his study about choosing fluid for a marine application find out that the following fluids are suitable and have a low hazard level: R-245ca, R-236ea, RC-138, C5F12, C-Propane, R-245fa, considering fire hazard, health hazard and physical hazard. Senian He [17] in his study about fluid selection on an LNG-carrier analyzes the following fluids to find the optimum one: C4F10, CF31, R-236ea, R236fa, RC-318.

1.3 Review on coupling engines-ORC

ORC are commonly used in waste heat recovery as to increase total energy production and improve the overall efficiency of the system. A very promising opportunity is to couple an internal combustion engine (ICE) with an ORC system. ICE have large amounts of waste heat energy aborted to the environment. The hot exhaust gases, the intercooler of the compressed air, the cooler of the jacket water and lubricating oil are the biggest part of them. A Sankey diagram of a typical tanker ship as proposed by Dimopoulos et. al. [32] is shown in Fig 2.11. This Sankey diagram is used to indicate the magnitude of waste heat losses in a ship's engine and the

possible gain of utilizing this waste. Although it is very promising to utilize the hot streams shown above, attention must be paid to the design of a system like this. In the literature there are several studies of coupling like this.

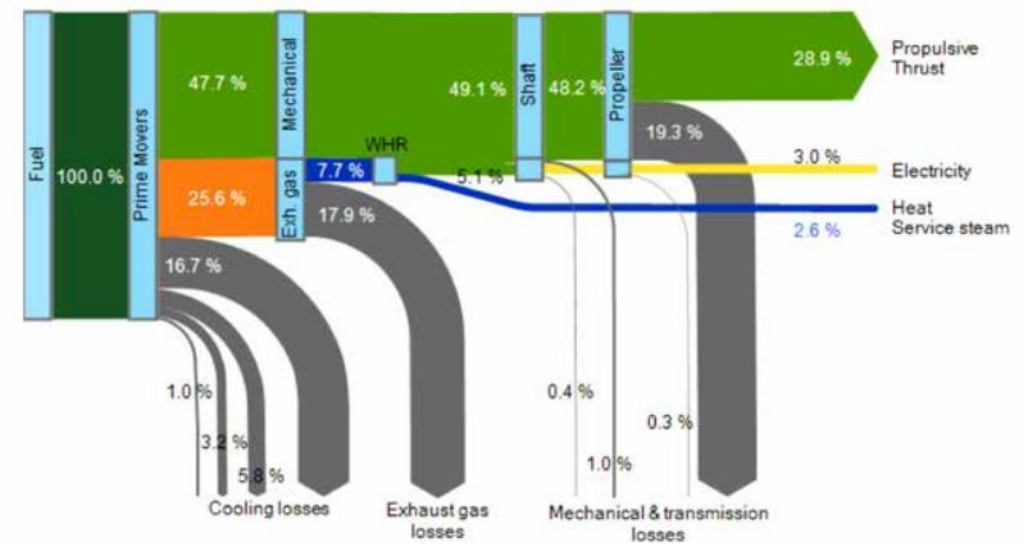

Fig 1.11 Typical energy flow diagram of a modern tanker at sailing condition [32]

Wang [18] performed an analysis of a novel system combining a dual loop ORC with a gasoline engine. In his study he recovered hear from an 130KW BL18T gasoline engine both from the cooling system and the exhaust gases and produced power through two expanders. The high pressure evaporator used the exhaust gases and was containing R-245fa while the low pressure evaporator was using the waste heat from the cooling system and was containing R-134a. The high pressure circuit after the expansion was preheating the low pressure circuit like in regenerative cycles. After them coupling of the two systems the maximum power is increased by 32 kW, meaning a 25% increase. The system's configuration is in Fig 2.12:

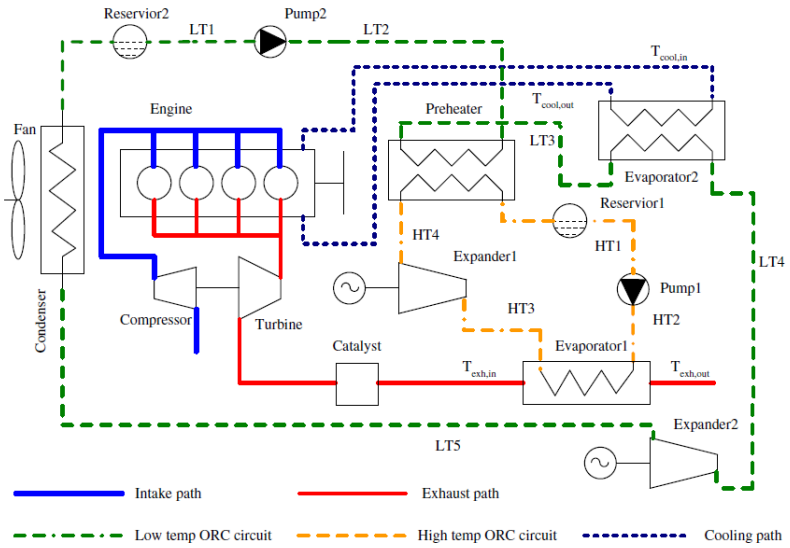

Fig. 1.12. Schematic of a dual loop ORC system combined with a gasoline engine [18]

Another analysis of ICE combined with a dual loop ORC was performed by Song [19]. The configuration was similar with the one performed by Wang [18] and the two circuits also use different working fluids. The ICE uses diesel fuel and has a 996 kW power output at 1500 rpm. In this analysis for the HT loop cyclohexane, benzene and toluene are selected while for the HT loop R-123, R-236fa and R-245fa are chosen. In the end the results show that the maximum power output is obtained by cyclohexane in the HT loop and R-236fa in the LT and is 111.2 kW. This leads to a 11.2% increase in the total power of the ICE. A T-s diagram in Fig. 2.13 shows the two loops:

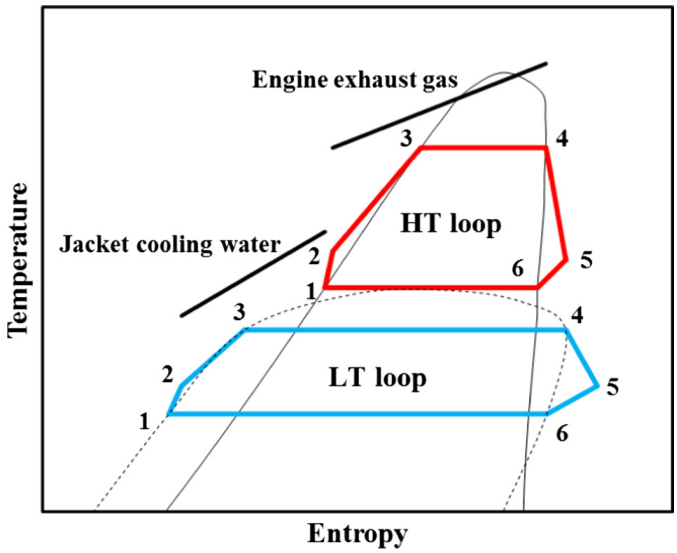

Fig. 1.13. T–s diagrams the dual loop ORC system for engine waste heat recovery [19]

Yu [20] also utilized waste heat from an internal combustion engine. He used R-245fa and used one loop. The as well used both jacket's water and exhaust gases waste heat, but he used a thermal oil to transfer heat from the exhaust gases to the organic fluid. The diesel engine he studied had 6 cylinders and was driving a generator, so the rotational speed was constant at 1500 rpm. Albeit the speed was constant the load was not. The study involves five different loads of the engine, at 285.3 kW, 235.8 kW, 211.6 kW, 176.2 kW and 117.7 kW. After the optimization of the cycle the power that the ORC produces in each case is 15.5 kW, 14.5 kW, 13.7 kW, 11.3 kW and 7.2 kW respectively.

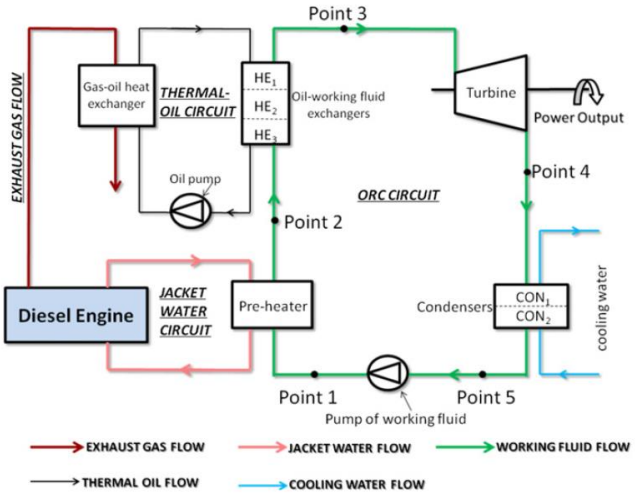

Fig. 1.14. Schematic diagram of the bottoming ORC [20]

Usitalo [21] made an experimental study in exploiting waste heat energy from the supercharged air before entering the ICE using one circuit with R-245fa and isopentane. He used a shell tube heat exchanger evaporator with a small superheat in order to be sure that there would be no liquid droplets in the expander. Both steady state and transient tests were run in order to evaluate the performance of the system. The steady state result showed that by increasing the evaporation pressure the heat rate introduced in the evaporator was decreased and the mass flow rate of the organic fluid too. Also the available heat drops significantly with the loads decrease from a certain point and on. The transient test showed that the ORC reaches steady state conditions 10 minutes after the start of the ICE's operation.

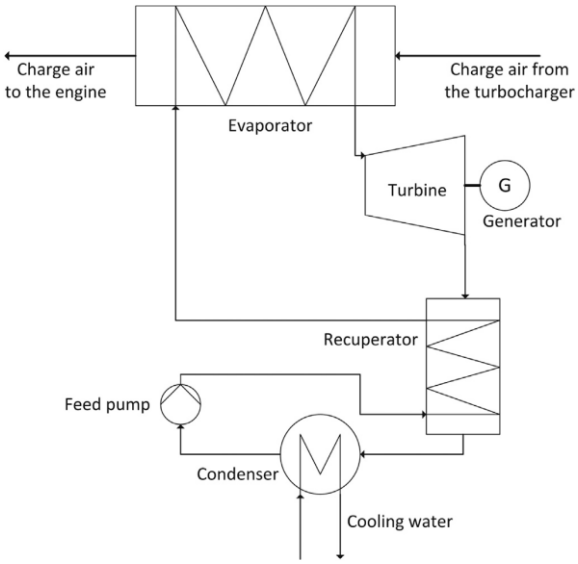

Fig. 1.15. A simplified process diagram of an ORC utilizing charge air heat [21]

1.4 Review on dynamic models and control strategies

The dynamic Off-Design models are a convenient way to predict the performance, safety and stability of a real system. They also allow the development of the proper control strategy, by evaluating the impact it has on the system's behavior through simulations. Off-design models are proposed in the literature and it is a scientific field that keeps developing as there is no global model to predict correctly the behavior of all the systems.

Astrom etc. [28] analyzed the complex dynamic behavior of a drum filled with vapor and liquid. His analysis indicates a way to predict the drum's behavior when the external parameters are known, such as mass flow rate entering and leaving and heat transferred to the drum. The calculations are done by solving the mass and energy balance equations that characterize the system. Astrom in order to avoid complex calculations proposes that the tubes temperature can be supposed to vary in the same way as the drums fluid does.

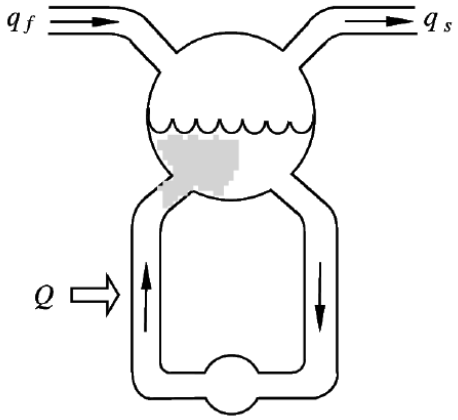

Fig. 1.16. Schematic of a drum [28]

Wei [8] made an experimental analysis in a real ORC system in order to validate the models he constructed. He considered two different types of models for the evaporator and the condenser, one moving boundary and one discretized. The moving boundary model does not have fixed bounders, but they are moving as the zones of different phases change. For example, as Wei stated, for the evaporator three zone are enough to form the model, one for the subcooled liquid, one for the two-phase mixture and one for the superheated vapor.

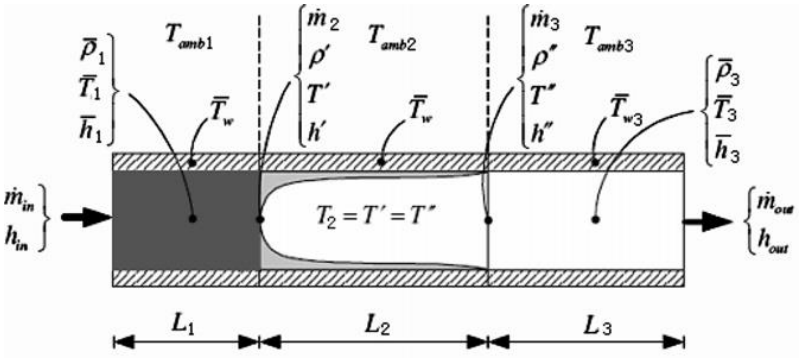

Fig. 1.17 Schematic of general moving boundary model [8]

For each of the three zones above the heat and mass balance equations are solved in order to obtain the results.

For the discretized model on the other hand, more areas are required in order to model the heat exchangers. Their boundaries are not moving as in the previous approach. They remain steady and in each cell friction and heat transfer are calculated. In his model Wei does not calculated mass entering and leaving cells through momentum balance, but it is a boundary condition for his model. Mass balance and energy balance problem in formulated for each unique cell as is usually

done for discretized models. The next figure is a nomenclature for his discretized model (design boundary conditions are shown in brackets, but these might be changed as required).

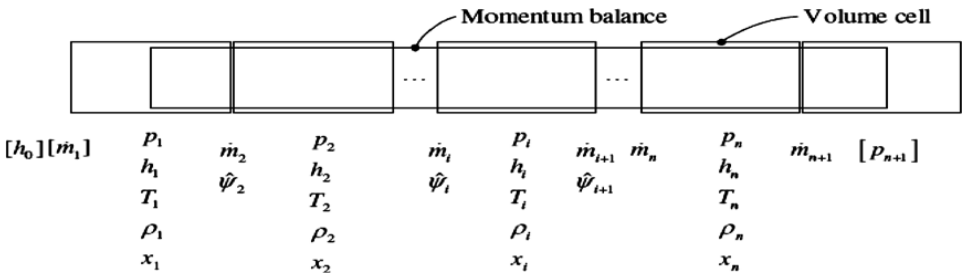

Fig. 1.18 Schematic of fixed boundary model [8]

Finally, Wei states that his fixed boundary model achieves an error of 4% and simulated the systems behavior correctly and without oscillations and chattering (which are common problem in dynamic simulations). What is more he states that the moving boundary models are less complex as they are characterized by a smaller order higher computational speed and so they are preferable for control design applications. His results indicate that the discretized model is more accurate than the moving boundary as is shown in his diagrams that follow:

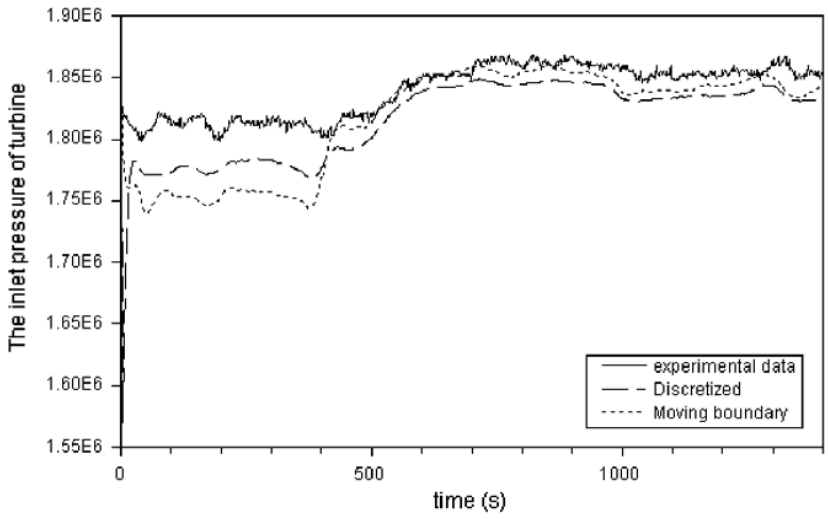

Fig. 1.19. Results of turbine inlet pressure for the dynamic simulation [8]

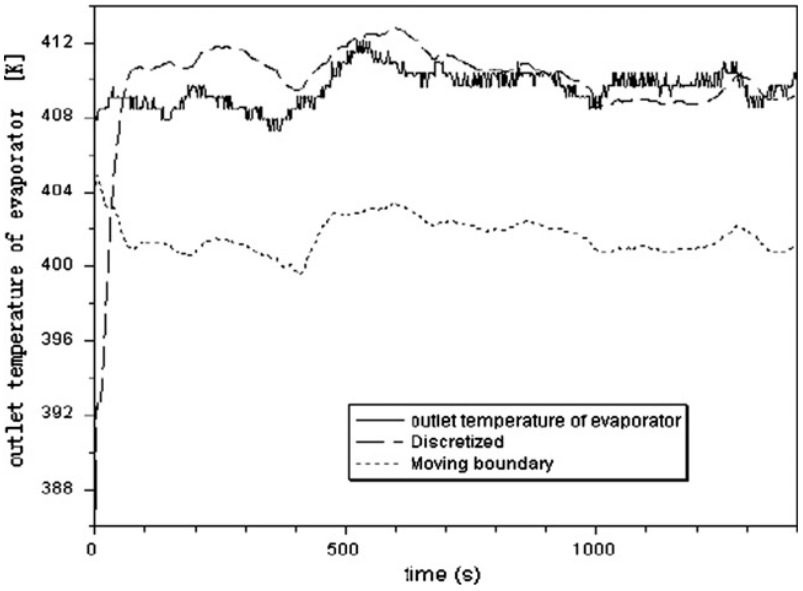

Fig. 1.20. Results of evaporator outlet temperature for the dynamic simulation [8]

Bamgbopa [9] also introduced a dynamic model of an ORC system and validate it through the comparison with other models proposed in the literature. He also used a finite volume model for the heat exchangers in his study.

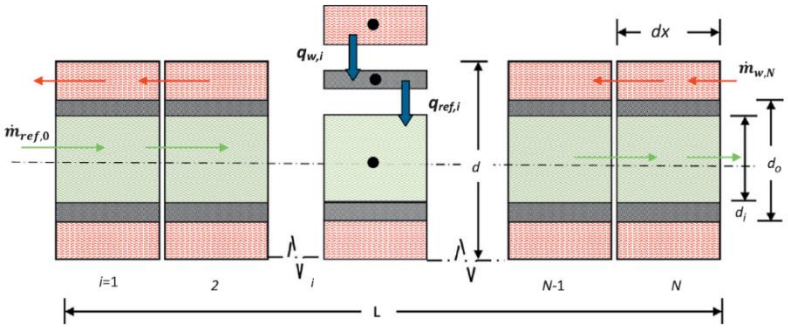

Fig. 1.21. Representation of a counter flow heat exchanger [9]

He tested his model to check the independence of the grid. His test variable was the $error_N$ which was defined as $error_N = \frac{\varepsilon_N - \varepsilon_{expected}}{\varepsilon_{expected}}$. The letter ε is used to symbolize the efficiency of heat exchanger. The results were that at 80 finite volumes the error was close to zero but at 70 volumes there was a good combination of accuracy and computational time.

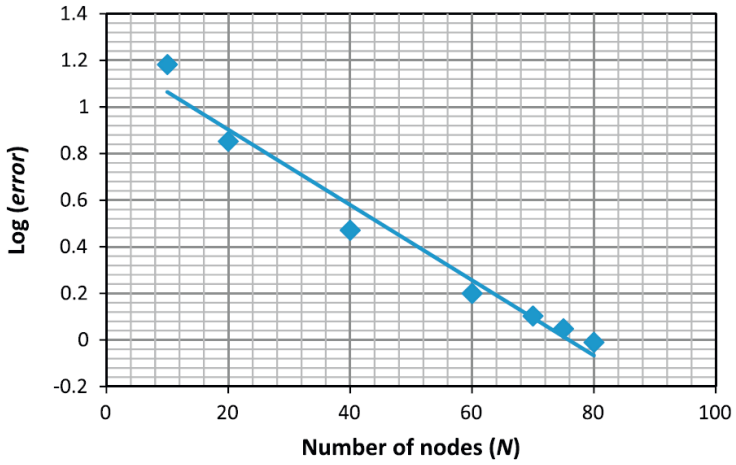

Fig. 1.22. Grid independency tests for N = 10, 20, 40, 60, 70, 75 and 80 [9]

Willatzen et. al. [11] in 1997 published a general dynamic simulation model for evaporators and condensers in refrigeration. Their model was a moving-boundary one with heat exchange. The analysis that was performed in mass and energy balance in the working fluid is very precise and has been the basis for further development of moving boundary models with phase change. The balance equations are developed for each of the three different phase regions and are properly connected together, forming a solvable system of equations by having as inputs the heat transferred in each region.

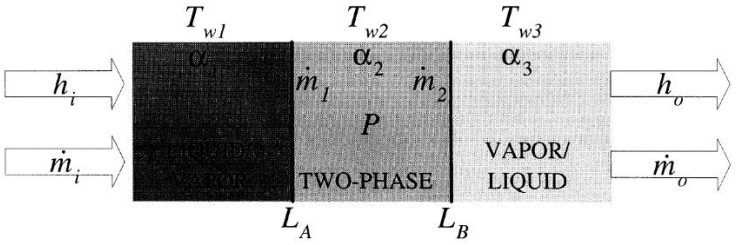

Fig. 1.22. A general two-phase heat exchanger structure [11]

Vaja [13] made an extensive research in various methodologies and tools for dynamic simulation. In his study he categorizes variables of dynamic systems according to their properties in two categories: flow variables and level variables. After this, he categorizes the components into two categories according to the way their performance is affected by the variables: flow control components and capacity/reservoir components.

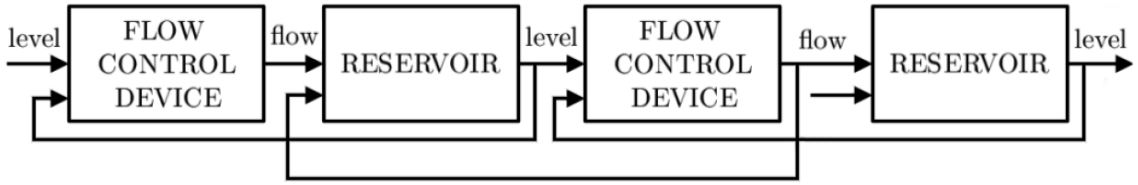

Fig. 1.23. Example of connection between state determined and not state determined components (reservoir and flow control devices) [13]

Vaja [13] also created an ORC power plant model with tools from Simulink® library. His approach is to model the overall system by connecting together models of individual components. The model that he used for the heat exchangers is shown in Fig. 224. Note that the counter flow heat exchanger with phase change that is used is connected with a capacity block. By using this approach Vaja separated the complex problem of modeling the heat exchanger into two different ones: one heat transfer problem and one mass and energy storage problem. As he states, it is necessary to take into account the mass and energy storage phenomena as they have significant impact on the cycles behavior.

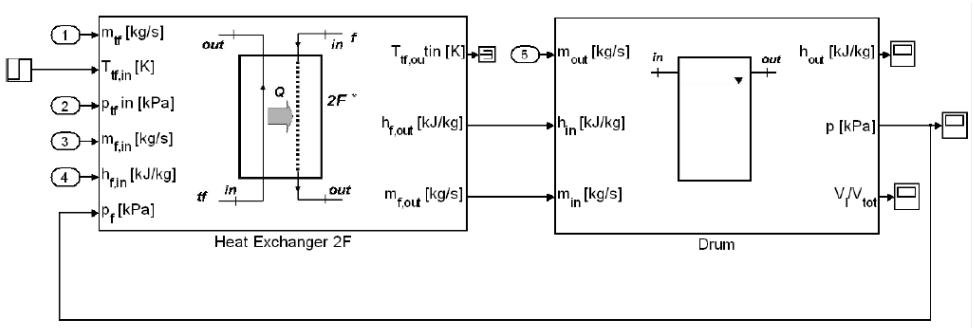

Fig. 1.24. Simulink® model of an evaporator-drum system [13]

Mazzi, et. al. [12] in their study also follow a similar approach. They subdivided the heat exchangers in two parts, one heat transfer component and one capacity component. The capacity component needs the initial values of pressure and temperature in the outlet and the values of inlet temperature and of mass flow rates at inlet and outlet during the simulation. The flow control components require the temperature at the inlet and pressure at the inlet and outlet in order to function. The heat transfer block requires the input conditions which are taken by the closest flow control component and capacity. The correct linking between the components is shown below.

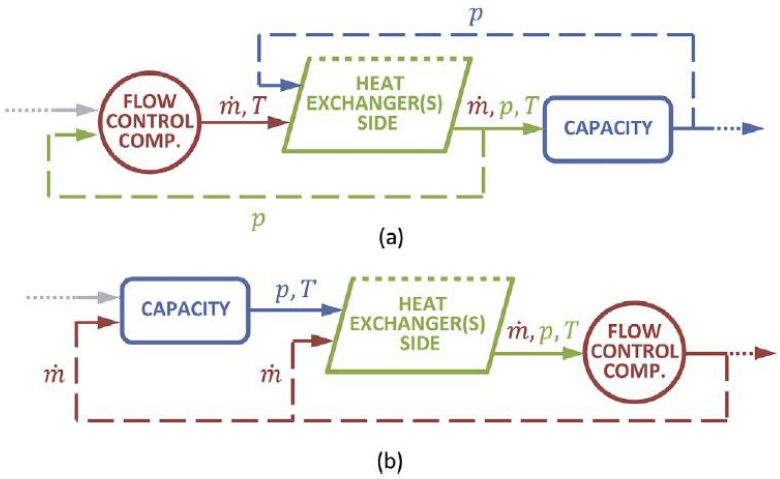

Fig. 1.25. Links between variables and heat exchangers sides in the off-design model: the capacity is downstream of the heat exchanger side (a) and capacity is upstream of the heat exchanger side (b). [12]

Quoilin [10] in his study tried to define the optimal control strategy for a small ORC application with a volumetric expander. For this, he created dynamic and steady state models to simulate the components of the cycle. He took into account the following general statement:

1. The condensation pressure must be maintained as low as possible
2. The superheating in the evaporator must be as low as possible
3. The optimal evaporation temperature results of an optimization of the overall heat recovery efficiency

In order to meet the following conditions, he considered two degrees of freedom: the rotational speed of the pump and the rotational speed of the expander. By changing these two he was able to control the main working conditions: evaporation pressure and superheating. Three different control regulations were introduced:

1. Constant evaporation temperature

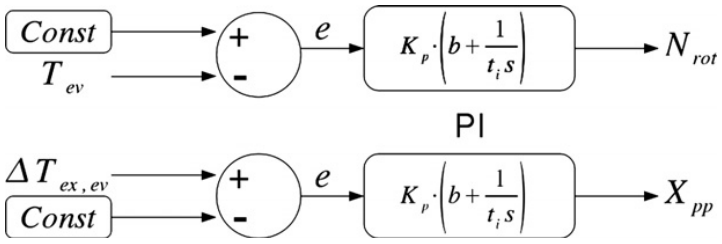

Fig. 1.26. First regulation strategy: constant evaporating temperature [10]

2. Optimal evaporation temperature. This required the predefinition of the optimal evaporation temperatures in various conditions with steady state models, which are stored in the control system

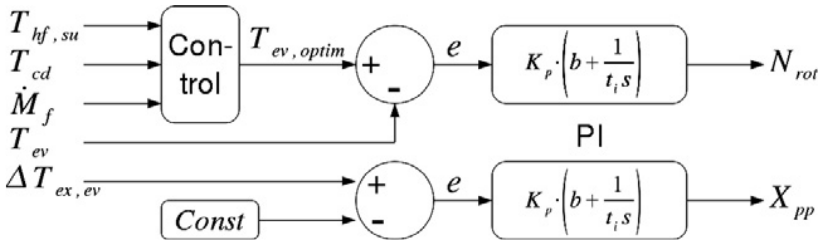

Fig. 1.27. Second regulation strategy: optimal evaporating temperature [10]

3. Correlated pump speed. This approach uses also data obtained by steady state model and tries to achieve faster response to varying conditions. The expander speed is selected because it constitutes an indirect measurement of the flow rate for a given evaporating temperature. Therefore, the correlated mass flow rate is the one which obtains the optimum evaporation temperature.

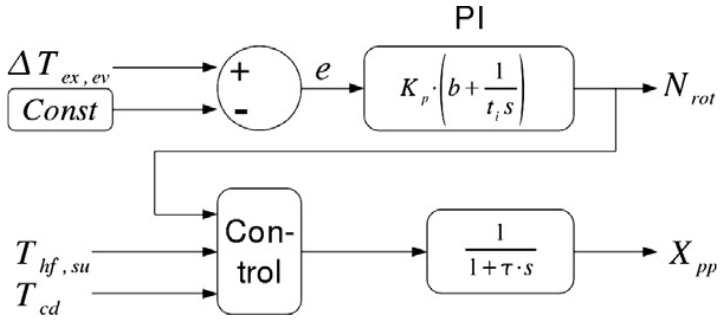

Fig. 1.28. Third regulation strategy: correlated pump speed [10]

He used PI controllers in all the cases above. The reasons that lead to the choice of PI over PID is their satisfactory behavior in the test that were run and their lack of sensitivity to noise.

1.5 Conclusions

In this chapter review in the literature that is connected with the thesis is done. It is shown that the choice of organic fluid is strictly depended on the application and the ORC layout. The layout is also depended on the application as different layout vary in the heat recovery factor, the thermal efficiency and the complexity. What is more different approaches for dynamic modelling have been presented. Unfortunately, this is a domain that is still developing and the literature is found relatively small since the authors neither describe precisely the work done nor publish all the results, as Vaja [13] also states. The current study follows the approach proposed by Vaja [13] and Mazzi [12] and the heat exchangers are modeled by two different blocks, on heat transfer and one capacity. Finally, a simple and effective control strategy found in literature and is presented. Considering the above, a moving boundary model is preferred to a fixed one, as it is simpler and faster. Three type of ORCs are considered, basic ORC, dual pressure subcritical and dual pressure supercritical. Also the working fluids that are available for usage are limited to the ones allowed onboard ships. Finally, the control variable of pump rotational speed is considered a proper one and easy to apply in any case. The speed of the turbine in this study will be constant, as in the ships there are many generators and it is considered more possible to operate in steady rotational speed than in changing.

2.Case study

The case that is studied in this thesis is a LNG carrier which was previously studied by Soffiato [7, 29]. Soffiato studied the LNG carrier's engine obtaining data for the ship's performance by the manufacture's brochure and after 3.5 years of measurements. It is considered that 3.5 years of measurement are enough in order to obtain a good statistic sample for the average year. The thesis was in developing design point models for different loads of the engine and performing an economical evaluation of the ORC installation. The data of this thesis will be used in order to select the hot streams which be utilized.

2.1 Main engine description

The plant is composed of four Dual Fuel Diesel Electric engines (DFDE) that supply electric power to the ship. No. 1 and No. 4 Diesel engines are Wärtsilä 12V50DF type, and No. 2 and No. 3 are Wärtsilä 6L50DF type. All the engines are four-stroke turbocharged inter-cooled ones and the pumps of the cooling systems are of the engine driven type. Each engine can be fueled either with natural gas or with heavy fuel oil (HFO). In case of natural gas, a small amount of Light Fuel Oil (LFO) is required as pilot injection. Wärtsilä 6L50DF is a six cylinders in-line engine and Wärtsilä 12V50DF is a twelve cylinders V engine.

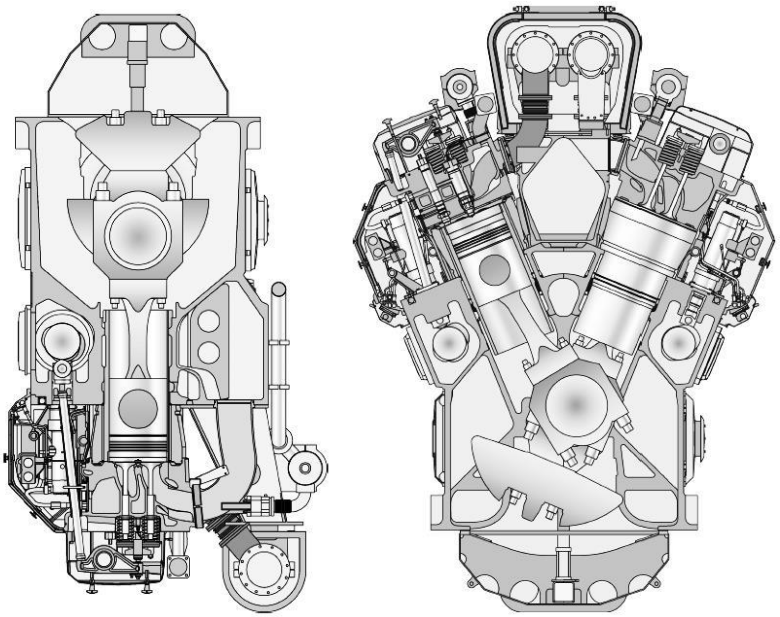

Fig 2.1 Cross section of the 6L50DF in-line engine (left) and of the 12V50DF V-engine (right) [29]

The design main characteristics of the two different engines are presented in Table 2.1. Most of the information that is reported is taken from the "Product guide" of the engines, as Soffiato states. The rest of the data are found by thermodynamic calculations. Considering the composition of this plant and the data of Table 2.1, the maximum available electrical power at generators outlet is 33000 kW.

Table 2.1 Main characteristic of the Diesel generator engines, [Wärtsilä (2012); Energy and steam balance of the ship] [29]

	Unit	12V50DF	6L50DF
[Wärtsilä (2012)]			
Mechanical output	kW	11400	5700
Cylinder bore	mm	500	500
Stroke	mm	580	580
Engine speed	rpm	500	500
Mean piston speed	m/s	9.7	9.7
Mean effective pressure	bar	20	20
[Energy and steam balance of the ship]			
Electric output	kW	11000	5500
Generator efficiency	%	96.49	96.49

All main engines that compose the generating power plant of the present ship have a similar cooling system that rejects heat at certain temperature levels to the cooling water provided by the "central cooler". This last component is a system mainly composed of heat exchangers which in turns dissipate heat to seawater.

In particular, the cooling system of each engine is composed of the low temperature circuit (LT) and of the high temperature one (HT) as shown in Fig. 2.2. In these circuits, the cooling flows (water) coming from the central cooler pass through various components and absorb heat, which increases their temperature.

The figure shows that the cooling flow in the HT circuit passes through the cylinder jackets and heads thus being heated from state *w1* to state *w2*. Then, it passes through the first stage of the charge air cooler (cooler *AC1* in the figure). A control valve after this cooler keeps the temperature of the HT water flow (T_{w3}) at an appropriate level, re-circulating a certain quantity of water. An additional valve is installed before the engine in order to maintain the temperature T_{w1} approximately constant.

The cooling flow of the LT circuit coming from the central cooler (state *w7*) passes through the second stage of the charge air cooler (cooler *AC2* in the figure) and then absorbs heat from the lubricating oil at the lubricating oil cooler (*LOC)*. A charge

air temperature control valve regulates the mass flow rate of the LT cooling water through the second stage of the charge air cooler (partly bypassing the cooler), in order to set the temperature of the air at state *a4*. Note that LT water flow comes directly from the central cooler so that its temperature depends on the operation of this component also in response to the climate conditions.

A tank of the lubricating oil is located just below the engine. From this, the oil is pumped into the lubricating oil cooler (*LOC)* where it is cooled down by transferring heat to the LT cooling flow, it passes through the engine and the turbocharger (*T/C)* and comes back to the tank. A temperature control valve is installed after the lubricating oil cooler to keep oil temperature constant at the engine inlet.

The arrangement shown in Fig 2.2igure 2.2 is valid for the two types of engines. The figure shows that the heat associated with the exhaust gas after the turbine of the T/C (state *eg2*) is exploited by an exhaust gas boiler (*EGB*).

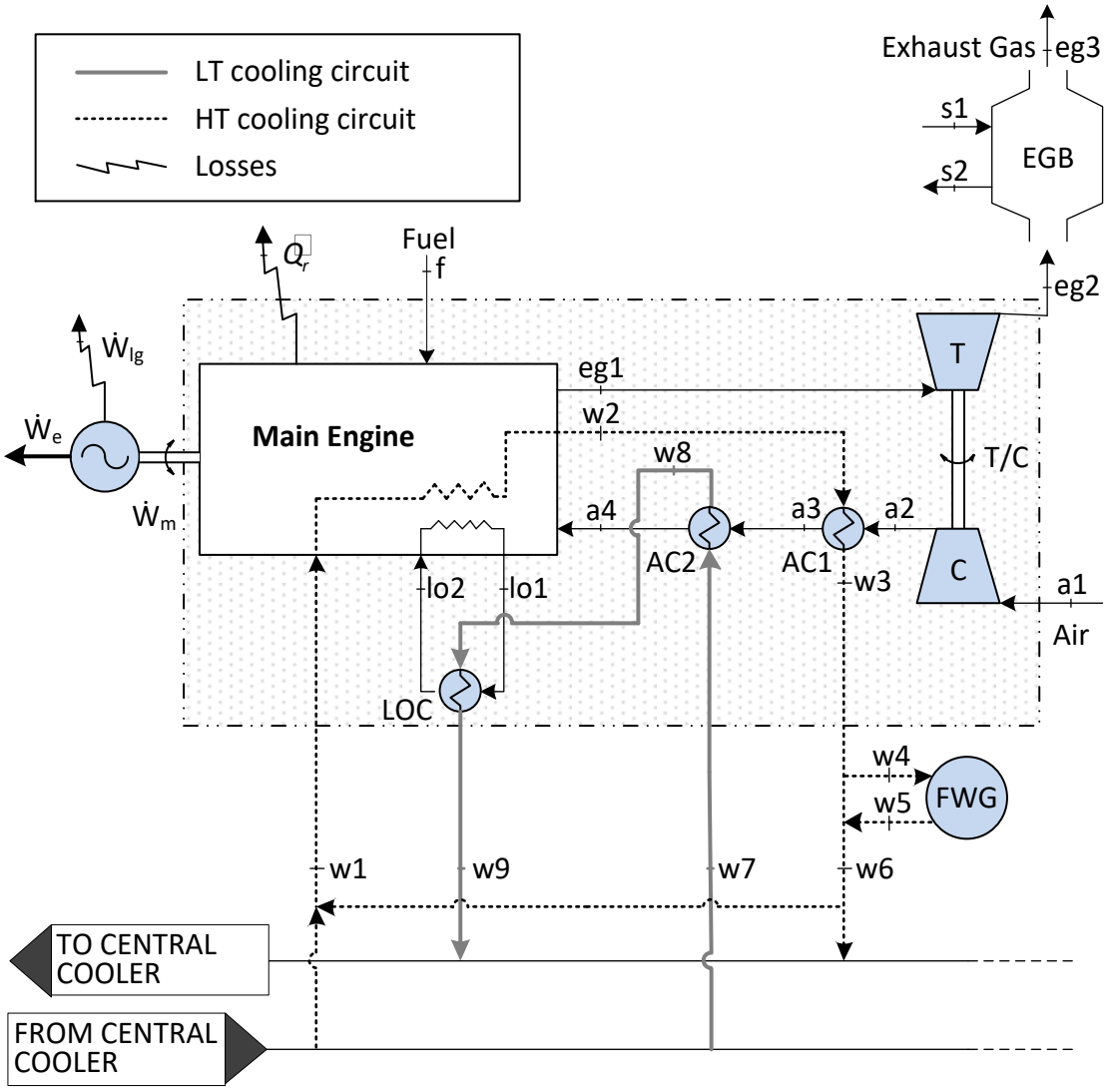

Fig 2.2 Arrangement of Main Engine and cooling circuits [29]

Thermodynamic calculations are done for many possible loads by Soffiato et. al. [29]. The results are on the table 2.2.

Table 2.2 Summary of the operating parameters [29]

		Wärtsilä 6L50DF					*Wärtsilä 12V50DF*				
Par.	Unit	100	90	85	75	50	100	90	85	75	50
T_{w1}	°C	74	74.6	75	76	78	76	76.4	76.6	77	78
T_{w2}	°C	79.4	78.3	78.6	79.5	81.0	80.1	79.8	79.9	80.5	81.0
T_{w3}	°C	83	82.2	82	82	82	85	83.3	83	83	82
T_{w7}	°C	36	36	36	38	38	36	36	36	36	36
T_{w8}	°C	45	43.7	43.1	43.9	41.4	45	43.7	43.1	41.9	39.4
T_{w9}	°C	54.2	52.6	51.9	52.6	49.7	54.2	52.6	51.9	50.6	47.2
T_{a2}	°C	187.0	177.6	170.5	151.9	113.1	183.3	176.8	169.6	151.9	113.1
T_{a3}	°C	97.8	95.2	94.1	91.1	79.3	96.3	94.9	93.7	91.1	79.6
T_{a4}	°C	44	44.6	45	46	50	45	44.2	44	45	51
T_{eg2}	°C	390	397	409.7	441	438	390	397	409.7	441	438
T_{lo1}	°C	76	75.4	75.3	75.1	73.6	76	75.4	75.3	75.1	73.6
T_{lo2}	°C	61	61	61	61	61	61	61	61	61	61
$\dot{m}_{lo}$	kg/s	18.1	18.1	18.1	18.1	18.1	36.2	36.2	36.2	36.2	36.2
$\dot{m}_{w1}$	kg/s	31.5	42.7	42.6	41.3	41.7	82.1	93.9	93.2	82.6	83.4
$\dot{m}_{w7}$	kg/s	13.3	13.3	13.3	13.3	13.3	26.6	26.6	26.6	26.6	26.6
$\dot{m}_{a}$	kg/s	9.15	8.27	7.78	6.9	5.26	18.3	16.64	15.67	13.81	10.52
$\dot{m}_{erg2}$	kg/s	9.4	8.5	8.0	7.1	5.4	18.8	17.1	16.1	14.2	10.8
p_{bar}	bar	1.028	1.028	1.028	1.030	1.031	1.015	1.015	1.015	1.016	1.016
p_{a2}	[bar-g]	2.4	2.14	2	1.7	1	2.3	2.16	2	1.6	0.9
p_{w1}	bar	3.15	3.15	3.15	3.15	3.15	3.15	3.15	3.15	3.15	3.15
p_{w7}	bar	3.15	3.15	3.15	3.15	3.15	3.15	3.15	3.15	3.15	3.15

In order to help the reader, understand better the results the Fig 2.3 shows the arrangement of the Wärtsilä 12V50DF Main Engine and cooling circuits with the values of temperature and mass flow rates for 100% load.

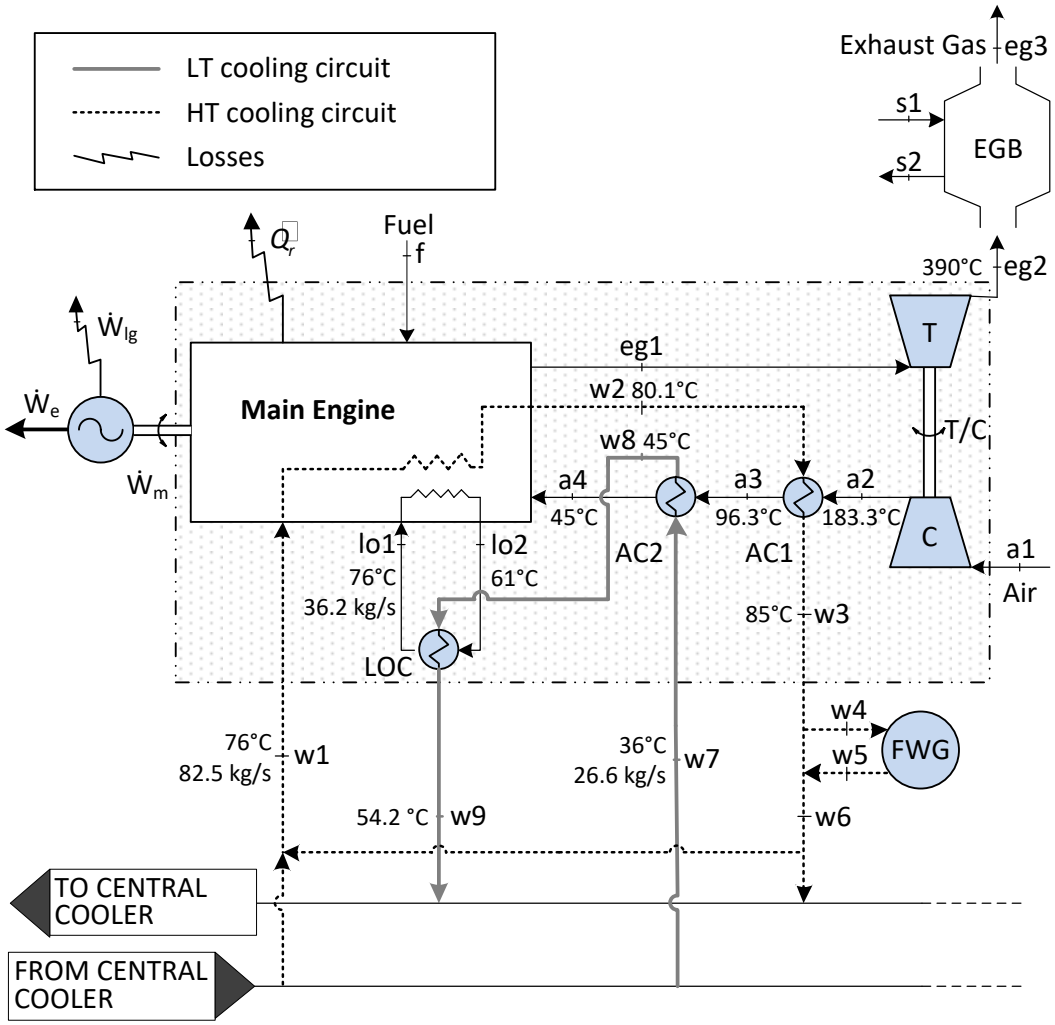

Fig 2.3 Arrangement of Wärtsilä 12V50DF Main Engine and cooling circuits; load 100% [29]

The two fresh water generators are not coupled with any engine in particular as to be more flexible. This is done because engines operate better at high load, so in normal voyage conditions it is preferred to operate three out of four in high load than all of them in medium load. Their main features are shown in the table 2.3.

Table 2.3 Main characteristics of the fresh water generators

First model		
Generator capacity	$m^3/24h$	30
Inlet temperature of the feeding water (range)	°C	55÷95
Inlet temperature of the feeding water (design)	°C	91
Outlet temperature of the feeding water	°C	73
Operation point steam flow	kg/s	11.8

Heat absorbed	kW	891.7
Second model		
Generator capacity	m^3/24h	30
Operation point steam flow	kg/s	7.08
Heat absorbed	kW	535.0

Power demands of a vessel are different in each phase of a trip and generally are a function of its service speed V_s. Propulsion represents the most important power need of a ship and, depending on the case, it can be satisfied directly by the mechanical power generated by the main engine plant or indirectly after conversion to electric energy. In this last case, electrical needs of the vessel can be expressed as:

$$W_e(V_s) = W_{e,p}(V_s) + W_{e,ep}(V_s)$$

where $W_{e,p}(V_s)$ is the electrical power demand for propulsion (usually proportional to the cube of the service speed) and $W_{e,ep}(V_s)$ represents the requirements of the additional electric loads (i.e., the electric loads except of propulsion). Considering the maximum electrical power that can be made available by the generation plant when all the diesel generators are in operation at the condition of 100% load (equal to 33000 kW) the maximum speed of the carrier in each case is:

$V_{s,laden}$ = 20.45 kn

$V_{s,ballast}$ = 20.75 kn

The results for various speed values are reported in Table2.**Error! Reference source not found.**4 for the laden and ballast voyage.

Table 2.4 Electrical needs of the ship, laden (left) and ballast (right) voyage [29]

V_s	$\dot{W}_{e,p}$	$\dot{W}_{e,ep}$	$\dot{W}_{e,laden}$
kn	kW	kW	kW
8	1848	1300	3148
10	3609	1300	4909
12	6237	1300	7537

V_s	$\dot{W}_{e,p}$	$\dot{W}_{e,ep}$	$\dot{W}_{e,ballast}$
kn	kW	kW	kW
8	1756	1170	2926
10	3429	1170	4599
12	5925	1170	7095

14	9904	1300	11204
16	14784	1300	16084
18	21050	1419	22469
20	28875	1581	30456

14	9409	1170	10579
16	14045	1170	15215
18	19998	1277	21275
20	27432	1423	28855

The operating profile of a vessel is a document which describes numerically how the vessel is operated during the year. The operating profile of the present LNG carrier considers three operating modes: “laden voyage”, “ballast voyage” and “staying in port”. Figure 2.4 presents the percentage of the time and the number of hours of the operation in each mode. During the “staying in port” only an engine-generator set is usually kept into operation and the result is low waste heat availability.

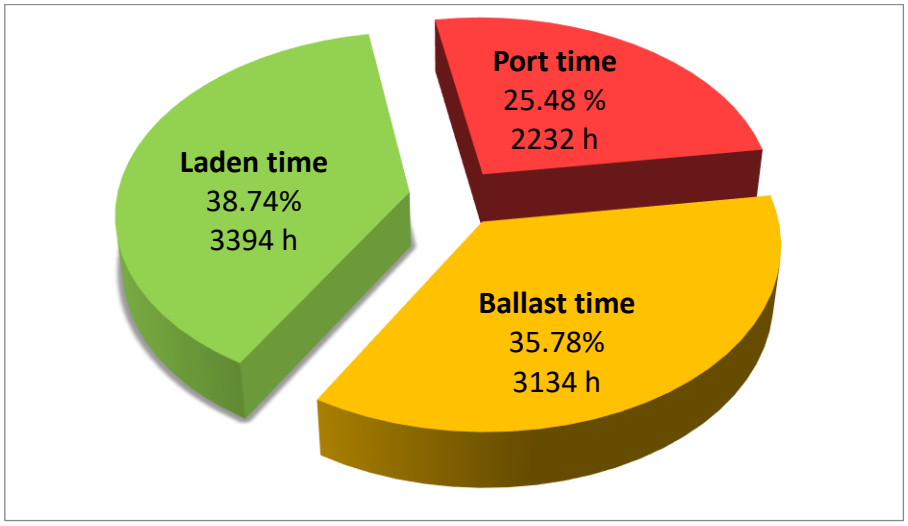

Fig 2.4 Operating modes of the current ship [29]

The vessel speed distribution profile is provided for laden and ballast modes. The overall range of the service speed (from 0 kn to 21 kn) is divided into 21 intervals of 1 kn, and for each of them, the number of hours is given as a percentage of total time in the mode; the number of hours of each interval is attributed to its average speed. The profile is presented in Fig. 2.5,**Error! Reference source not found.** where values for the service speed below 6 kn are not considered. The two percentages that are reported for each interval are referred to the laden and ballast modes, respectively. Note that most of the time the speed of the vessel is lower than the maximum value. Thus, the vessel sails in “slow steaming” mode: a lower service speed

leads to a significant reduction in power for propulsion reducing at the same time the fuel consumption.

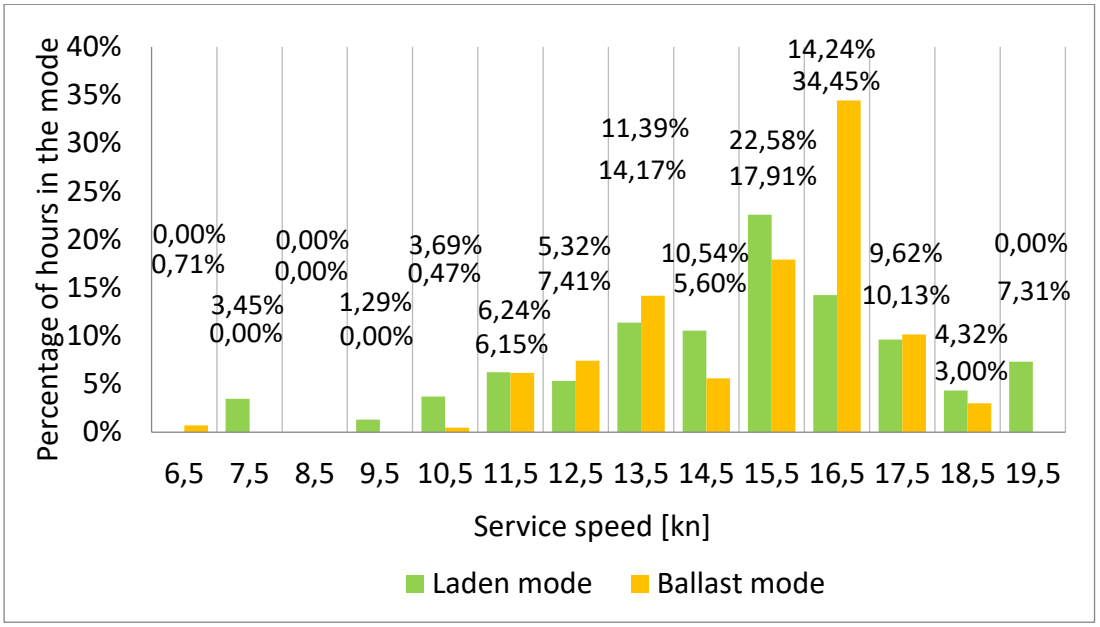

Fig. 2.5 Distribution profile of the vessel speed at laden and ballast voyage. The percentages are referred to the hours in laden and ballast modes, respectively. [29]

Soffiato [7, 29] during his study made two assumptions in order to overcome the missing information and calculate all the necessary data: the electrical power is generated by the lowest possible number of engine-generator sets, and tried to operate them at a load that is closed to the maximum efficiency; the second assumption considers that the total electric load is distributed to the operating generators in proportion to their nominal power.

Table 2.5 shows the electrical power that has to be generated, in case of laden voyage. For each condition, the engines that are kept in operation are presented and the corresponding power production is reported in accordance with the two aforementioned assumptions. The load of the engines is reported as well. Table 2.6 Table 2.provides similar information relating to the case of ballast voyage.

Table 2.5 Operating profile of the engines, laden voyage [29]

No.	Average speed	Hours	Hours	W_e	12V50DF No.1	6L50DF No. 2	6L50DF No. 3	12V50DF No.4	Load
-	kn	%	-	kW	kW	kW	kW	kW	%
1	7.5	3.5	117.1	2823	0	0	2823	0	51
2	8.5	0.0	0.0	3517	-	-	-	-	-
3	9.5	1.3	43.8	4395	0	0	4395	0	80
4	10.5	3.7	125.2	5478	0	0	5478	0	100
5	11.5	6.2	211.8	6789	0	0	0	6789	62
6	12.5	5.3	180.6	8350	0	0	0	8350	76
7	13.5	11.4	386.6	10180	0	0	0	10180	93
8	14.5	10.5	357.7	12304	0	0	4101	8202	75
9	15.5	22.6	766.4	14741	0	0	4914	9827	89
10	16.5	14.2	483.3	17514	0	4378	4378	8757	80
11	17.5	9.6	326.5	20711	0	5178	5178	10355	94
12	18.5	4.3	146.6	24315	9726	0	4863	9726	88
13	19.5	7.3	248.1	28302	9434	4717	4717	9434	86

Table 2.6 Operating profile of the engines, ballast voyage [29]

No.	Average speed	Hours	Hours	W_e	12V50DF No.1	6L50DF No. 2	6L50DF No. 3	12V50DF No.4	Load
-	kn	%	-	kW	kW	kW	kW	kW	%
14	6.5	0.7	22.3	2112	0	0	2112	0	38
15	7.5	0.0	0.0	2617	-	-	-	-	-
16	8.5	0.0	0.0	3276	-	-	-	-	-
17	9.5	0.0	0.0	4110	-	-	-	-	-
18	10.5	0.5	14.7	5139	0	0	5139	0	93
19	11.5	6.2	192.8	6385	0	0	0	6385	58
20	12.5	7.4	232.3	7867	0	0	0	7867	72

21	13.5	14.2	444.1	9607	0	0	0	9607	87
22	14.5	5.6	175.5	11624	0	0	3875	7749	70
23	15.5	17.9	561.4	13939	0	0	4646	9293	84
24	16.5	34.5	1079.8	16573	8287	0	0	8287	75
25	17.5	10.1	317.5	19607	9804	0	0	9804	89
26	18.5	3.0	94.0	23027	9211	0	4605	9211	84

2.2 Previous study ORC configurations

With the current data Soffiato [29] considered that the ORC will be designed for the operating point that is presented in Table 2.6. Three engines are in operation while the engine No.2 is turned off. The load of the working engines is equal to 85%. The choice takes into consideration the observations on the speed distribution profile of the vessel that have been presented.

Table 2.7 Operating point for the engines [29]

W_e	12V50DF No.1	6L50DF No. 2	6L50DF No. 3	12V50DF No.4	Load
kW	kW	kW	kW	kW	%
23375	9350	0	4675	9350	85

The choice allows the calculation of the thermal flows that are rejected to the engines cooling systems. The quality of the heat (in terms of temperature) that is possible to exploit coupling an ORC system with the cooling systems depends on their configuration. Soffiato considered three different layouts of coupling the ORC with the engines, utilizing many hot streams. In the current study not all of them are going to be utilized as this involves the design of many different components which excides the point of the current study.

In the first case of Soffiato, the ORC system absorbs heat from the cooling flows of the engines cooling circuits and no modification in the layout of the cooling systems is introduced. Fig 2.6 presents this first cooling system configuration showing the coupling with the ORC system and the FWG. Two thermal sources are available from each engine-generator set that is considered as operating in accordance with the

choice of the operating point. The ORC system absorbs heat from the water flows of the HT and LT circuits at the point *HE1* and *HE2*, respectively. *HE1* and *HE2* are defined as positions where heat can be transferred. The data after the calculations for the available heat for extraction are presented in Table 2.7

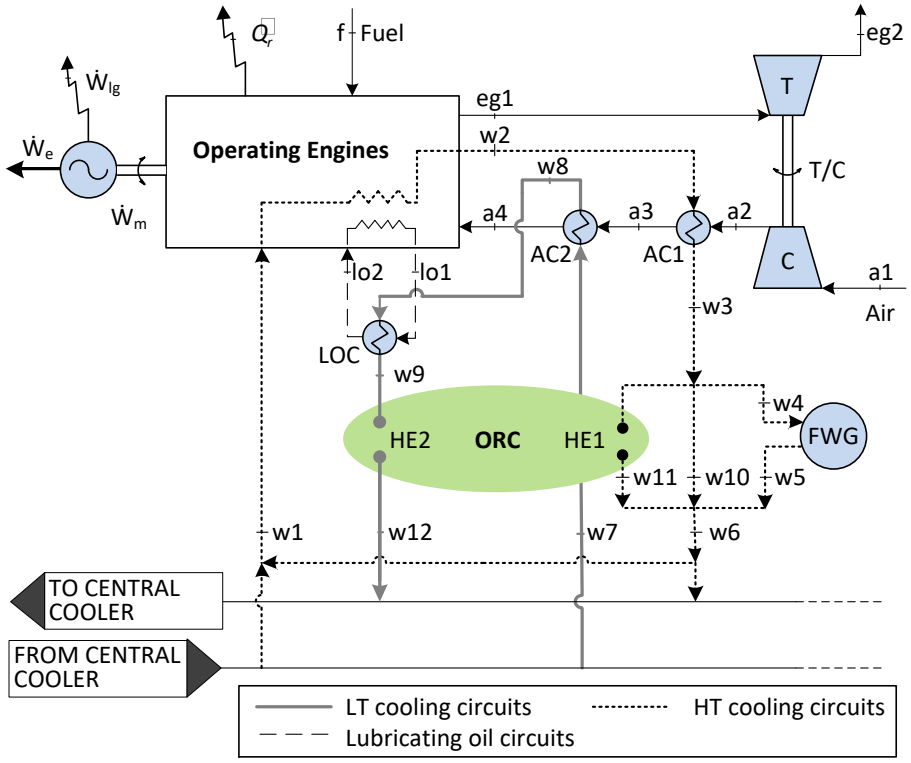

Fig. 2.6 Configuration of the cooling systems and coupling with the ORC, first case [29]

Table 2.8 Calculation of various parameters, first configuration [29]

Parameter	Unit	Value
T_{w3}	°C	82.8
T_{w1}	°C	76.3
T_{w7}	°C	36.0
T_{w9}	°C	51.9
$\dot{m}_{w4}$	Kg/s	21.67
$\dot{m}_{w1}$	Kg/s	229.0
$\dot{m}_{w10}$	Kg/s	10.97
$\dot{m}_{w11}$	Kg/s	196.36
$\dot{m}_{w7}$	Kg/s	66.5

In the second case, Soffiatio investigates the possibility to split the LT cooling circuits into two parts as shown in Fig2.7. This allows a direct heat transfer between lubricating oil and organic fluid of the ORC system at the point *HE3*. The water flows heated by the charge air in the heat exchanger *AC2* are also considered as thermal sources even if the quality of the heat associated with is low. These flows transfer heat to the ORC system at the point *HE2*. Water flows belonging to the HT circuits represent the third thermal source for the ORC system (*HE1*). The data after the calculations for the available heat for extraction are presented in Table 2.8

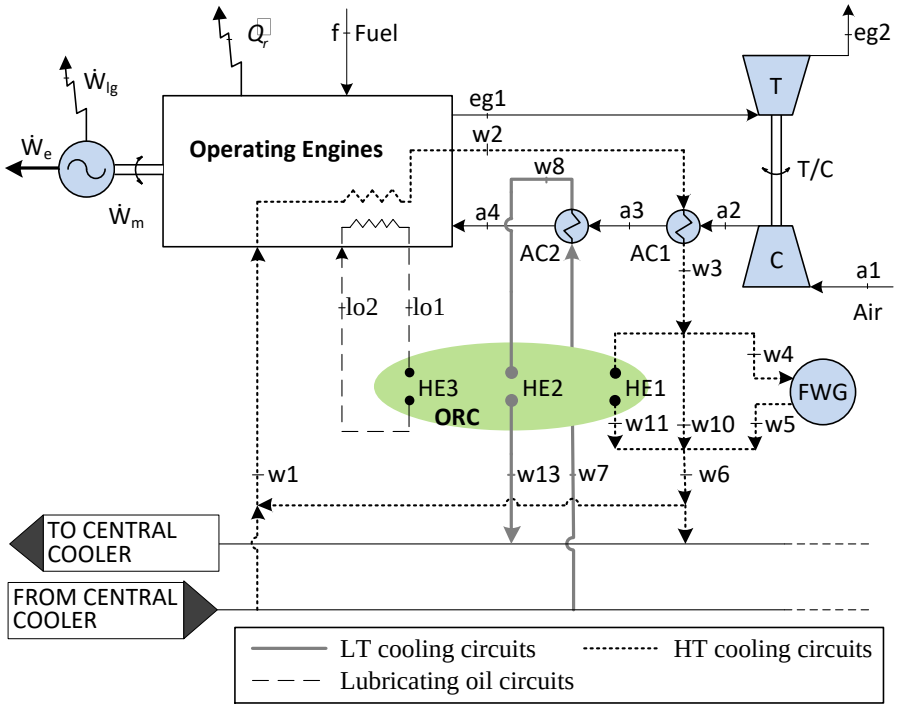

Fig. 2.7 Configuration of the cooling systems and coupling with the ORC, second case [29]

Table 2.9 Calculation of various parameters, second configuration [29]

Parameter	Unit	Value
T_{w3}	°C	82.8
T_{w1}	°C	76.3
T_{w7}	°C	36.0
T_{w8}	°C	43.1
T_{lo1}	°C	75.3
T_{lo2}	°C	61
$\dot{m}_{w11}$	Kg/s	196.36

$\dot{m}_{w7}$	Kg/s	66.5
$\dot{m}_{lo}$	Kg/s	90.5

The third study case considers the possibility of proposing a new design for the engines cooling systems in order to better exploit the quality of the rejected heat. According with this new design presented in Fig. 2.7 Fig, thermal sources for the ORC are the jacket water, the lubricating oil and the charge air that has to be cooled after the compressor of the T/C. This layout allows the higher heat extraction to be performed. The temperature of the air at the beginning of the cooling (state *a2*) is relatively high so that the removal of the intermediate heat transfer with the HT cooling flows allows the occurring irreversibility to be reduced significantly. As it is shown in the figure, the water flow resulting from the mixing of the jacket flows is split into three flows: one of them is heated by the air and then feeds the FWG, another one is exploited by the ORC system and the third one is bypassed in order to keep the temperature at the state *w6* at an appropriate value. In Table 2.8 the results of the study are presented

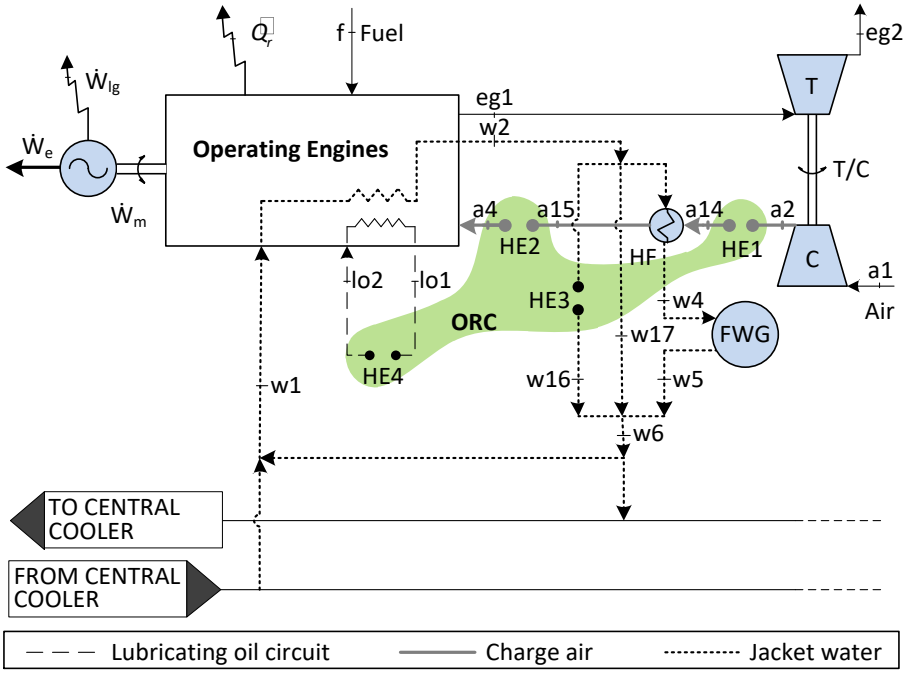

Fig. 2.8 Configuration of the cooling system and the heat sources of the ORC, third case [29]

Table 2.10 Calculation of various parameters, second configuration [29]

Parameter	Unit	Value
T_{a2}	°C	169.75
T_{a4}	°C	44.15
T_{w2}	°C	79.66
T_{w1}	°C	76.3
$\dot{m}_{w16}$	kg/s	186.05
$\dot{m}_{w17}$	kg/s	21.29
$\dot{m}_{a}$	kg/s	39.12

2.3 Current study ORC configurations

In the current study some of the hot sources shown above are chosen in order to utilize and produce electrical power. Three different case are studied. For these, also the configurations of the system are changed. The fresh water generator in all cases is coupled with the hot oil stream, as there is enough energy and high temperature for its operation. The first configuration refers in utilizing the jacket water and supercharge air by a one evaporation pressure level ORC. The second utilizes both jacket water and supercharge air by two different subcritical evaporation pressure. The third utilizes both jacket water and supercharge air by two different evaporation pressure levels, one subcritical and one supercritical, as proposed in the second layout. The cases are presented below, showing the coupling of the cooling system with the heat exchangers of the ORC, the ORC layout, the design point values of the hot steams and the constrains in temperature.

1) Only jacket water's heat is utilized, one subcritical pressure level

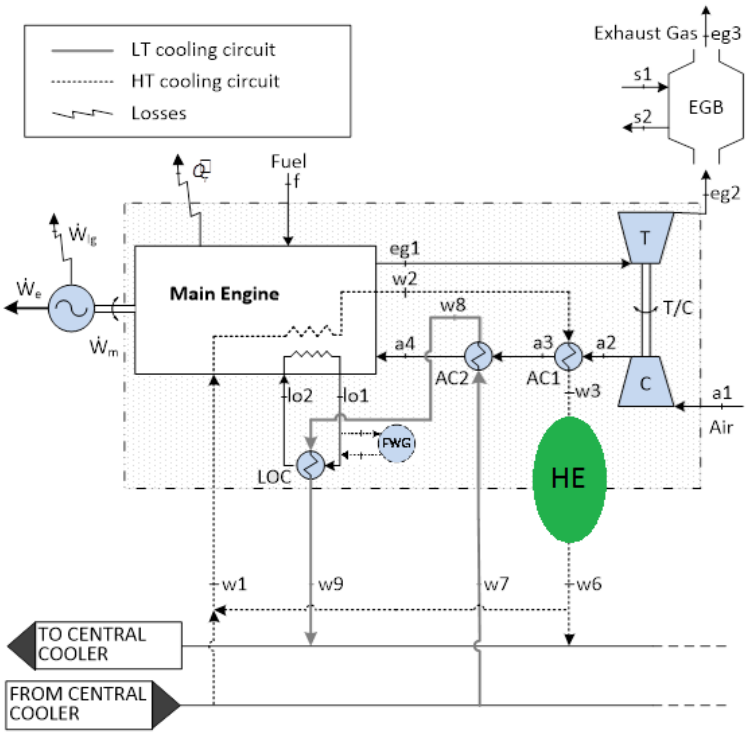

Fig. 2.9 Configuration of the cooling system and the heat sources of the ORC for case 1

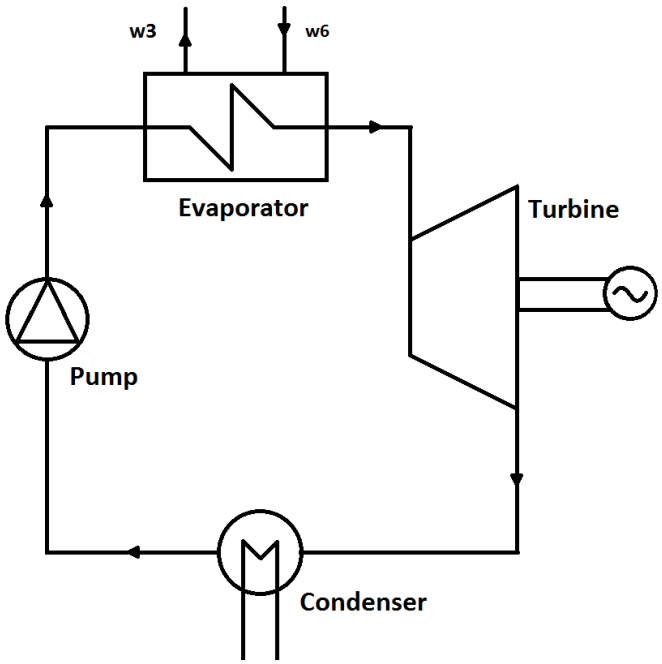

Fig. 2.10 Schematic of first ORC system

Table 2.11 Calculation of various parameters, first case

Parameter	Unit	Value
T_{w3}	°C	83
$T_{w6\ min}$	°C	76.3
$\dot{m}_{w1}$	Kg/s	229.1

2) Both jacket water's and supercharged air heat are utilized, two subcritical pressure levels exist

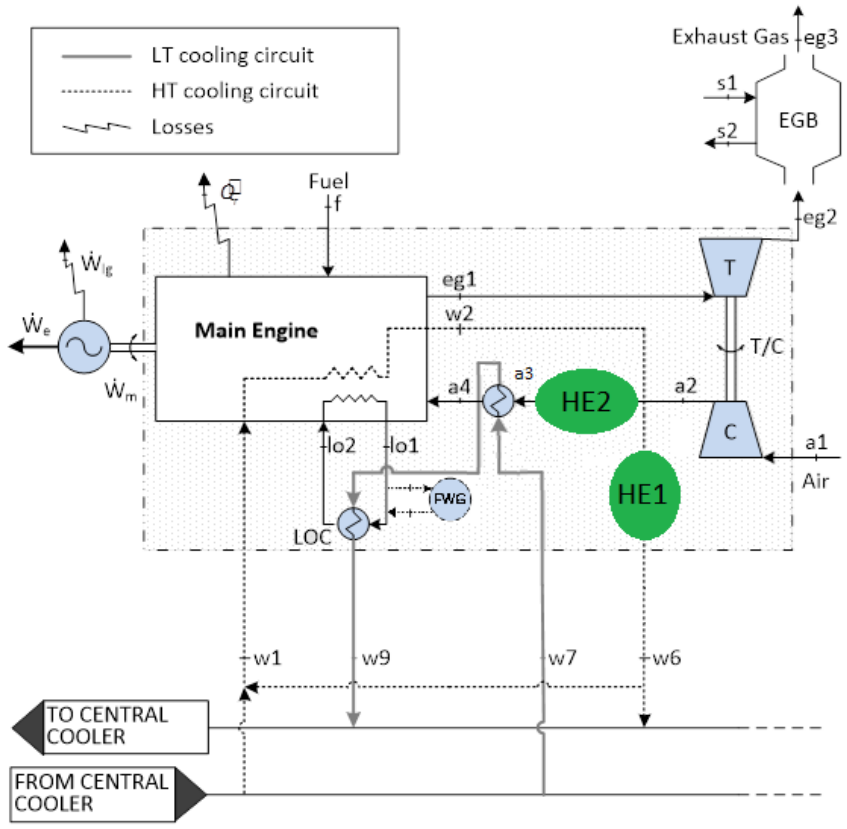

Fig. 2.11 Configuration of the cooling system and the heat sources of the ORC for case 2

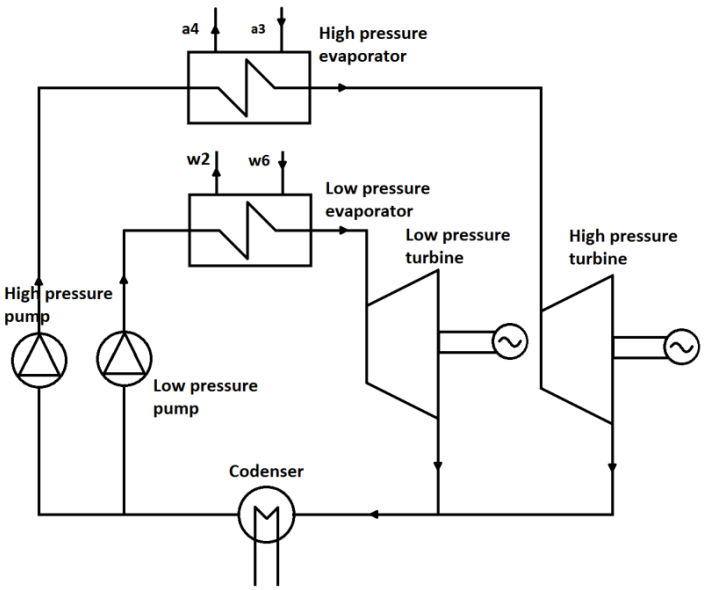

Fig. 2.12 Schematic of second ORC system

Table 2.12 Calculation of various parameters, second case

Parameter	Unit	Value
T_{w2}	°C	79.2
T_{w6}	°C	76.3
$\dot{m}_{w1}$	Kg/s	229.1
T_{a2}	°C	177.0
$T_{a3,min}$	°C	44.2
$\dot{m}_{a2}$	Kg/s	41.6

3) Both jacket water's and supercharged air heat are utilized, one subcritical and one supercritical pressure levels exist. The configuration is the same as to case number

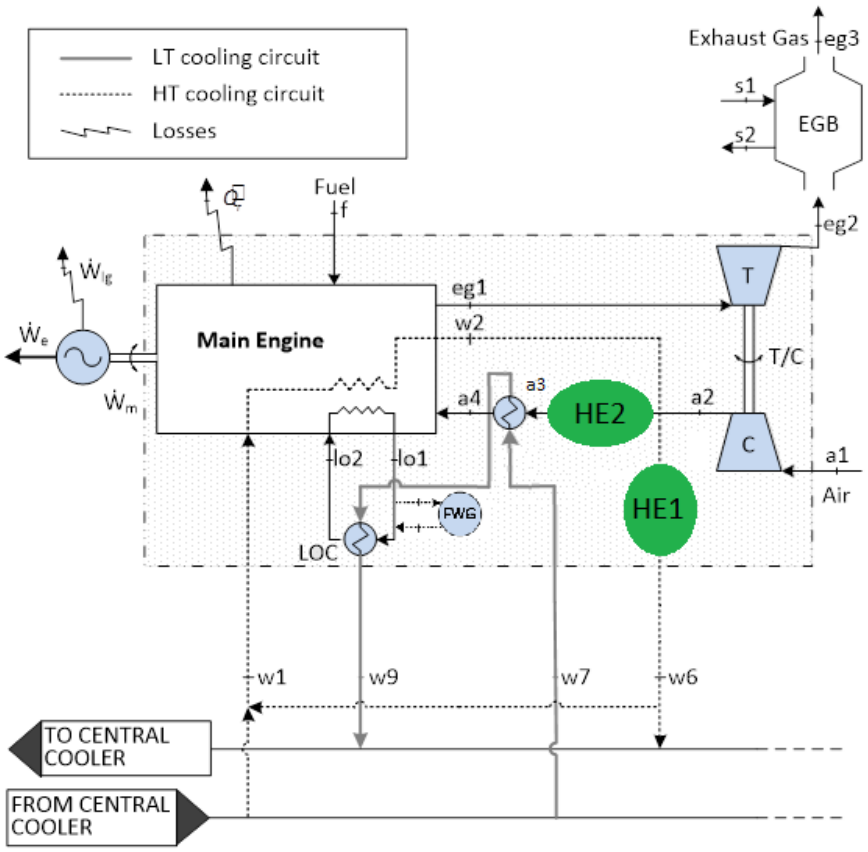

Fig. 2.13 Configuration of the cooling system and the heat sources of the ORC for case 3

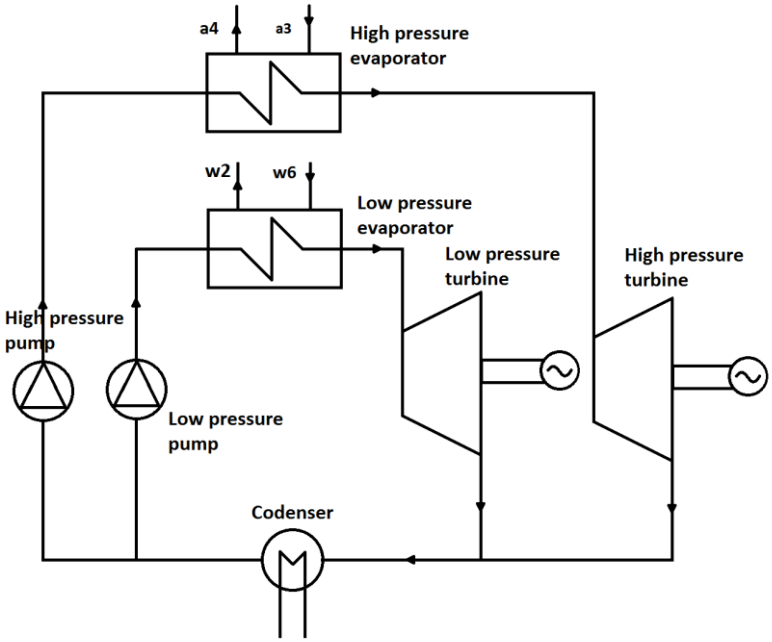

Fig. 2.14 Schematic of third ORC system

Table 2.13 Calculation of various parameters, third case

Parameter	Unit	Value
T_{w2}	°C	79.2
$T_{w6,min}$	°C	76.3
$\dot{m}_{w1}$	Kg/s	229.1
T_{a2}	°C	177.0
$T_{a3,min}$	°C	44.2
$\dot{m}_{a2}$	Kg/s	41.6

2.4 Conclusions

In this chapter the case study is presented. First the main engine is analyzed and then the operation profile of the ship is given. After, the possible configurations that were proposed on the previous study are presented. Then, from the analysis of the hot streams that was done by Soffiato three new cycles are proposed and studied, by changing the placement of the two fresh water generators and introducing new heat exchangers. These choices will lead to deferent results in comparison with the previous study, as not all possible hot sources are utilized. This is done because it is very difficult to construct dynamic models for such a complex system that contains many heat exchangers.

3.Methodology-Modelling approach

In this chapter the methodology that is followed and the modeling approach that is done are presented. Design point models, design of components, dynamic off-design models and control systems are created in this thesis. The design point models have as objective function to maximize the net power at the design point conditions. This is achieved by choosing properly the cycle parameters as pressure. After the determination of the design point, it is possible to calculate the components characteristics. The design of components includes essential data for the off-design dynamic models such as number of tubes in the shell-n-tube heat exchangers and operation maps of some components. The dynamic off design models are created in order to simulate the dynamic behavior of the system as the ship load changes. This has an impact on the hot sources that are utilized and as a result the operating point of the cycle changes. The control systems are developed to reassure that the ORC system is operating steadily and safely, which is critical on board a ship.

3.1 Methodology

In this subchapter he methodology that is followed in this study is presented. Two different kinds of models are developed in this thesis, design point and dynamic. The purpose of the two kinds of models is different and so, different methodologies are followed in order to create each model

3.1.1 Design point methodology and components' design

In this subchapter the way that the design point functions will be explained. Decision variables are the evaporation pressures for subcritical the cycle and both evaporation pressures and the entropy in the turbine inlet for the supercritical pressure level. The objective function is the maximization of the power output. The condensation pressure is not a decision variable as it is maintained as low as possible. Each hot source from the engine corresponds to a different pressure level and all the different pressure level ORC's streams end after the expansion in the same low pressure level where condensation takes place. Input data for the model are the inlet temperature and mass flow rate of hot sources, the inlet temperature of the cold sink, the values of the Pinch Point temperature differences and the minimum exit temperature of the hot source. This allows the mass flow rates of ORC and cooling water of the ORC to be calculated through the heat balance. Superheating and subcooling are included even though they decrease the performance, as they guarantee safe operation for the components. The Design model also designs the type

E shell-tube heat exchangers. Approximations that are done is the efficiency of the pumps are 0.7 and for high pressure turbines 0.75 respectively. For low pressure turbines a correlation from the literature is used to predict the efficiency. No pressure drops are taken into account in this study.

3.1.2 Dynamic models methodology

In this subchapter the way that the off-design model functions will be explained. The model has to simulate the dynamic behavior of a thermodynamic cycle. A thermodynamic cycle is a series thermodynamic transformations in order to absorb or to produce energy. The system is preferred to reach equilibrium conditions although it usually operates under transient ones. In real systems the pressure and temperature reach equilibrium conditions due to the existence of components that are having the function of a capacity. Capacity function means the ability keep pressure and temperature relatively constant by mass and energy storage. In real systems other components exist also, mass flow control components, that allow the communications between capacities by mass transfer.

A thermodynamic cycle is carried out by components which perform thermodynamic changes as stated. They are asked to increase or decrease enthalpy in order to perform the desired changes. Components that increase the enthalpy are pumps, heat exchangers, combustion chambers etc. components that decrease the enthalpy are turbines, heat exchangers, valves etc. we make a distinction between components that change enthalpy through work transfer and components that change enthalpy through heat transfer. The formal fixes the mass flow rate passing through them, given the values of pressure at inlet and outlet. These values are imposed by the capacities, which are at the inlet and outlet of the components respectively.

Every component is modeled as individual block or blocks receiving input variables and calculating the output variables which feed other blocks respectively. This makes the overall system very flexible, as it is easy to replace a component without changing the rest of the model. Thermo-fluid systems can be described by two types of variables as Vaja [13] indicates. These are:

Level variables: in general, they are differential variables provided by fundamental equations (exp. mass balance equation) that indicate the magnitude of thermodynamic properties stored inside a component (exp. pressure). They are an expression of state variables in state determined systems.

Flow variables: they usually refer to fluxes of extensive properties through boundary surfaces or components and can be considered as outputs of not state determined systems (exp. mass flow rate).

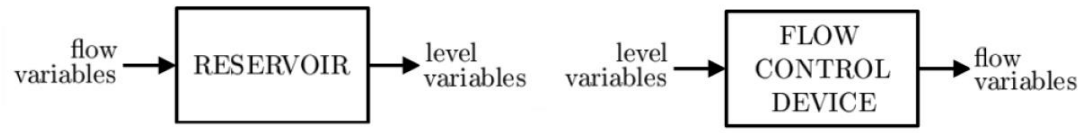

Fig 3.1.1 Schematic of the connections of reservoirs-flow control components [13]

The simulation starts from the design point that all variables values are known and then calculates the systems behavior by solving the equations that characterize it. The model is consisted by three types of blocks as is proposed by Mazzi et. al. [12], flow control components, capacities and heat transfer blocks. In the current study the volumes of each different phase area are calculated by the heat exchanger block and the capacity only solves the heat and mass balance equation, as will be explained below.

Flow control blocks: they receive level variables as input variables and have in general flow variables as outputs. Their behavior is characterized by the characteristic curves (operation maps). In the current study the flow control components that are used more specifically receive as inputs the inlet enthalpy and pressure, the outlet pressure and rotational speed and calculate the mass flow rate that runs through them and the outlet enthalpy (or enthalpy flow rate).

Capacities/Reservoirs blocks: They act as storage tank, storing mass and energy. They receive as input variables both level variables and flow variables and calculate as output only level variables. In this study the capacities that are used have as inputs the inlet and outlet mass flow rate, inlet enthalpy, the heat that is transferred to them and the volume of the various phases of the organic fluid inside them. They have as outputs the pressure change and outlet enthalpy change. By feeding them with the initial pressure and outlet enthalpy they calculate the pressure and enthalpy values throughout the simulation.

Heat transfer block: They are like flow control components but they are fed also by flow variables. They receive as input variables but the mass flow rate of both the organic fluid and the hot (or cold) heat sources. They calculate the heat that is transfers to the organic fluid and the volumes of each different phase inside (superheating area or two phase area for example).

Between two flow control components there is a capacity/reservoir and between two capacities there is a flow component so that they feed each other respectively. After connecting all the blocks together, a loop is created that keeps

feeding its blocks as simulation time progresses, representing the overall systems behavior in the end. This is shown in the next figure.

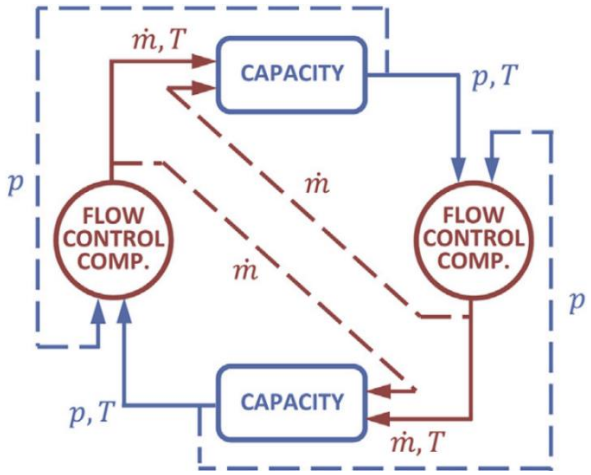

Fig 3.1.2 Connections between capacities and flow control components [12]

In the present work the components of the cycle are modeled as following:

Centrifugal one stage Pump: flow control component

Axial one stage turbine: flow control component

Subcritical Evaporator: capacity coupled with a heat exchanger

Supercritical Evaporator: capacity coupled with a heat exchanger

Condenser: capacity coupled with a heat exchanger

After the connection of the components the feed each other respectively throughout the simulation as the figure indicates

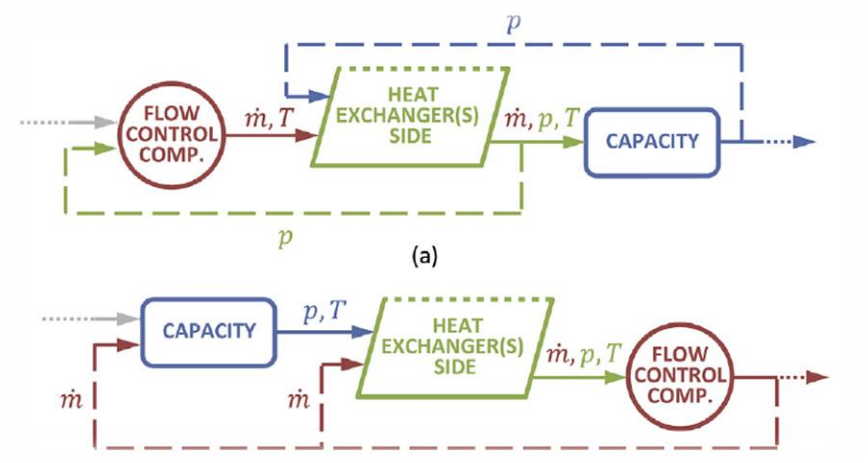

Fig 3.1.3 Correct connection of the different types of blocks [12]

It is important to clarify that the arrows represent signals and not mass flow between the components. They are used to show the block which calculates each variable (having the same color) and the inputs that each individual block needs (arrow point at them). The model with the one evaporation temperature is presented as example below in order to make the way the connections function clearer. In the single stage ORC, the pump is followed by the evaporator, meaning one heat exchanger block and one capacity block. The evaporator is followed by the turbine, which expands till the pressure of the condenser that follows. In the end the pump is pumping fluid from the condenser to the evaporator and the cycle is completed.

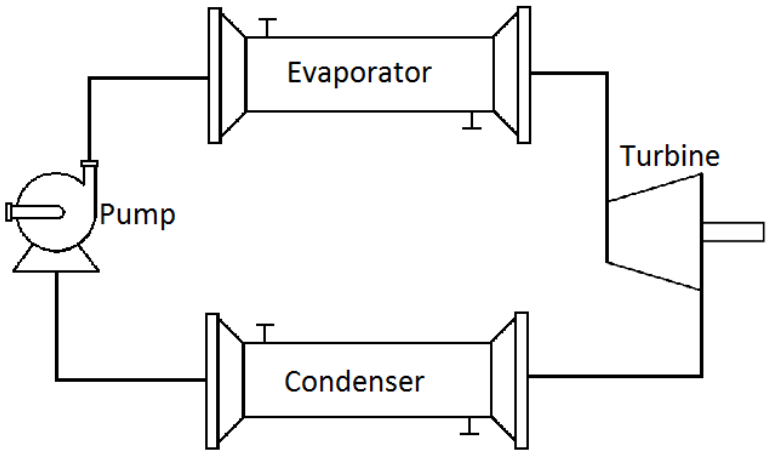

Fig 3.1.4 First case ORC, one evaporation pressure level

Now the signal flow will be explained. The signal flow is different from the mass flow and is presented in the following figure. The color shows which block calculates the signal. The arrows represent the block which is feed by the specific signal. For example, the pump calculates the mass flow rate and enthalpy outlet as a flow control component and it is feed by the pressure in its inlet an outlet (calculated by the capacities) and the enthalpy inlet.

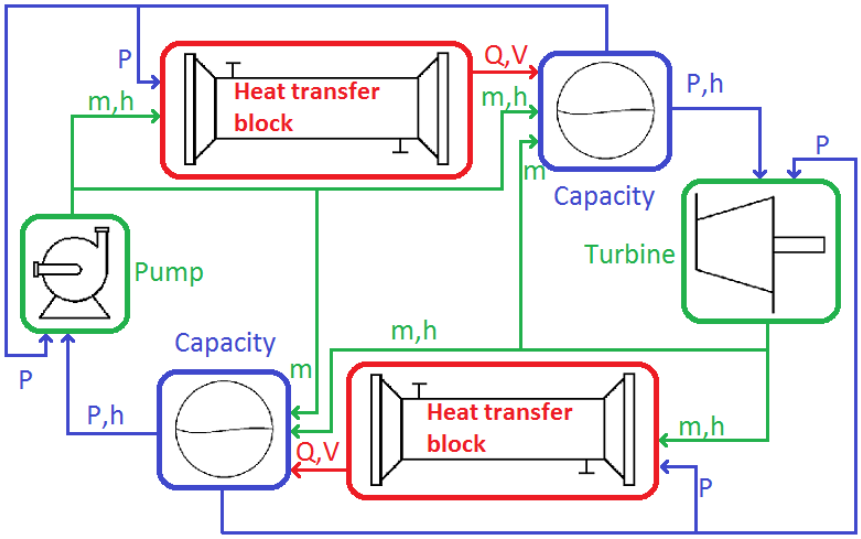

Fig 3.1.5 Schematic of the signals of the first case ORC

The same approach is used and to the two other cases that are studied respectively for each pressure level.

3.1.3 Control strategy

The safety of the process and the high efficiency are necessary to be guaranteed in every application. To this end, a proper control strategy must be developed according to the specific needs of each application. It is obvious that the liquid level inside the heat exchangers cannot be measured easily, as is done inside the drums in water-steam Rankine cycles, because it is located in the tube side and the ship oscillations. The pump needs to receive subcooled liquid in order to avoid cavitation and the turbine needs to be fed at least with saturated vapor in order to avoid corrosion in its blades in most cases. In the current one, the ship oscillations make superheating a necessary safety factor against liquid drops. The control strategy proposed in this thesis is to measure the superheating of the subcritical evaporators

and the subcooling of the condenser and alter the pump's rotational speed and the mass flow rate of cooling water respectively. For the supercritical evaporator in the third case studied, as measured variable is proposed the entropy instead of the superheating. The measurement of the values of the control variables can be calculated by a software which receives the measured temperature and pressure. To change the pump's rotational speed and the mass flow rate of the cold water PI controllers can be used as is also proposed by Quoilin [10]. The reasons for this choice are:

1) PI controllers will not amplify the noise that exists on ships
2) Will result a steady state error of zero with the time of inputs that the system has
3) There is no need for a fast response as changes are slow in these systems

For the above reasons the PI controller is thought to be the proper one. The gains of the system are chosen according to the needs of the system through multiple simulations. In the next figure a schematic of the control strategy for the subcritical evaporators, the supercritical evaporators and the condensers is shown.

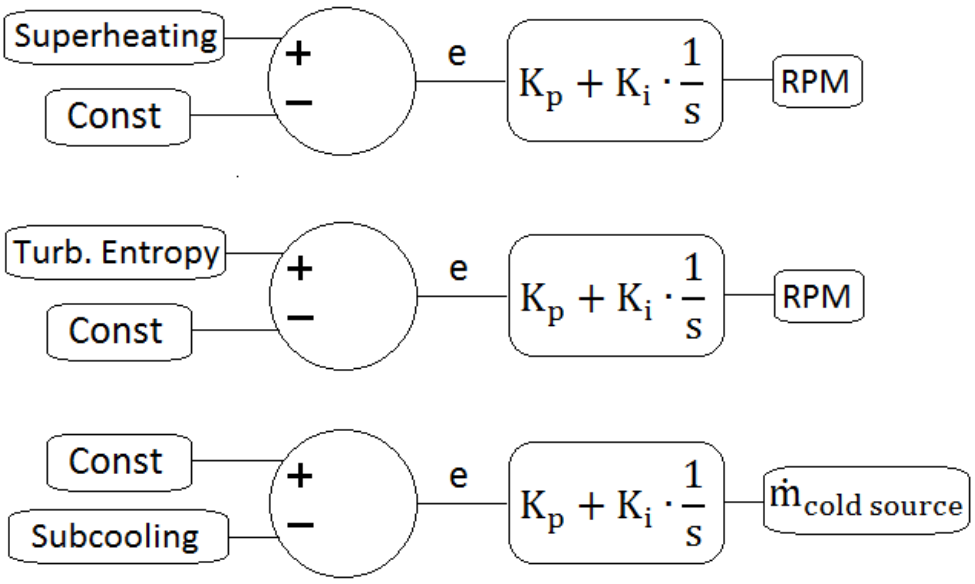

Fig. 3.1.6. Control strategies

3.2 Design models of the cycles

The way the design point models function is explained in the subchapter. There are three different cycles studied in this thesis. A different design point model is created for each cycle, as to obtain the maximum power output in each case.

3.2.1 One pressure level subcritical cycle

The way the one pressure level design point model functions is explained in the subchapter. As stated above, decision variable is only the evaporation pressure (P_{evap}) of the cycle and not condensation pressure (P_{cond}) as it affects the cycle's efficiency always in the same way. Input data are the organic fluid, the inlet temperature and mass flow rate of heat source, the inlet temperature of the cold sink, and the values of the Pinch Point temperature differences (ΔT_{pp}) which are equal to 10 °C. The approximations that are done is the efficiency of the pump is 0.7 and not taking account of the pressure drops. Also an important feature taken into account is the return temperature of the hot source in the jacket. Turbines efficiency is calculated by a correlation of Luca Da Lio et. al. [23]. The correlation uses as input the fluid's critical temperature (T_{cr}), the expansion ratio (VR) and size parameter (SP). The literature defines them as:

$$VR = \frac{\rho_{in}}{\rho_{out}} \qquad SP = \frac{\dot{m}^{0.5}}{{\rho_{out}}^{0.5} \cdot (h_{in} - h_{out})^{0.25}}$$

After all the parameters needed are defined the calculation starts. The models start the calculation from choosing the maximum available evaporation pressure. This can be defined either by the critical pressure of the fluid or by the hot source if it's temperature is lower than the critical temperature plus the superheating. The optimum evaporation pressure is between the maximum one and the condensation pressure.

$$\eta_{total} = f(P_{evap})$$

$$P_{evap,max} = \min\left[P_{crit}, P_{sat}\left(T_{hot} - \Delta T_{sup}\right)\right]$$

$$P_{evap,max} < P_{evap,opt} < P_{cond}$$

$$T_{hot,out} > T_{hot,out,min}$$

A loop solves the problem for every pressure. After this all the cycle's points are known for this pressure except the point after the expansion as it needs the expanders efficiency, which calculated by the correlation of Da Lio et. al. [23]. The correlation gives the turbine's efficiency by knowing the fluid's critical temperature T_{cr}, the expansion ratio VR and size parameter SP, so the correlation needs both the inlet and output conditions of the turbine in order to calculate the efficiency.

$$n_{t,is} = f(T_{cr}, VP, SP)$$

To solve the problem another loop is added which is starting by an initial value of 0.75 and calculates all the cycle points. Then a first value of the $n_{t,is}$ is obtained and is used in the next loop. When the $n_{t,is}$ converges all the cycle point are known and by energy balance equations in the pinch point both the ORC mass flow and the cold water's mass flow are obtained. The power now can be easily calculated. Also the thermal efficiency, heat recovery factor and total efficiency are calculated:

$$W_{net} = W_t - W_p$$

$$\eta_{thermal} = \frac{W_{net}}{\dot{Q}_{in}}$$

$$\varphi = \frac{\dot{Q}_{in}}{\dot{m_{hot}} \cdot (T_{hot} - T_{cold})}$$

$$\eta_{total} = \eta_{thermal} \cdot \varphi$$

The same procedure is followed for all the possible evaporation pressures by the external loop. After that, the optimum pressure is obtained and all the points of the cycle are recalculated for this pressure. The useful results are being obtained in the end.

N° of variables: 42

$VP, SP, T_{cr}, n_{t,is}, n_{p,is}, W_{net}, W_t, W_p, P_{evap,opt}, T_{hot,in}, T_{hot,out}$, $\dot{m}_{hot}, Cp_{hot}, T_{cold,in}, \dot{m}_{cold}, Cp_{cold}, T_{cold,out}, P_{cond}, \Delta T_{sup}, \Delta T_{sub}, \Delta T_{pp}$, wf, $\dot{m}_{wf}, \eta_{total}, \eta_{thermal}$, ϕ, $\sum_{i=1}^{8} T_i$, $\sum_{i=1}^{8} s_i$

N° of dependent variables: 33

$VP, SP, T_{cr}, n_{turb,is}, n_{pump,is}$, W, $W_{turb}, W_{pump}, P_{evap,opt}, \dot{m}_{cold}, P_{cond}, \dot{m}_{wf}, \eta_{total}, \eta_{thermal}, \eta_{HR}, T_{hot,out}, T_{cold,out}, \sum_{i=1}^{8} T_i$, $\sum_{i=1}^{8} s_i$

N° of independent variables: 6

$T_{hot,in}, \dot{m}_{hot}, Cp_{hot}, Cp_{cold}, T_{cold,in}$, wf

N° of fixed variables: 4

$\Delta T_{sup}, \Delta T_{sub}, \Delta T_{pp}, n_{p,is}$

N° of output variables: 29

$n_{t,is}, W_{net}, W_t, W_p, P_{evap,opt}, \dot{m}_{cold}, P_{cond}, \dot{m}_{wf}, \eta_{total}, \eta_{thermal}$, ϕ, $T_{hot,out}, T_{cold,out}, \sum_{i=1}^{8} T_i$, $\sum_{i=1}^{8} s_i$

A flow chart of this program is presented below in order to make these steps clearer:

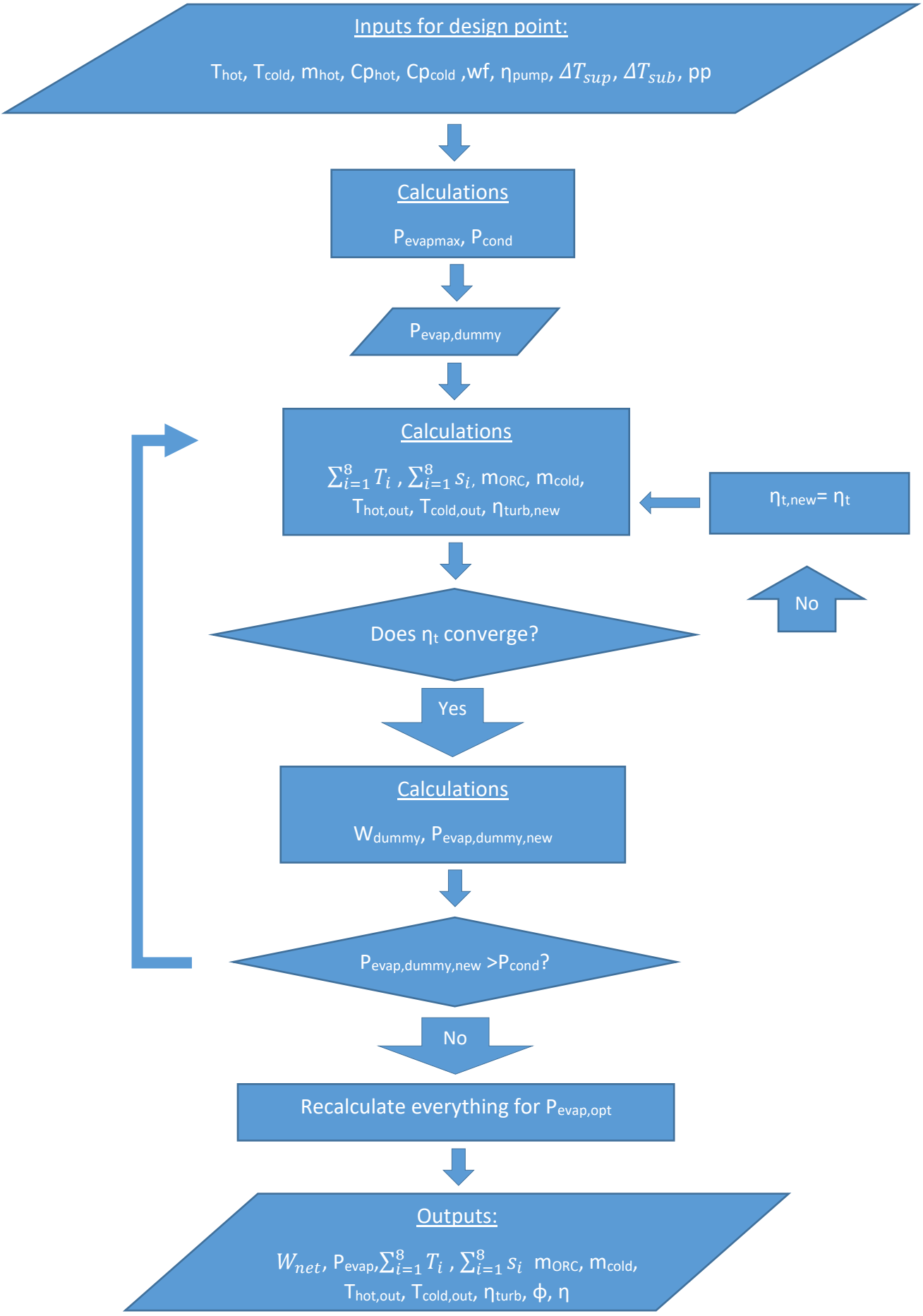
Inputs for design point:
T_{hot}, T_{cold}, m_{hot}, Cp_{hot}, Cp_{cold} ,wf, η_{pump}, ΔT_{sup}, ΔT_{sub}, pp
Calculations
$P_{evapmax}$, P_{cond}
$P_{evap,dummy}$
Calculations
$\sum_{i=1}^{8} T_i$, $\sum_{i=1}^{8} s_i$, m_{ORC}, m_{cold}, $T_{hot,out}$, $T_{cold,out}$, $\eta_{turb,new}$
$\eta_{t,new}= \eta_t$
No
Does η_t converge?
Yes
Calculations
W_{dummy}, $P_{evap,dummy,new}$
$P_{evap,dummy,new} > P_{cond}$?
No
Recalculate everything for $P_{evap,opt}$
Outputs:
W_{net}, P_{evap},$\sum_{i=1}^{8} T_i$, $\sum_{i=1}^{8} s_i$ m_{ORC}, m_{cold}, $T_{hot,out}$, $T_{cold,out}$, η_{turb}, ϕ, η

3.2.2 Two pressure level subcritical cycle

In the case of the two evaporation pressure levels the principles that have been followed are the same as in the one pressure level. Again there is a small subcooling in the evaporator and a small superheating in both the evaporators. The correlation that was used to calculate the turbine's efficiency is used only in the lower pressure turbine as the higher pressure turbine operates out of the range of the correlation. Also now the ΔT_{pp} is equal to 10K for the LP evaporator and the condenser, while it is 20K for the HP evaporator due to the big size that the heat exchanger has otherwise. A constrain for the outlet temperatures of hot sources exists here as well. An efficiency equal to 0.75 is supposed for this reason. Each pressure level is optimized independently, as the condensation pressure is not a decision variable. In the end the characteristics of the cycle for the optimum pressures are obtained.

$$\eta_{total} = f(P_{evap,LP}, P_{evap,HP})$$

$$P_{evap,LP,max} = \min\left[P_{crit}, P_{sat}\left(T_{hot,LP} - \Delta T_{sup,LP}\right)\right]$$

$$P_{evap,LP,max} < P_{evap,LP,opt} < P_{cond}$$

$$P_{evap,HP,max} = \min\left[P_{crit}, P_{sat}\left(T_{hot,HP} - \Delta T_{sup,HP}\right)\right]$$

$$P_{evap,HP,max} < P_{evap,HP,opt} < P_{cond}$$

$$T_{hot,out,LP} > T_{hot,out,LP,min}$$

$$T_{hot,out,HP} > T_{hot,out,HP,min}$$

N° of variables: 71

$VR_{LP}, SP_{LP}, T_{cr}, n_{t,HP,is}, n_{p,HP,is}, n_{t,LP,is}, n_{p,LP,is}, W_{net,HP}, W_{turb,HP}, W_{pump,HP}, P_{evap\ HP,opt}, T_{hot,HP,in}, T_{hot,HP,out}, \dot{m}_{hot,HP}, Cp_{hot,HP}, W_{net,LP}, W_{turb,LP}, W_{pump,LP}, P_{evap\ LP,opt}, T_{hot,LP,in}, T_{hot,LP,out}, \dot{m}_{hot,LP}, Cp_{hot,LP}, T_{cold,in}, \dot{m}_{cold}, Cp_{cold}, T_{cold,out}, P_{cond}, \Delta T_{sup,HP}, \Delta T_{sup,LP}, \Delta T_{sub}, \Delta T_{pp,LP}, \Delta T_{pp,HP}$, wf, $\dot{m}_{wf,HP}, \dot{m}_{wf,LP}, \eta_{total}, \eta_{total,HP}, \eta_{thermal,HP}, \varphi_{HP}, \eta_{total,LP}, \eta_{thermal,LP}, \varphi_{LP}\ \sum_{i=1}^{14} T_i, \sum_{i=1}^{14} s_i$

N° of dependent variables: 57

$VR_{LP}, SP_{LP}, T_{cr}, n_{t,HP,is}, n_{p,HP,is}, n_{t,LP,is}, n_{p,LP,is}, W_{net,HP}, W_{t,HP}, W_{p,HP}, P_{evap\ HP,opt}, T_{hot,HP,out}, W_{net,LP}, W_{t,LP}, W_{p,LP}, P_{evap\ LP,opt}, T_{hot,LP,out}, T_{cold,in}, \dot{m}_{cold}, T_{cold,out}, P_{cond}, \dot{m}_{wf,HP}, \dot{m}_{wf,LP}, \eta_{total}, \eta_{total,HP}, \eta_{thermal,HP}, \varphi_{HP}, \eta_{total,LP}, \eta_{thermal,LP}, \varphi_{LP}\ \sum_{i=1}^{14} T_i, \sum_{i=1}^{14} s_i$

N° of independent variables: 9

$T_{hot,HP,in}, \dot{m}_{hot,HP}, Cp_{hot,HP}, T_{hot,LP,in}, \dot{m}_{hot,LP}, Cp_{hot,LP}, T_{cold,in}, Cp_{cold}$, wf

N° of fixed variables: 8

$\Delta T_{sup,HP}, \Delta T_{sup,LP}, \Delta T_{sub}, \Delta T_{pp,LP}, \Delta T_{pp,HP}, n_{turbHP,is}, n_{pumpHP,is}, n_{pumpLP,is}$

N° of output variables: 51

$n_{t,LP,is}, W_{net,HP}, W_{t,HP}, W_{p,HP}, P_{evap\ HP,opt}, T_{hot,HP,out}, W_{net,LP}, W_{t,LP}, W_{p,LP}, P_{evap\ LP,opt}, T_{hot,LP,out}, T_{cold,in}, \dot{m}_{cold}, T_{cold,out}, P_{cond}, \dot{m}_{wf,HP}, \dot{m}_{wf,LP}, \eta_{total}, \eta_{total,HP}, \eta_{thermal,HP}, \varphi_{HP}, \eta_{total,LP}, \eta_{thermal,LP}, \varphi_{LP}\ \sum_{i=1}^{14} T_i, \sum_{i=1}^{14} s_i$

3.2.3 Two pressure level supercritical cycle

For the lower evaporation pressure the principles that are applied are the same as in the one pressure level. The supercritical pressure though was approached in a different way. In the supercritical area there is no superheated vapor, as it is a different state of matter. For pressure above the critical there is no vapor, but a state different from solid, liquid and vapor. This is shown in Fig 3.2.1

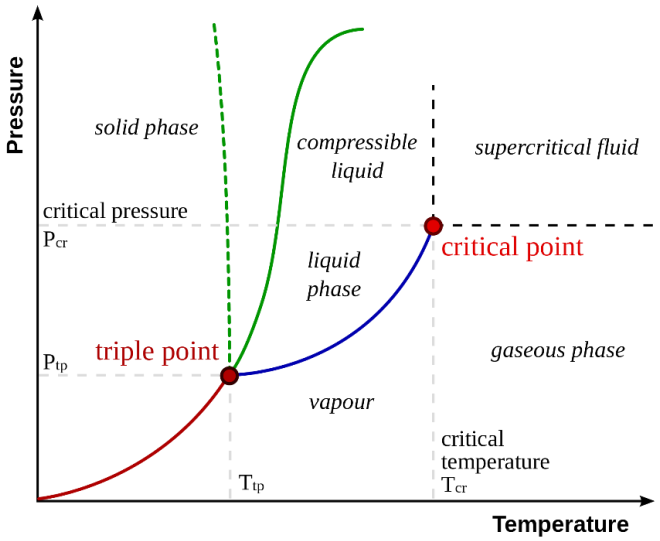

Fig. 3.2.1 States of matter

The negative result that superheating had on the cycle efficiency then is not valid for this occasion. So both the enthalpy and the pressure of the fluid in the turbine inlet are decision variables. In order to determine the range in which the entropy varies some calculations need to be done first. The maximum entropy of saturated vapor curve from condensation pressure till critical pressure is found. If entropy in the outlet of the evaporator is greater than this value, then even with $\eta_{turb,is}$ there will be no two phase state in the expander during the expansion. The Fig 3.2.2 and 3.2.3 are used to show this clearer:

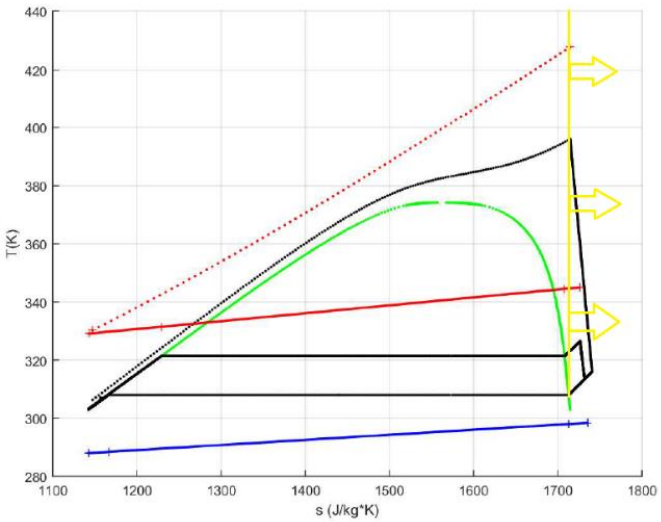

Fig. 3.2.2 Supercritical ORC of wet fluid

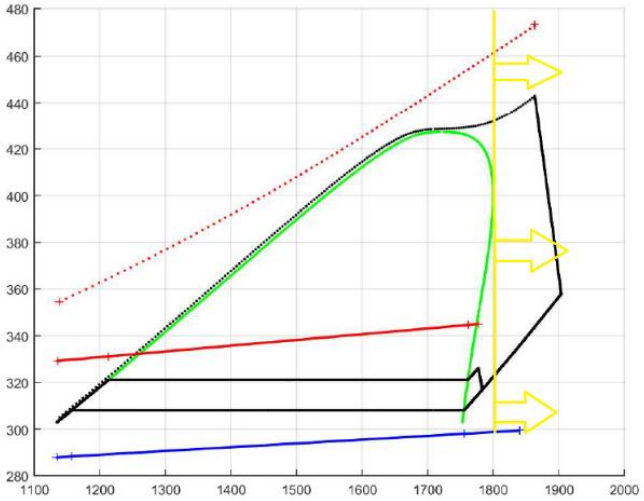

Fig. 3.2.3 Supercritical ORC of dry fluid

In Fig. 3.2.2 and Fig. 3.2.3 two pressure level ORCs are depicted. The area which can be the end of the supercritical evaporation is marked by the yellow lines and the arrows. In this way the expansion does not enter the two phase area in any point, both for dry and wet fluids. Pinch Point temperature differences are set again as $\Delta T_{pp,LP} = 10K$, $\Delta T_{pp,HP} = 20K$. For the subcritical evaporator the pinch point is obviously going to be at the point of saturated liquid, and by energy balance between the two streams (organic and hot source) the mass flow rate of the low pressure level of the ORC is calculated. For the supercritical evaporation the pinch point position is not known a priori. To solve the problem of the supercritical mass flow rate, the temperature difference is calculated through energy balance in 90 points along the evaporation curve, for various mass flow rates. The mass flow rate starts from zero and increases till the pinch point difference reaches the value of 20K in at least one point. After this, the maximum mass flow rate of the cycle is obtained and the power is calculated for this evaporation pressure and turbine inlet entropy. The procedure is followed for all possible evaporation pressures and turbine inlet entropy in two loops. In the end the optimum pair is obtained.

$$\eta_{total} = f(P_{evap,LP}, P_{evap,HP}, s_{turb,in,HP})$$

$$P_{evap,LP,max} = \min\left[P_{crit}, P_{sat}\left(T_{hot,LP} - \Delta T_{sup,LP}\right)\right]$$

$$P_{evap,HP,max} < P_{evap,HP,opt} < P_{cond}$$

$$P_{evap,HP,max} = \min\left[P_{crit}, P\left(T_{hot,HP}, s_{max}\right)\right]$$

$$P_{evap,HP,max} < P_{evap,HP,opt} < P_{cond}$$

$$s_{turb,in,HP,min} = \max[s_{sat\ vapor}]$$

$$s_{turb,in,HP,max} = s_{turb,in,HP,min} + 100\,\frac{J}{kg \cdot K}$$

$$s_{turb,in,HP,max} < s_{turb,in,opt,HP} < s_{turb,in,HP,min}$$

$$T_{hot,out,LP} > T_{hot,out,LP,min}$$

$$T_{hot,out,HP} > T_{hot,out,HP,min}$$

N° of variables: 67

VR_{LP}, SP_{LP}, T_{cr}, $n_{turbHP,is}$, $n_{pumpHP,is}$, $n_{turbLP,is}$, $n_{pumpLP,is}$, W_{HP}, $W_{turb,HP}$, $W_{pump,HP}$, $P_{evap\ HP,opt}$, $T_{hot,HP,in}$, $T_{hot,HP,out}$, $\dot{m}_{hot,HP}$, $Cp_{hot,HP}$, W_{LP}, $W_{turb,LP}$, $W_{pump,LP}$, $P_{evap\ LP,opt}$, $T_{hot,LP,in}$, $T_{hot,LP,out}$, $\dot{m}_{hot,LP}$, $Cp_{hot,LP}$, $T_{cold,in}$, $\dot{m}_{cold}$, Cp_{cold}, $T_{cold,out}$, P_{cond}, $s_{turb,in,opt,HP}$, $\Delta T_{sup,LP}$, ΔT_{sub}, $\Delta T_{pp,LP}$, $\Delta T_{pp,HP}$, wf, $\dot{m}_{wf,HP}$, $\dot{m}_{wf,LP}$, η_{total}, $\eta_{total,HP}$, $\eta_{thermal,HP}$, $\eta_{HR,HP}$, $\eta_{total,LP}$, $\eta_{thermal,LP}$, $\eta_{HR,LP}$ $\sum_{i=1}^{12} T_i$, $\sum_{i=1}^{12} s_i$

N° of dependent variables: 51

VR_{LP}, SP_{LP}, T_{cr}, $n_{turbLP,is}$, W_{HP}, $W_{turb,HP}$, $W_{pump,HP}$, $P_{evap\ HP,opt}$, $T_{hot,HP,out}$, W_{LP}, $W_{turb,LP}$, $W_{pump,LP}$, $P_{evap\ LP,opt}$, $T_{hot,LP,out}$, $T_{cold,in}$, $\dot{m}_{cold}$, $T_{cold,out}$, P_{cond}, $\dot{m}_{wf,HP}$, $\dot{m}_{wf,LP}$, η_{total}, $\eta_{total,HP}$, $\eta_{thermal,HP}$, $\eta_{HR,HP}$, $\eta_{total,LP}$, $\eta_{thermal,LP}$, $\eta_{HR,LP}$ $\sum_{i=1}^{12} T_i$, $\sum_{i=1}^{12} s_i$

N° of independent variables: 9

$T_{hot,HP,in}$, $\dot{m}_{hot,HP}$, $Cp_{hot,HP}$, $T_{hot,LP,in}$, $\dot{m}_{hot,LP}$, $Cp_{hot,LP}$, $T_{cold,in}$, Cp_{cold}, wf

N° of fixed variables: 7

$\Delta T_{sup,LP}$, ΔT_{sub}, $\Delta T_{pp,LP}$, $\Delta T_{pp,HP}$, $n_{turbHP,is}$, $n_{pumpHP,is}$, $n_{pumpLP,is}$

N° of output variables: 48

$n_{turbLP,is}$, $s_{turb,in,HP}$, W_{HP}, $W_{turb,HP}$, $W_{pump,HP}$, $P_{evap\ HP,opt}$, $T_{hot,HP,out}$, W_{LP}, $W_{turb,LP}$, $W_{pump,LP}$, $P_{evap\ LP,opt}$, $T_{hot,LP,out}$, $T_{cold,in}$, $\dot{m}_{cold}$, $T_{cold,out}$, P_{cond}, $\dot{m}_{wf,HP}$, $\dot{m}_{wf,LP}$, η_{total}, $\eta_{total,HP}$, $\eta_{thermal,HP}$, $\eta_{HR,HP}$, $\eta_{total,LP}$, $\eta_{thermal,LP}$, $\eta_{HR,LP}$ $\sum_{i=1}^{12} T_i$, $\sum_{i=1}^{12} s_i$

3.3 Design models of the components

After the basic parameters of the ORC are defined the calculation of some characteristics of the components is done. This involves the following: pump, turbine, heat exchangers. These characteristics are going to be used in the dynamic model to calculate the transient response of the ORC system

3.3.1 Subcritical heat exchangers

The heat exchangers are type E shell-n-tube. The reason for this choice is the small space for oscillations that exists in the tubes side. It is considered the best scenario for the phase change. The assumptions that are made are the following:

1) They are adiabatic, meaning heat losses are neglected
2) No pressure losses have been calculated
3) The axial heat transfer is not taken into account
4) Thermal resistance of the tubes is neglected as it is considered too small compared with the convection ones
5) The properties of the heat source are calculated one time only in the inlet of the exchanger while the properties of the organic fluid are calculated again for each different phase area

The selected layout is the following:

1) The organic fluid is in the tube side and the heat source in the shell side
2) The tubes are in triangular pitch formation
3) The heat exchange is done counter-currently

The following characteristics are predefined in the model and therefor are as inputs:

1) Inlet diameter of the tube, d_{in}
2) Reynolds number of organic fluid in the liquid area.

The inputs from the design point model are:

1) Mass flow rate of organic fluid and the outer source
2) Temperatures and specific enthalpies in inlet and outlet of the heat exchanger $T_{ORC,in}, T_{ORC,out}, T_{Source,in}, T_{Source,out}, h_{ORC,in}, h_{ORC,out}$
3) Temperature and pressure of phase change T_{sat}, P_{sat}

All the needed fluid properties are calculated using the Refprop®. In order to calculate the total length of the exchanger, it is subdivided in three areas, according to the phase that exists in the interior of each area. In the case of the evaporator these are the preheater (subcooled area), the evaporation area (two phase area) and the superheater (superheating area). In the case of the condenser there are respectively the same areas. The number of tubes is defined by the Reynolds number of organic fluid in the liquid area that the heat exchange will take place and the tube's inner diameter d_{in}.

$$Nt = f(Re, d_{in})$$

Then all the other crucial parameters of the heat exchangers geometry can be calculated by empirical correlations except from the length. These are the outer diameter of the tube d_{out}, the triangular pitch P_t of the tubes, the baffles spacing B_s, the inner diameter of the shell D_s, the shell-side cross flow area A_s, and the shell-side hydraulic diameter D_e. All the equations used except the estimation of outer diameter are proposed by Edwards et. al. [25] and Kern et. al. [2] and can be found on the Appendix.

$$d_{out} = 1.2 d_{in}$$

$$P_t = f(d_{out})$$

$$B_s = f(d_{out})$$

$$D_s = f(P_t, Nt)$$

$$A_s = f(d_{out}, P_t, B_s, D_s)$$

$$D_e = f(d_{out}, P_t)$$

After the calculation of these geometrical parameters it possible to evaluate the velocity of the fluid in the shell side and as result the Reynolds number too.

$$u'' = f(A_s, m_{source})$$

$$Re'' = f(u'', D_e)$$

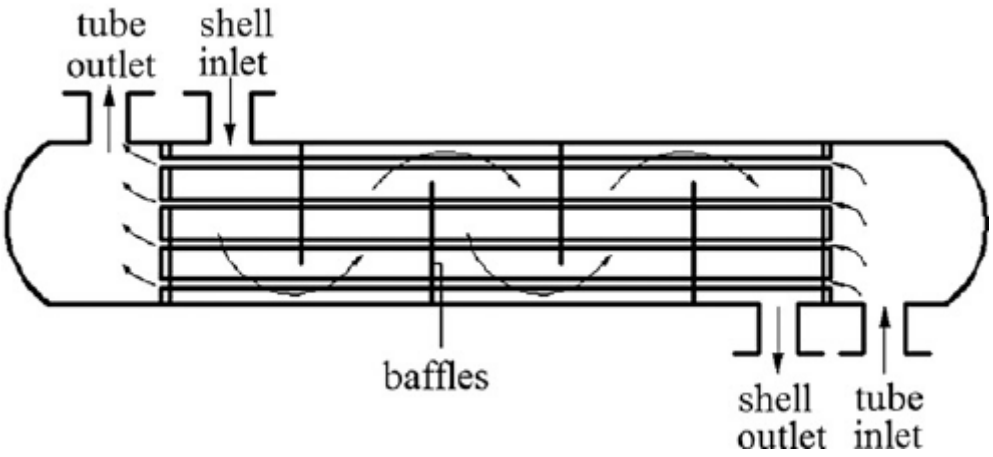

Fig. 3.3.1 Type E counter flow shell and tube heat exchanger

For each area, all the unknown temperatures of the heat source are calculated. Then the heat transfer problem is solved for each area separately and in the end the total length of the heat exchanger is the sum of the length of the different areas. The equations that define the problem are:

$$Q_i = m_{ORC} \cdot (h_{i,out} - h_{i,in})$$

$$Q_i = m_{source} \cdot Cp_{source} \cdot (T_{i,in} - T_{i,out})$$

$$Q_i = U_i \cdot A_i \cdot \Delta T_{LMTD}$$

$$\Delta T_{LMTD} = \frac{\Delta T_1 - \Delta T_2}{\ln(\frac{\Delta T_1}{\Delta T_2})}$$

$$A_i = Nt \cdot \pi \cdot d_{in} \cdot L_i$$

$$U_i = \frac{1}{\frac{1}{a'} + \frac{d_{in}}{De \cdot a''}}$$

a’ is calculated by the Nusselt number that Dittus-Boelter equation predicts as a function of Reynolds and Prandle numbers. This is for single phase flow

$$Nu = 0.023 \cdot Re^{0.8} \cdot Pr^{n}$$

$$\text{where } n = 0.4 \text{ for heat and } 0.3 \text{ for cooling}$$

$$a' = \frac{Nu \cdot \lambda}{d_{in}}$$

For the evaporation heat transfer coefficient, the Dittus-Boelter equation cannot be used as it is not valid for this conditions. Instead, Winterton [14, 24] correlation is used, which takes into account various phenomena that take place when evaporation takes place:

$$a'_{evap} = \sqrt{(F \cdot a'_L)^2 + (S \cdot a'_{pool})^2}\text{, where}$$

$$a'_L = 0.023 \cdot (\frac{\lambda_L}{d_{in}}) \cdot Re_L^{0.8} \cdot Pr_L^{0.4}$$

$$F = \left[1 + x \cdot Pr_L \left(\frac{\rho_L}{\rho_V} - 1\right)\right]^{0.35}$$

$$a'_{pool} = 55 \cdot {P_{cr}}^{0.12} \cdot q^{\frac{2}{3}} \cdot (-\log_{10} P_{cr})^{-0.55} \cdot M^{-0.5}$$

$$S = \frac{1}{1 + 0.055 \cdot F^{0.1} \cdot Re_L^{0.16}}$$

For the condensation heat transfer coefficient also the Dittus-Boelter is not valid. A correlation proposed by Cavallini et. al. [30, 31] is used:

$$a'_{cond} = 0.023 \cdot (\frac{\lambda_L}{d_{in}}) \cdot Re_{eq}^{0.8} \cdot Pr_L^{0.33}$$

where the equivalent Reynolds number can be expressed as

$$Re_{eq} = Re_V \cdot \left(\frac{\rho_L}{\rho_V}\right)^{0.5} \cdot \frac{\mu_V}{\mu_L} + Re_L$$

a'' is calculated as a function of Reynolds and Prandle numbers as proposed by John Edwards [25] for the equivalent outer diameter De

$$Nu = 0.36 \cdot Re^{0.55} \cdot Pr^{0.33} \left(\frac{\mu_b}{\mu_w}\right)^{0.14}$$

$$a'' = \frac{Nu \cdot \lambda}{De}$$

Finally, the total length of the shell-n-tube is obtained by the sum of the single lengths and total area is calculated respectively

$$L_{total} = \sum L_i$$

$$A_{total} = Nt \cdot \pi \cdot d_{in} \cdot L_{total}$$

The previous procedure is presented in flow chart:

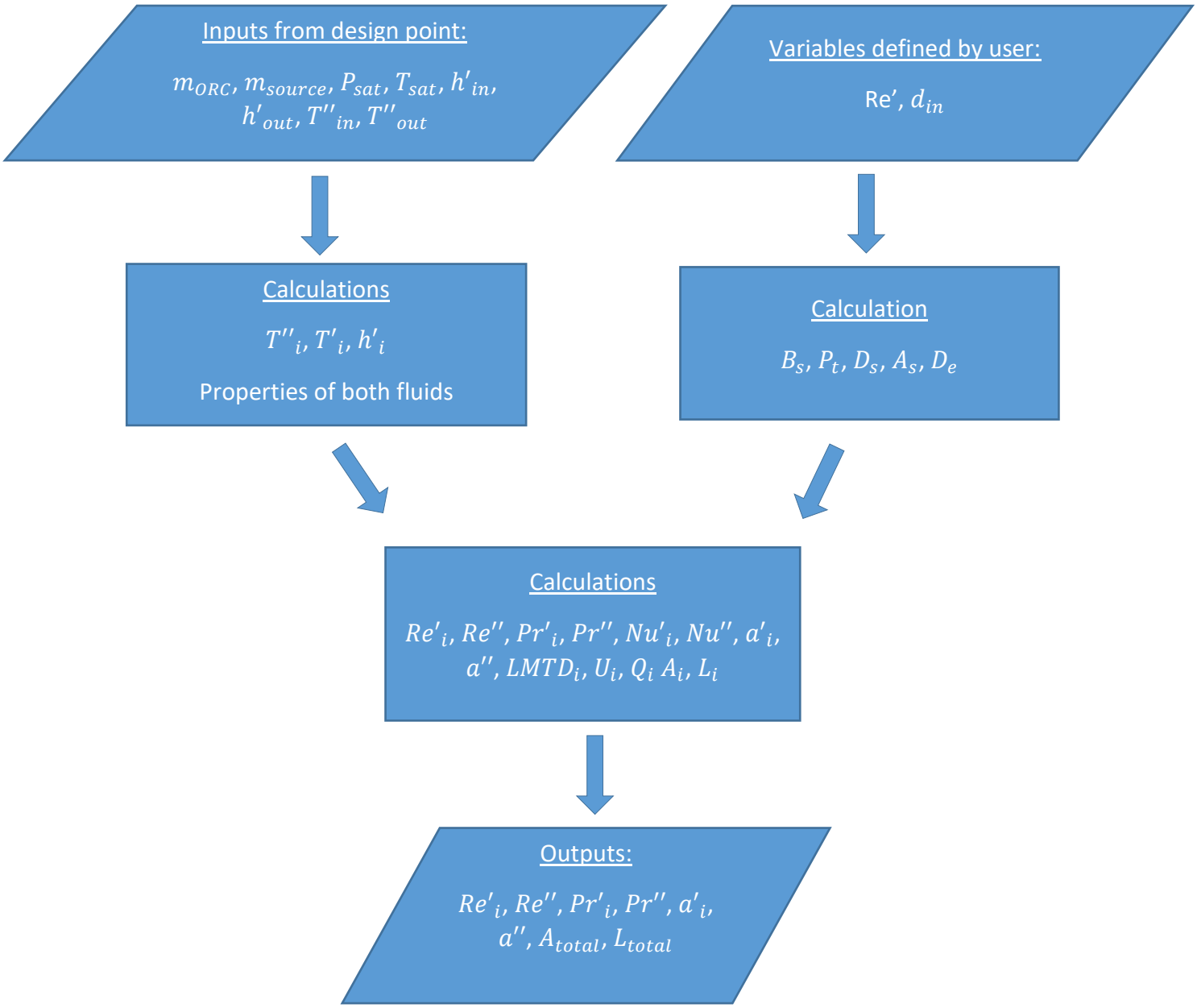

3.3.2 Supercritical heat exchangers

The supercritical heat exchanger is different from the subcritical ones as no phase change takes place inside. The equations that define the heat transfer properties of the shell side are the same as in the subcritical one. The correlation that is used for the supercritical heat transfer Nusselt number is Jackson's correlation [34, 35]. It is proposed by Karellas et. al. [26] because the Dittus-Boelter equation that is used usually for subcritical heat transfer does not predict that quarterly the heat transfer coefficient near the critical point.

$$\mathrm{Nu_b} = 0.0183 \cdot \mathrm{Re_b^{0.82}} \cdot \mathrm{Pr^{0.5}} \left(\frac{\rho_w}{\rho_b}\right)^{0.3} \left(\frac{\overline{Cp}}{Cp_b}\right)^n$$

$$\overline{Cp} = \frac{h_w - h_b}{T_w - T_b}$$

If pc is the pseudo-critical point, then the exponent n is defined as:

$$n = 0.4 \text{ for } T_b < T_w < T_{pc} \text{ and } T_w > T_b > 1.2 \cdot T_{pc}$$

$$n = 0.4 + 0.2\left(\frac{T_w}{T_{pc}} - 1\right) \text{ for } T_b < T_{pc} < T_w$$

$$n = 0.4 + 0.2\left(\frac{T_w}{T_{pc}} - 1\right)\left(1 - 5\left(\frac{T_b}{T_{pc}} - 1\right)\right) \text{ for } T_{pc} < T_b < 1.2 \cdot T_{pc}$$

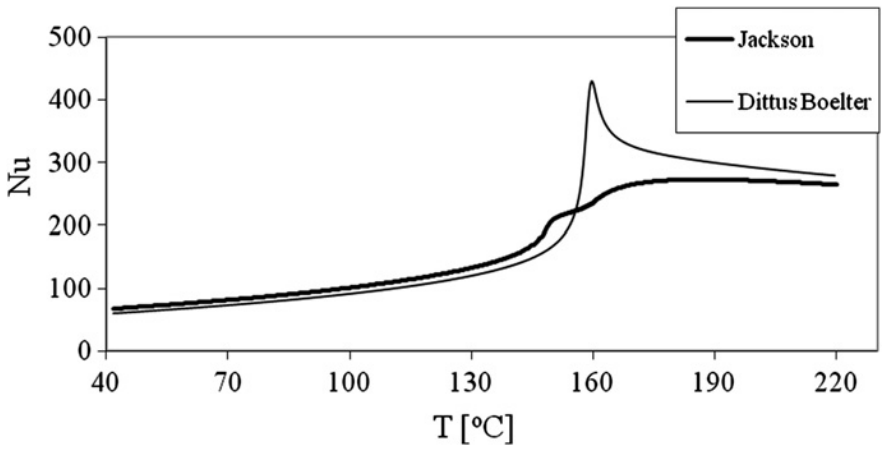

Fig. 3.3.2 Nusselt number, according to Jackson and Dittus Boelter, as a function of temperature of the organic fluid [26]

3.3.3 Pumps

The pump is a centrifugal one stage pump which provides the necessary head in order for the cycle to operate. It's speed at the design point is 3000 rpm. In the off-design conditions it is changed by the control system in order to keep the cycle's parameters steady. The operation and performance are described by the operation map, which indicates the head provided in accordance to the volume flow rate and the rotational speed of the pump. The map also provides information about the efficiency of the pump according to the head, the volume flow rate and the rotational speed. Useful data can be exported from the design point model in order to create an operation map which will be used in the off-design point conditions. These are the nominal head of the pump, the volume flow rate, the nominal rotational, the efficiency at that point and the volume flow rate in which the head is equal to zero, dead flow rate. The equations that provide these values are:

$$Y_{dp} = \frac{P_{out} - P_{in}}{\rho_{in} \cdot g}$$

$$\dot{V_{dp}} = \frac{m_{ORC,dp}}{\rho_{in}}$$

$$\dot{V_{0,dp}} = \frac{V_{dp}}{0.7}$$

$$\eta_{is,dp} = 0.7 = known$$

$$\omega_{dp} = 3000rpm = known$$

The efficiency of the pump and the rpm at the design point are known as they are values defined in the design point model. The characteristic curve of the pump, for constant RPM, is assumed to be a second order polynomial function (parabola) with symmetry around the Y axis and the efficiency is calculated by the correlation that Vaja [13] proposes:

$$\eta_{p,is} = \eta_{p,is,dp} \cdot \left[2\frac{\dot{V}}{\dot{V_{dp}}} - \left(\frac{\dot{V}}{\dot{V_{dp}}} \right)^2 \right]$$

The characteristic curve is fully defined for the nominal rotational speed. In the off-design conditions the rotational speed changes and so the affinity laws are used to predict the performance of the pump. As the speed varies, the parameters of the pump change as shown below:

$$\frac{\dot{V}_1}{\dot{V}_2} = \frac{rpm_1}{rpm_2}$$

$$\frac{Y_1}{Y_2} = \left(\frac{rpm_1}{rpm_2}\right)^2$$

$$\frac{W_1}{W_2} = \left(\frac{rpm_1}{rpm_2}\right)^3$$

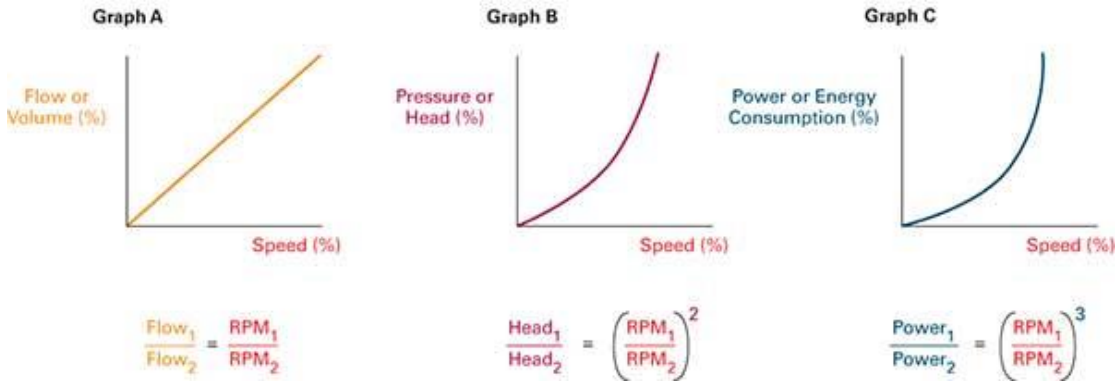

Fig. 3.3.3 Affinity laws

By applying the affinity laws to the design point and the dead volume flow rate point two new operation point for the new speed are obtained. Then by applying the assumption of the parabola, the characteristic curve in the new speed is fully defined. The isentropic efficiency is calculated by the correlation that Vaja [13] proposes:

$$\eta_{p,is} = \eta_{p,is,dp} \cdot \left[2\frac{\dot{V}}{\dot{V_{dp}}} - \left(\frac{\dot{V}}{\dot{V_{dp}}}\right)^2\right]$$

Where the $\dot{V_{dp}}$ is the one at the nominal rotation speed, ω_{dp}. In this way the operation map of the pump is created. A figure is shown below just to give an example of an operation map of a pump.

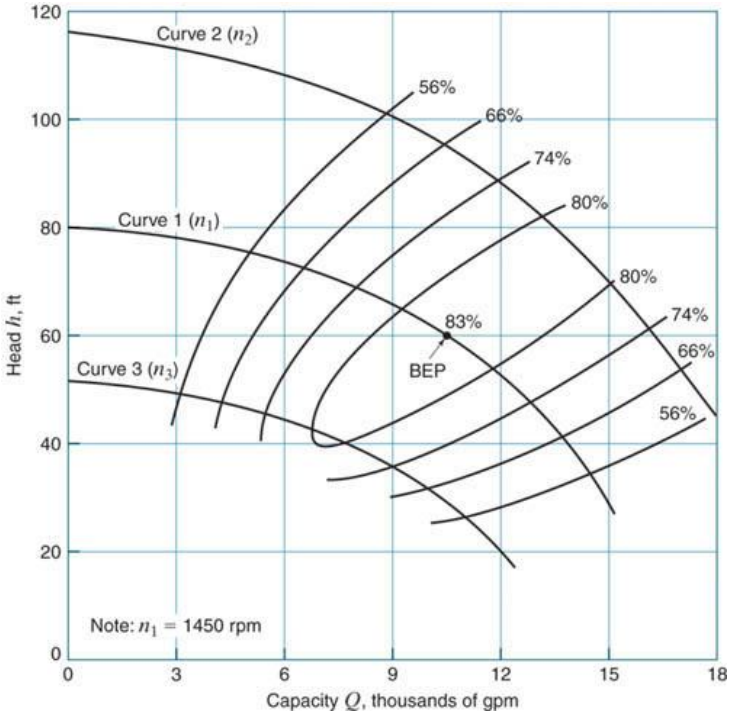

Fig. 3.3.4 Pump operation map example

3.3.4 Turbines

The turbine is a one stage axial turbine, working on constant RPM. It is the component producing the power, so it is a very crucial component to the cycle. In the literature seems that there is not yet a standard correlation to define the performance of a turbine expanding organic fluid in all operating conditions. This is because of the very big number of organic fluids in usage and the different operation conditions that may exist.

Since the turbine revolves at constant speed it's map is actually a curve. In order to create the curve, information must be exported from the design point conditions. The Stodola coefficient K_s and the non-dimensional mass flow rate m_R proposed by Mazzi et. al. [12]. The isentropic efficiency of the turbine at the design point $\eta_{t,is,dp}$ is known.

$$K_s = \frac{\dot{m_{dp}}}{\rho_{in,dp} \cdot \left(P_{in,dp}^2 - P_{out,dp}^2\right)}$$

$$m_{R,dp} = \frac{\dot{m_{dp}} \cdot T_{in,dp}^{0.5}}{P_{in,dp}}$$

$$\eta_{t,is,dp} = known$$

These values are used to create the curve as shown below. The efficiency is calculated by the correlation that Vaja [13] is proposing:

$$\dot{m} = K_s \cdot \rho_{in} \cdot (P_{in}^2 - P_{out}^2)$$

$$m_R = \frac{\dot{m} \cdot T_{in}^{0.5}}{P_{in}}$$

$$\eta_{t,is} = \eta_{t,is,dp} \cdot \left[2\frac{m_R}{m_{R,dp}} - \left(\frac{m_R}{m_{R,dp}} \right)^2 \right]$$

Note must be taken in the fact that K_s is constant in all operating conditions while m_R changes. Since the turbine is axial and one stage the cone law describes the operation as shown in Fig 3.3.5

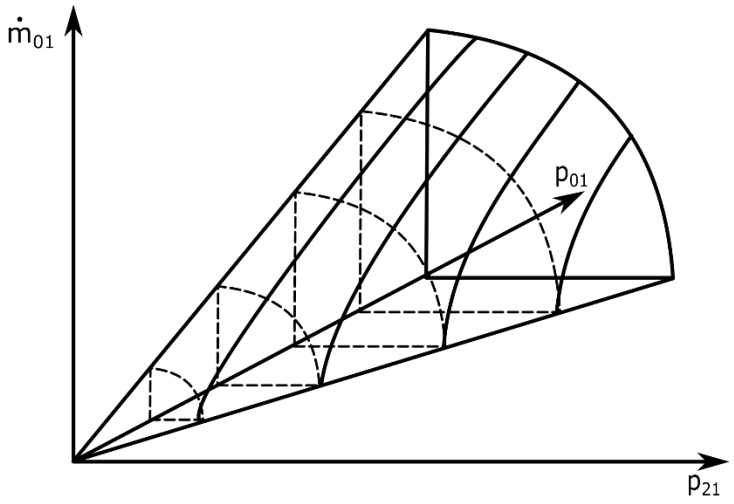

Fig. 3.3.5. Stodola law of eclipse

3.4 Dynamic off-design models

In this chapter the dynamic off-design models of the components are presented. In this study the components are modeled by one or more Simulink® blocks. The pump and the turbine are modeled by one block each, while the shell-n-

tube heat exchangers are modeled by two. The creation of the models needs data that are taken from the design point model, such as $\dot{m}_{ORC,dp}$.

3.4.1 Pump block

The pump is a one stage centrifugal pump with variable speed. It is a flow control component. It mainly receives level variables and calculates flow variables. The mass and energy storage of the component is neglected, as it is considered very small in comparison with the one of the shell-n-tubes. No mass and energy storage is taken into account because the mass and energy storage phenomena of the heat exchangers are considered much more impactful. Also its inertia is neglected. The equations that characterize the block are the following:

Mass balance equation:

$$\frac{d\dot{m}}{dt} = 0 \leftrightarrow \sum \dot{m} = 0 \leftrightarrow \dot{m}_{in} = \dot{m}_{out}$$

Energy balance equation:

$$\frac{dE}{dt} = 0 \leftrightarrow \sum E = 0 \leftrightarrow E_{out} = E_{in} + W_{pump}$$

$$W_{pump} = \dot{m}_{pump} \cdot (h_{out} - h_{in})$$

The inputs from other blocks are: h_{in}, P_{in}, P_{out}, ω

The outputs towards other blocks are: $\dot{m}_{pump}$, h_{out}

This is shown in the next figure:

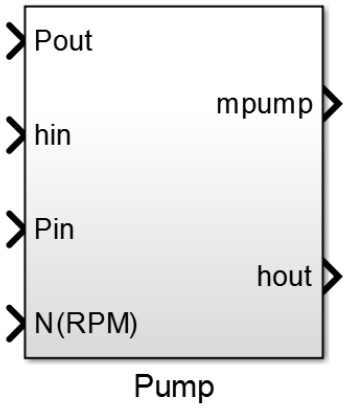

Fig. .3.4.1. Pump Simulink® block

In order to calculate the outputs, the map developed in the design of the components is used. The volume flow rate is determined by the present rotational speed ω and head implied in the pump, Y. This means that the pump's mass flow rate is determined by speed ω, pressure difference in inlet and outlet and the inlet density ρ_{in}.

$$\dot{m}_{pump} = f(P_{in}, P_{out}, \rho_{in}, \omega)$$

The enthalpy in the outlet is calculated using the inlet enthalpy, the isentropic efficiency $\eta_{p,is}$ of the pump and the isentropic enthalpy $h_{out,is}$

$$\eta_{pump,is} = \eta_{pump,is,dp} \cdot \left[2\frac{\dot{V}}{\dot{V_{dp}}} - \left(\frac{\dot{V}}{\dot{V_{dp}}} \right)^2 \right]$$

$$h_{out} = h_{in} + \frac{h_{out,is} - h_{in}}{\eta_{p,is}}$$

All the fluid properties needed are calculated by the Refprop® program in Matlab® environment.

3.4.2 Turbine block

The turbine is a one stage axial turbine operating at constant speed. It is a flow control component as the pump and mainly receives level variables and calculates flow variables. Also the mass and energy storage of the component is neglected as

done in the pump, as it is considered very small in comparison with the one of the shell-n-tubes.

Mass balance equation:

$$\frac{d\dot{m}}{dt} = 0 \leftrightarrow \sum \dot{m} = 0 \leftrightarrow \dot{m}_{in} = \dot{m}_{out}$$

Energy balance equation:

$$\frac{dE}{dt} = 0 \leftrightarrow \sum E = 0 \leftrightarrow E_{out} = E_{in} - W_{turb}$$

$$W_{turb} = \dot{m}_{turb} \cdot (h_{in} - h_{out})$$

The inputs from other blocks are: h_{in}, P_{in}, P_{out}

The outputs towards other blocks are: $\dot{m}_t$, h_{out}

This is shown in the next figure:

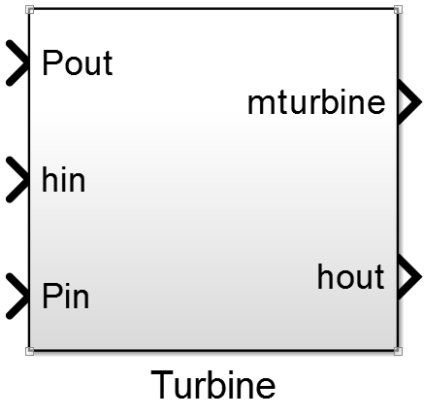

Fig. .3.4.2. Turbine Simulink® block

In order to calculate the outputs, the curve developed in the design of the components is used. The turbine's mass flow rate is determined by pressures in inlet and outlet and the inlet density ρ_{in}.

$$\dot{m}_{turb} = f(P_{in}, P_{out}, \rho_{in})$$

$$\dot{m}_{turb} = K_s \cdot \rho_{in} \cdot (P_{in}^2 - P_{out}^2)$$

The enthalpy in the outlet is calculated using the inlet enthalpy, the isentropic efficiency $\eta_{t,is}$ of the turbine and the isentropic enthalpy $h_{out,is}$. Also the non dimentional mass flow rate m_R is used, as indicated below:

$$m_R = \frac{\dot{m}_t \cdot T_{in}^{0.5}}{P_{in}}$$

$$\eta_{turb,is} = \eta_{t,is,dp} \cdot \left[2\frac{m_R}{m_{R,dp}} - \left(\frac{m_R}{m_{R,dp}} \right)^2 \right]$$

$$h_{out} = h_{in} - \eta_{t,is} \cdot (h_{in} - h_{out,is})$$

All the fluid properties needed are calculated by the Refprop® program in Matlab® environment.

3.4.3 Subcritical heat transfer block

The subcritical heat transfer block belongs in the block category of heat exchangers. It is one of the two block that models a subcritical shell-n-tube exchanger. It is similar to a flow control component as it calculates flow variables (heat transferred between two fluids) but it receives both level variables, such as pressure, and flow variables, such as mass flow rate, as input. It is important to clarify from the beginning that the subcritical heat transfer blocks do not have mass and energy storage phenomena, and these phenomena are taken into account in the capacity blocks, with which they are coupled. In the capacity block that follows the storage phenomena are taken into consideration for the organic fluid only. For the hot or cold source fluid are not taken into account in general as they go further than the purpose of this study. The mass flow rate of the organic fluid with which the calculations are done is the one that enters the shell-n-tube, meaning is the one calculating from the previous flow control component. This means that for the evaporator is the pump's mass flow rate and for the condenser the turbine's.

$$\dot{m}_{evaporator} = \dot{m}_{pump}$$

$$\dot{m}_{condenser} = \dot{m}_{turbine}$$

The subcritical heat transfer block is subdivided in three parts according to the phase of the organic fluid inside:

Preheater: the part of the heat exchanger from the inlet of the organic fluid till the two phase region

Evaporator/Condenser: the part in which the phase change is done

Superheater/Subcooler: the part of the heat exchanger after the two phase region in which the superheating/subcooling is done, which in the last area of the heat exchangers and stretches till the outlet.

For each of the areas above the block calculates the amount of energy that is transferred and the surface/length that is required for the heat exchange also. So the different phases volumes inside the tubes are calculated in this bock. The inputs and outputs that the block receives and gives from and to others blocks of the models during the simulation are presented below. The model also receives inputs that have been calculated during the design-point model and the components design programs. These are information related to the geometry and heat transfer as well

Inputs from other model blocks: $\dot{m}'_{in}$, $\dot{m}_{source}$, T''_{in}, h'_{in}, P_{in}

Inputs from design-point conditions: d_{in} , d_{out} , De , L_{total} , Nt, $a'_{i,dp}$, $a''_{i,dp}$, $\dot{m}_{source,dp}$, $\dot{m}_{wf,dp}$, $Pr_{wf,i,dp}$

Outputs: T''_{out}, V_i, Q_i

The volumes occupied inside the tubes be different organic fluid phases and the energy given to each area are the V_i and Q_i respectively. A figure of the Simulink® block is shown in order to give a supervisory view the variables. On the left side are the input variables, while on the right are the output ones.

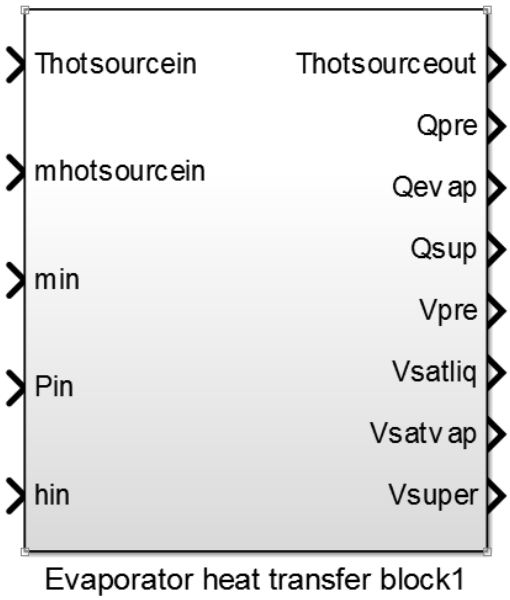

Fig. .3.4.3. Subcritical evaporator heat transfer Simulink® block

The equations that define the problem are:

Mass balance equations:

$$\sum \dot{m} = 0 \leftrightarrow \frac{dm}{dt} = 0$$

For the organic fluid:

$$\dot{m}'_{in} = \dot{m}'_{out}$$

$$\dot{m'}_{in,i} = \dot{m'}_{out,i} = \dot{m}_{wf}$$

For the source's fluid:

$$\dot{m}''_{in} = \dot{m}''_{out} = \dot{m}_{source}$$

Energy balance equations:

$$\sum \dot{E} = 0 \leftrightarrow \frac{dE}{dt} = 0$$

$$Q'_{i} = Q''_{i} = Q_i$$

$$Q' = Q''$$

For the organic fluid:

$$Q' = \dot{m}'_{in} \cdot (h'_{out} - h'_{in})$$

$$Q'_{\iota} = \dot{m}_{wf} \cdot (\Delta h'_{i})$$

For the source's fluid:

$$Q'' = \dot{m}_{source} \cdot Cp_{source} \cdot (T''_{in} - T''_{out})$$

$$Q''_{\iota} = \dot{m}_{source} \cdot Cp_{source} \cdot (\Delta T''_{i})$$

Heat transfer:

$$Q_i = U_i \cdot A_i \cdot \Delta T_{LMTD,i}$$

$$A_i = Nt \cdot \pi \cdot d_{in} \cdot L_i$$

$$U_i = \frac{1}{\frac{1}{a'_i} + \frac{d_{in}}{De \cdot a''_i}}$$

For the convective coefficients in the off-design points, a correlation proposed by Manente et. al. [33] is used. By using this correlation, the calculation of the heat transfer coefficients in each area is simple. The correlation is the one following:

$$a'_i = a'_{i,dp} \cdot \left(\frac{\dot{m}_{wf,i}}{\dot{m}_{wf,dp}}\right)^{n1} \cdot \left(\frac{Pr_{wf,i}}{Pr_{wf,i,dp}}\right)^{n2}$$

$$a'' = a''_{dp} \cdot \left(\frac{\dot{m}_{source,odp}}{\dot{m}_{source,dp}}\right)^{n3}$$

$$\text{where } i = \text{pre}, \text{evap/cond}, \text{sup/sub}$$

In the current case that Dittus-Boelter, Winterton , Cavallini and Edward correlations are used the exponents are:

$$n_1 = 0.8$$

$$n_2 = 0.3 \text{ for the evaporator and } 0.4 \text{ for the condenser}$$

$$n_3 = 0.55$$

The temperatures in the heat exchanger outlet are unknown and cannot be found without interactions. Therefor a superheating (subcooling for the condenser) is assumed for the organic working fluid (ΔT_{sup} or ΔT_{sub}) and by solving the energy balance equation the temperatures and enthalpies of both fluids are calculated in every characteristic point for the current time step.

$$\sum T''_i = \text{known}$$

$$\sum h'_i = \text{known}$$

After this assumption, by solving the heat transfer problem for this situation the total surface needed for the heat exchange is calculated. Then it is compared to the actual one. If it is not equal to the actual one, the assumption of the ΔT_{sup} (or ΔT_{sub}) in the outlet changes and the calculations are repeated. When the surface converges the problem is solved and the outputs can be obtained in order to feed the capacity block that follows.

$$A_i = \frac{Q_i}{(U_i \cdot \Delta T_{LMTD,i})}$$

$$A_{total\ dummy} = \sum_{i=1}^{3} A_i = A_{pre} + A_{evap/cond} + A_{sup/sub}$$

After the determination of the heat exchange areas, the volume occupied by each phase is calculated. For the determination of the volume occupied by saturated vapor, and the one by saturated liquid, in the saturated area the average void fraction γ is used. The homogenous model proposed by Butterworth [27] is used for reasons of simplicity:

$$\gamma = \int_{x=0}^{1} \frac{x \cdot \rho_L}{x \cdot \rho_L + (1-x) \cdot \rho_V} dx$$

where x is the vapor quality

The variables used by the block are summarized:

N° of variables: 45

$\dot{m}_{wf}$, $\dot{m}_{source}$, T''_{in}, h'_{in}, P_{in}, T''_{out}, V_i, Q_i, d_{in} , d_{out} , De , L_{total} , Nt, $a'_{i,dp}$, a''_{dp}, $\dot{m}_{source,dp}$, $\dot{m}_{wf,dp}$, $Pr_{wf,i,dp}$, $\Delta h'_i$, Cp_{source}, $\Delta T''_i$, U_i, $\Delta T_{LMTD,i}$, A_i, a'' , a'_i,γ

N° of independent variables: 5

$\dot{m}_{wf}$, $\dot{m}_{source}$, T''_{in}, h'_{in}, P_{in},

N° of dependent variables: 26

T''_{out}, V_i, Q_i, $\Delta T''_i$, $\Delta h'_i$, U_i, $\Delta T_{LMTD,i}$, A_i, a'', a'_i,γ

N° of fixed variables: 13

d_{in} , d_{out} , De , L_{total} , Nt, $a'_{i,dp}$, a''_{dp}, $\dot{m}_{source,dp}$, $\dot{m}_{wf,dp}$, $Pr_{wf,i,dp}$, Cp_{source}

N° of outputs: 7

T''_{out}, V_i, Q_i

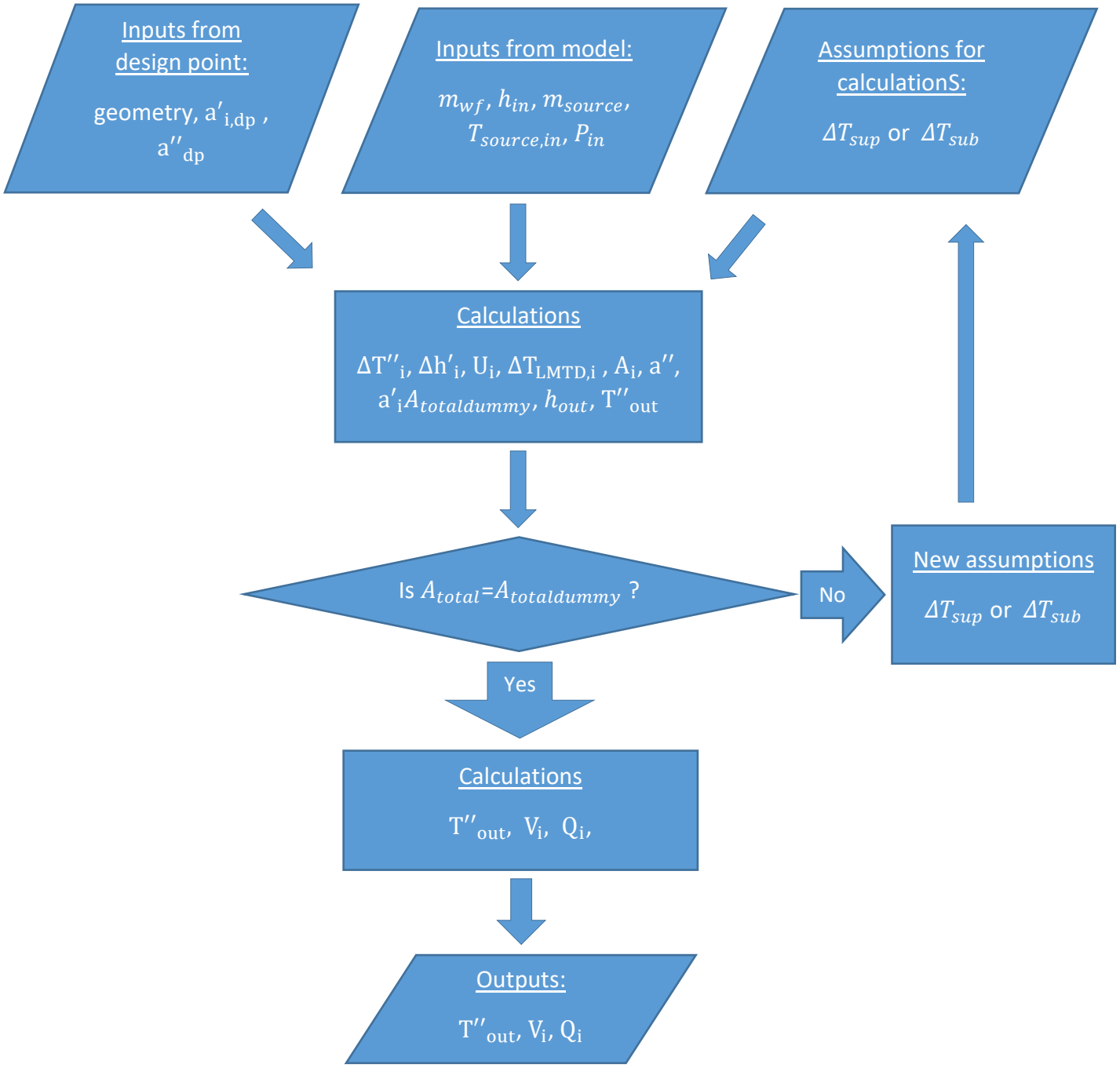
Inputs from design point:
geometry, $a'_{i,dp}$, a''_{dp}
Inputs from model:
m_{wf}, h_{in}, m_{source}, $T_{source,in}$, P_{in}
Assumptions for calculationS:
ΔT_{sup} or ΔT_{sub}
Calculations
$\Delta T''_i$, $\Delta h'_i$, U_i, $\Delta T_{LMTD,i}$, A_i, a'', $a'_i A_{totaldummy}$, h_{out}, T''_{out}
Is A_{total}=$A_{totaldummy}$?
No
New assumptions
ΔT_{sup} or ΔT_{sub}
Yes
Calculations
T''_{out}, V_i, Q_i,
Outputs:
T''_{out}, V_i, Q_i

3.4.4 Subcritical capacity block

The capacity block is the second block used to model the shell-n-tube, together with the heat exchanger one. It receives flow variables as inputs (such as mass flow rate) and calculates level variables (such outlet enthalpy). Its role is to simulate the storage phenomena that exist in the system. The two storage phenomena that are modeled are the mass and energy storage of the organic fluid. The heat sources phenomena are not taken into account. It is a very important component as it describes very crucial parameters of a thermodynamic cycle.

Inputs from the design point model: d_{in}, d_{out}, N_t, Cp_{tube}, $L_{evap,tot}$, $\mathrm{P_{initial}}$, $\mathrm{h'_{out,initial}}$

Inputs from other blocks: $\mathrm{\dot{m}_{ORC\ in}}$, $\mathrm{\dot{m}_{ORC\ out}}$, $\mathrm{h'_{in}}$, $\mathrm{V_i}$, $\mathrm{Q_i}$

Inputs from previous interaction: $\mathrm{P_{previews}}$, $\mathrm{h'_{out,previews}}$

Outputs: $\mathrm{P_{new}}$, $\mathrm{h'_{out,new}}$, ΔT_{sup} or ΔT_{sub}

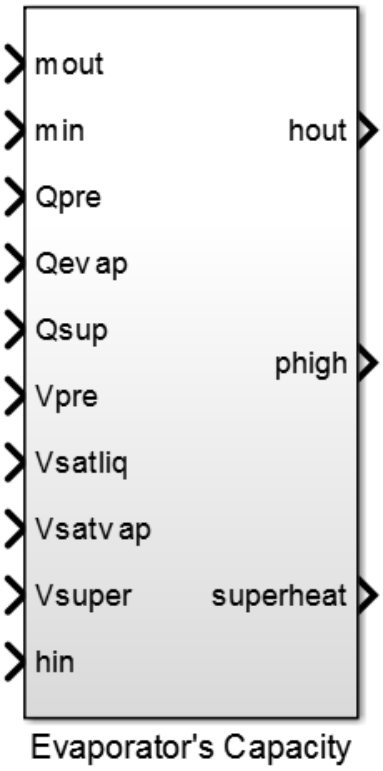

Fig. 3.4.4. Subcritical evaporator capacity Simulink® block

The equations that are solved are the mass balance, energy balance and volume preservation. The analysis is similar to the one done by Willatzen et. al. [11], with the difference that here the thermal inertia of the tubes is added to the energy balance of the working fluid and is not written as a separate equation. In the Fig.3.4.5 the general structure is shown:

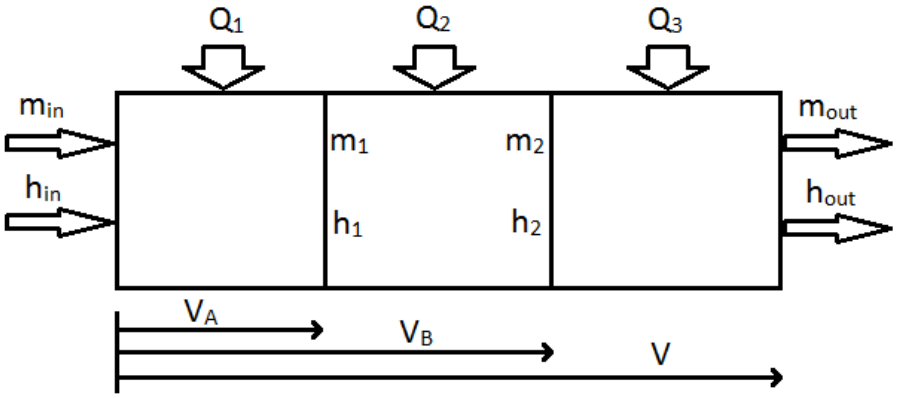

Fig. .3.4.5. Subcritical evaporator capacity structure

<u>The Volume preservation in differential form is written as:</u>

$$\frac{dV}{dt} = 0, \rightarrow$$

$$\frac{dV_A}{dt} + \frac{dV_B}{dt} + \frac{dV_C}{dt} = 0$$

<u>The Mass Balance equation in differential form is written as:</u>

$$\dot{m'}_{in} - \dot{m'}_{out} = \frac{dM}{dt}$$

$$\frac{\partial \rho}{\partial t} + \frac{\partial(\rho \cdot u)}{\partial z} = 0$$

After the integration in the hole volume of the heat exchanger it is written for each of the three different areas as:

<u>First area (preheating/precooling):</u>

$$\frac{dV_A}{dt}(\bar{\rho}_1 - \rho_1) + V_A\frac{d\bar{\rho}_1}{dt} = \dot{m}_{in} - \dot{m}_1$$

Second area (evaporation/condensing):

$$(V_B - V_A)\left[\frac{d\rho_V}{dP}\gamma + (1-\gamma)\frac{d\rho_L}{dP}\right]\frac{dP}{dt} + \frac{dV_B}{dt}(\bar{\rho}_2 - \rho_2) - \frac{dV_A}{dt}(\bar{\rho}_2 - \rho_1) = \dot{m}_1 - \dot{m}_2$$

Third area (superheating/subcooling):

$$\frac{dV_B}{dt}(\rho_2 - \bar{\rho}_3) + (V - V_B)\frac{d\bar{\rho}_3}{dt} = \dot{m}_2 - \dot{m}_{out}$$

The Energy Balance equation in differential form is written as:

$$\dot{E_{in}} - \dot{E_{out}} = \frac{dE}{dt}$$

$$\frac{\partial(\rho h - P)}{\partial t} + \frac{d\left(m_{tube}\cdot C_{p,tube}\cdot(T_{tube} - T_{ref})\right)}{dt} + \frac{\partial(\rho\cdot u\cdot h)}{\partial z} = Q$$

The reference temperature of the tube does not change, so:

$$\frac{d\left(m_{tube}\cdot C_{p,tube}\cdot(T_{tube} - T_{ref})\right)}{dt} = \frac{d\left(m_{tube}\cdot C_{p,tube}\cdot T_{tube}\right)}{dt}$$

What is more, the tube temperature is assumed to change in the same way as the one of the organic fluid, as is proposed by Astrom et. al. [28], meaning:

$$\frac{dT_{tube,i}}{dt} = \frac{dT_{wf,i}}{dt}$$

After the integration in the hole volume of the heat exchanger it is written for each of the three different areas as:

First area (preheating/precooling):

$$\frac{dV_A}{dt}\left(\bar{\rho}_1\bar{h}_1 - \rho_1 h_1\right) + V_A\left(\bar{h}_1\frac{d\bar{\rho}_1}{dt} + \bar{\rho}_1\frac{d\bar{h}_1}{dt} - \frac{dP}{dt}\right) + m_{tube,1}\cdot C_{p,tube}\frac{d(T_{tube,1})}{dt} = \dot{m}_{in}h_{in} - \dot{m}_1 h_1 + Q_1$$

Second area (evaporation/condensing):

$$(V_B - V_A)\left[\frac{d(\rho_V h_V)}{dP}\gamma + (1-\gamma)\frac{d(\rho_L h_L)}{dP} - 1\right]\frac{dP}{dt} + \frac{dV_B}{dt}\left(\bar{\rho}_2\bar{h}_2 - \rho_2 h_2\right) - \frac{dV_A}{dt}\left(\bar{\rho}_2\bar{h}_2 - \rho_1 h_1\right) + m_{tube,2}\cdot C_{p,tube}\frac{d(T_{tube,2})}{dt} = \dot{m}_1 h_1 - \dot{m}_2 h_2 + Q_2$$

Third area (superheating/subcooling):

$$\frac{dV_B}{dt}\left(\rho_2 h_2 - \bar{\rho}_1\bar{h}_1\right) + (V - V_B)\left(\bar{h}_3\frac{d\bar{\rho}_3}{dt} + \bar{\rho}_3\frac{d\bar{h}_3}{dt} - \frac{dP}{dt}\right) + m_{tube,3}\cdot C_{p,tube}\frac{d(T_{tube,3})}{dt} = \dot{m}_2 h_2 - \dot{m}_{out}h_{out} + Q_3$$

Each thermodynamic magnitude like $\frac{d(\rho_i)}{dt}$ can be written as a function of the temperature and pressure derivative over time for the single phase regions 1 and 3:

$$\frac{d(\rho_i)}{dt} = \left(\frac{\partial\rho}{\partial T}\cdot\frac{dT}{dt} + \frac{\partial\rho}{\partial P}\cdot\frac{dP}{dt}\right)$$

For the two phase region the pressure and the temperature are not independent values, so the derivative of the temperature can be expressed as a function of the pressure derivative. Therefore, for the saturated region thermodynamic magnitudes like $\frac{d(\rho)}{dt}$ can be written as:

$$\frac{d(\rho)}{dt} = \left(\frac{\partial \rho}{\partial T} \cdot \frac{dT}{dt} + \frac{\partial \rho}{\partial P} \cdot \frac{dP}{dt}\right) = \left(\frac{\partial \rho}{\partial T} \cdot \frac{\partial T}{\partial P} + \frac{\partial \rho}{\partial P}\right) \cdot \frac{dP}{dt}$$

For the area of the preheating/precooling it is supposed that the fluid inside has average temperature equal to the average between the inlet and the saturation one. For the area of the superheating/subcooling it is supposed as well that the average temperature is equal to the average between the saturation and the outlet one.

$$\overline{T}_1 = \frac{T_{in} + T_{sat}}{2}, \qquad \overline{T}_3 = T_{sat}, \qquad \overline{T}_3 = \frac{T_{sat} + T_{out}}{2}$$

And so:

$$\frac{d\overline{T}_1}{dt} = \frac{\frac{dT_{in}}{dt} + \frac{dT_{sat}}{dt}}{2}, \qquad \frac{d\overline{T}_3}{dt} = \frac{dT_{sat}}{dt}, \quad \frac{d\overline{T}_3}{dt} = \frac{\frac{dT_{sat}}{dt} + \frac{dT_{out}}{dt}}{2}$$

The outlet enthalpy derivative is expressed as:

$$\frac{dh_{out}}{dt} = C_p \cdot \frac{dT_{out}}{dt} + \frac{\partial h}{\partial P} \cdot \frac{dP}{dt}$$

All the fluid's properties like $\frac{\partial \rho}{\partial P}$ are calculated with the Refprop® tool. In the end there is a system of linear equations, containing 7 equations and 7 unknown variables. Through its solution the outputs of the capacity are obtained. Note that ΔT_{sup} or ΔT_{sub} is not an independent value, as it is calculated from P_{new}, $h'_{out,new}$.

<u>7 equations:</u> 3 mass balance equations, 3 energy balance equations, 1volume preservation
<u>7 unknowns:</u> $\frac{dP}{dt}$, $\frac{dh_{out}}{dt}$, $\dot{m}_{sat\,liq}$, $\dot{m}_{sat\,vap}$, $\frac{dV_A}{dt}$, $\frac{dV_B}{dt}$, $\frac{dV_C}{dt}$

N° of variables: 24

$\dot{m}_{wf,in}, \dot{m}_{wf,out}, h'_{in}, V_i, Q_i, P_{previews}, h'_{out,previews}, \frac{dP}{dt}, \frac{dh_{out}}{dt},$

$\dot{m}_{sat\ liq}, \dot{m}_{sat\ vap}, \frac{dV_A}{dt}, \frac{dV_B}{dt}, \frac{dV_C}{dt}, \Delta T_{sup}$ or ΔT_{sub}

N° of independent variables: 12

$\dot{m}_{wf,in}, \dot{m}_{wf,out}, h'_{in}, V_i, Q_i, P_{previews}, h'_{out,previews}, \Delta T_{sup}$ or ΔT_{sub}

N° of dependent variables: 7

$\frac{dP}{dt}, \frac{dh_{out}}{dt}, \dot{m}_{sat\ liq}, \dot{m}_{sat\ vap}, \frac{dV_A}{dt}, \frac{dV_B}{dt}, \frac{dV_C}{dt}$

N° of fixed variables: 5

d_{in}, d_{out}, Nt, $Cp_{tube}, L_{evap,tot}$

N° of outputs: 3

$P_{new}, h'_{out,new}, \Delta T_{sup}$ or ΔT_{sub}

The next flow chart presents the way that calculations are done:

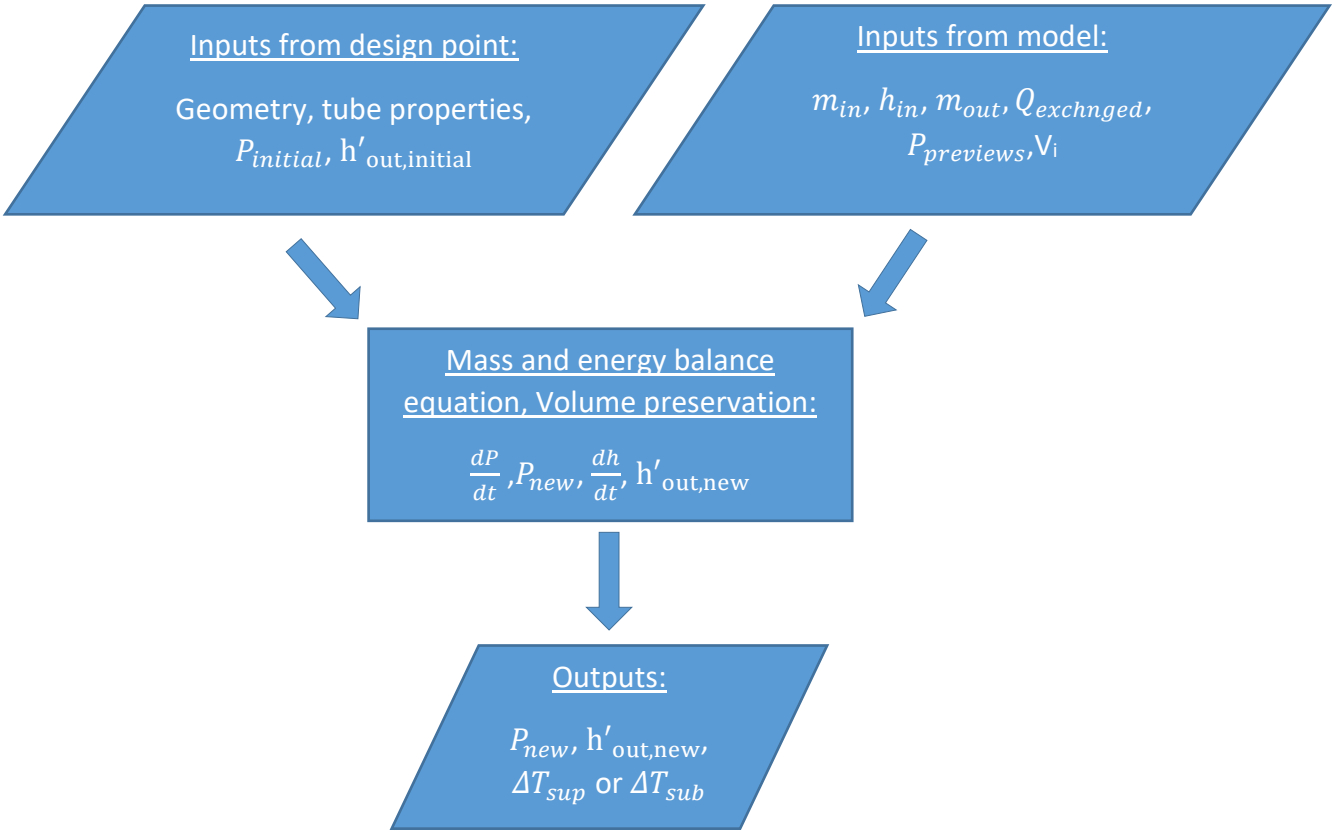

The Fig. 3.4.6 that following shows the overall connections in the one pressure level dynamic model. The connections are the signals representing values of thermodynamic values as is already stated.

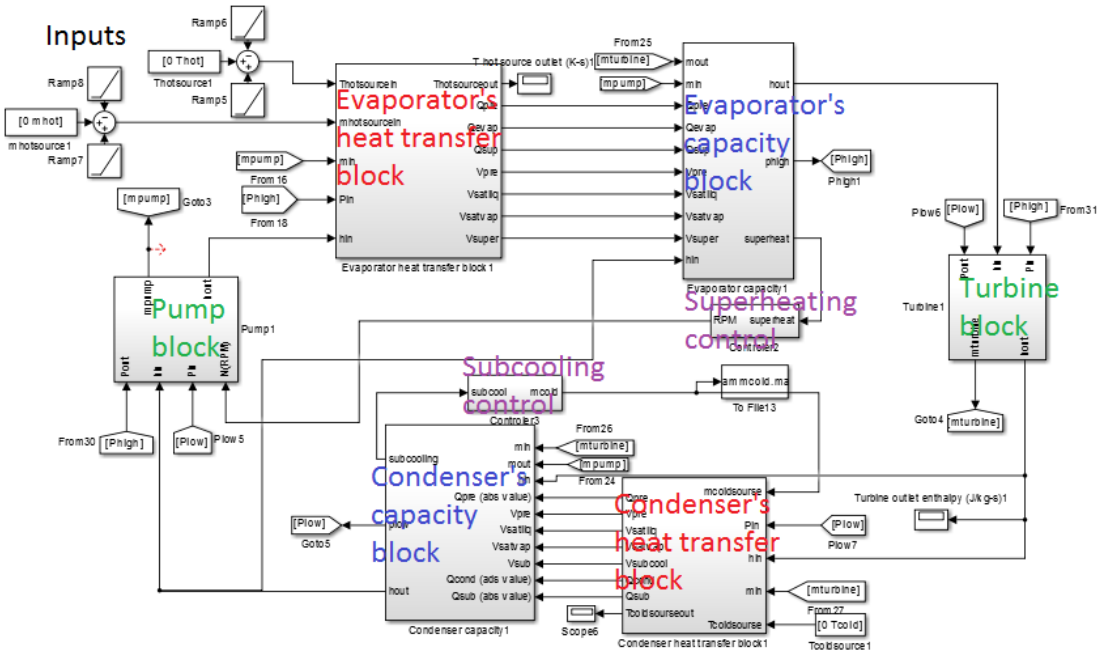

Fig.3.4.6 Simulink® model of one pressure level

For comparison, in figure 3.4.7 is shown the ORC model created by Vaja. As the Figure indicates, the modeling approach and the connections between the components are similar.

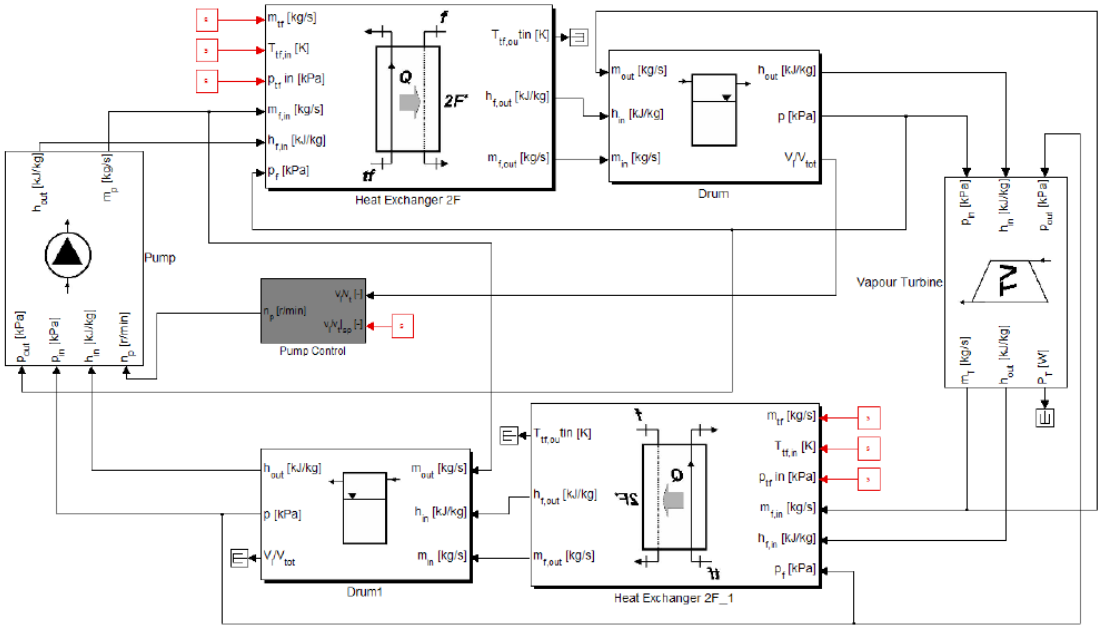

Fig. 3.4.7. Simulink® model of an ORC power plant [13]

3.4.5 Supercritical heat transfer block

The supercritical heat transfer block belongs in the block category of heat exchangers. It is one of the two block that models the supercritical shell-n-tube exchanger. The supercritical heat transfer block does not have mass and energy storage phenomena, and these phenomena are taken into account in the capacity block which follows and are taken for the organic fluid only. The mass and energy storage phenomena for the hot source fluid are not taken into account in general as they go further than the purpose of this study. The mass flow rate of the organic fluid with which the calculations are done is the one that enters the shell-n-tube, meaning is the one calculating from the previous flow control component. This means that for the supercritical evaporator is the pump's mass flow rate and for the condenser the turbine's.

$$\dot{m}_{evap,super} = \dot{m}_{pump}$$

Mass balance equations:

$$\sum \dot{m} = 0 \leftrightarrow \frac{dm}{dt} = 0$$

For the organic fluid:

$$\dot{m}'_{in} = \dot{m}'_{out} = \dot{m}_{wf}$$

For the source's fluid:

$$\dot{m}''_{in} = \dot{m}''_{out} = \dot{m}_{source}$$

Energy balance equations:

$$\sum \dot{E} = 0 \leftrightarrow \frac{dE}{dt} = 0$$

$$Q' = Q''$$

For the organic fluid:

$$Q' = \dot{m}_{wf} \cdot (h'_{out} - h'_{in})$$

For the source's fluid:

$$Q'' = \dot{m}_{source} \cdot Cp_{source} \cdot (T''_{in} - T''_{out})$$

Heat transfer equations:

$$Q = U \cdot A \cdot \Delta T_{LMTD}$$

$$A = Nt \cdot \pi \cdot d_{in} \cdot L_{total}$$

$$U = \frac{1}{\frac{1}{a_i} + \frac{d_{in}}{De \cdot a_i}}$$

$a' = a'_{dp} \cdot \left(\frac{\dot{m}_{wf}}{\dot{m}_{wf,dp}}\right)^{n1} \cdot \left(\frac{Pr_{wf}}{Pr_{wf,dp}}\right)^{n2}$, where Pr_{wf} is calculated in the inlet only

$$a'' = a''_{dp} \cdot \left(\frac{\dot{m}_{source,ı}}{\dot{m}_{source,dp}}\right)^{n3}$$

In the current case that Jackson's correlation and the one proposed by Kern are used the exponents are:

$$n_1 = 0.82$$

$$n_2 = 0.3$$

$$n_3 = 0.55$$

The temperatures in the outlet of the heat exchanger are considered unknown and cannot be found without interactions. Therefore, an output temperature is supposed for the organic working fluid and by solving the energy balance equation the temperatures and enthalpies of both fluids are calculated in each point for this temperature.

$$T''_{out} = \text{known}$$

$$h'_{out} = \text{known}$$

After by solving the heat transfer problem for this situation the total length needed is calculated. Then it is compared to the actual one. If it is not right the assumption of temperature in the outlet changes and the calculations are repeated. When the length converges the problem is solved and the outputs can be obtained in order to feed the capacity block that follows.

$$A = \frac{Q}{(U \cdot \Delta T_{LMTD})}$$

Now the inputs and outputs that the block receives and gives from and to others blocks of the models during the simulation will be presented

Inputs from other blocks: $\dot{m}_{wf}$, $\dot{m}_{source}$, T''_{in}, h'_{in}, P_{in}

Inputs from design-point conditions: d_{in} , d_{out} , De , L_{total} , Nt, a'_{dp} , a''_{dp} ,

$\dot{m}_{wf,dp}$, $\dot{m}_{source,dp}$, $Pr_{ORC,i,dp}$

Outputs: T''_{out}, Q, V

Mind that the volume V does not change during the simulation, so the block has as output a constant value.

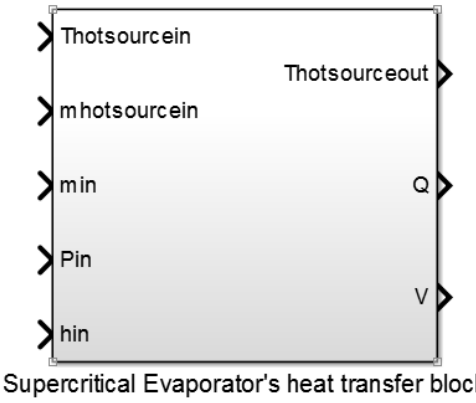

Fig. .3.4.8 Supercritical evaporator heat transfer Simulink® block

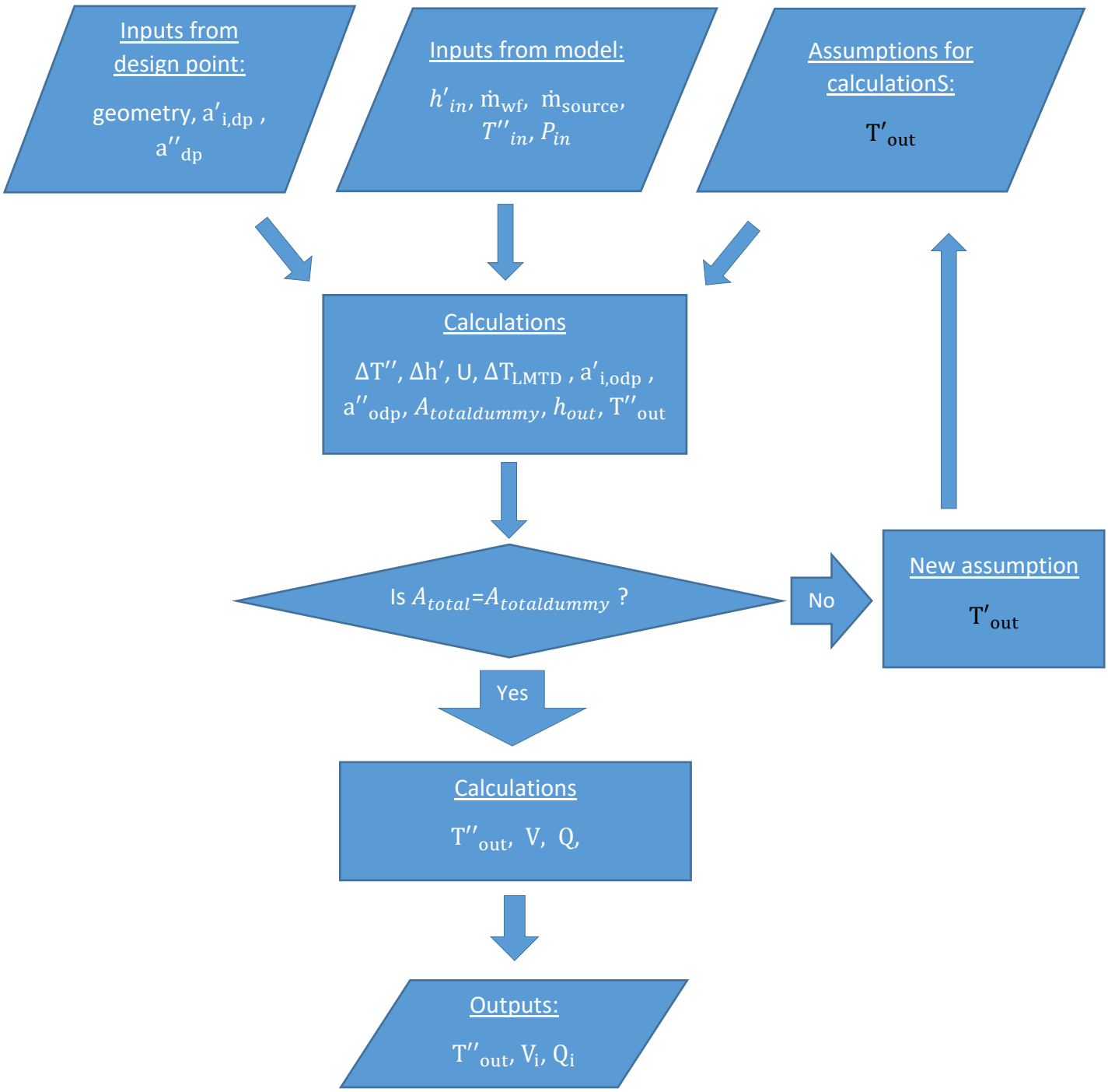
Inputs from design point:
geometry, $a'_{i,dp}$, a''_{dp}
Inputs from model:
h'_{in}, $\dot{m}_{wf}$, $\dot{m}_{source}$, T''_{in}, P_{in}
Assumptions for calculationS:
T'_{out}
Calculations
$\Delta T''$, $\Delta h'$, U, ΔT_{LMTD} , $a'_{i,odp}$, a''_{odp}, $A_{totaldummy}$, h_{out}, T''_{out}
Is A_{total}=$A_{totaldummy}$?
No
New assumption
T'_{out}
Yes
Calculations
T''_{out}, V, Q,
Outputs:
T''_{out}, V_i, Q_i

3.4.6 Supercritical capacity block

In the supercritical shell-n-tube heat exchanger the capacity block that is used to model the storage phenomena is different from the subcritical one. This is because there is only one phase inside. This results in a different dynamic response as the mass balance and energy balance equations that are used are different. Also the volume preservation equation has no impact as there is no volume change between different phases.

Inputs from the design point model: d_{in}, d_{out}, Nt, Cp_{tube}, $L_{evap,tot}$, $P_{initial}$, $h'_{out,initial}$

Inputs from other blocks: $\dot{m}_{ORC\ in}$, $\dot{m}_{ORC\ out}$, h'_{in}, V, Q

Inputs from previous interaction: $P_{previews}$, $h'_{out,previews}$

Outputs: P_{new}, $h'_{out,new}$, $s'_{out,new}$, $T'_{out,new}$

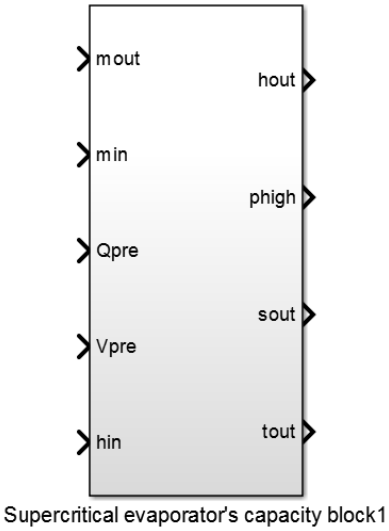

Fig. .3.4.9. Supercritical evaporator capacity Simulink® block

The equations that define the problem are:

Mass balance:

$$\dot{m}_{in} - \dot{m}_{out} = V \cdot \frac{d(\rho)}{dt} = V \cdot \left(\frac{\partial \rho}{\partial T} \cdot \frac{dT}{dt} + \frac{\partial \rho}{\partial P} \cdot \frac{dP}{dt}\right)$$

Energy balance:

$$\dot{m}_{in} \cdot h_{in} - \dot{m}_{out} \cdot h_{out} + Q = \rho \cdot V \frac{d(u)}{dt} + u \cdot V \frac{d(\rho)}{dt} + m_{tube} \cdot C_{p,tube} \cdot \frac{d(T_{tube})}{dt}$$

Where:

$$\frac{d(\rho)}{dt} = \left(\frac{\partial \rho}{\partial T} \cdot \frac{dT}{dt} + \frac{\partial \rho}{\partial P} \cdot \frac{dP}{dt}\right)$$

$$\frac{d(u)}{dt} = \left(\frac{\partial u}{\partial T} \cdot \frac{dT}{dt} + \frac{\partial u}{\partial P} \cdot \frac{dP}{dt}\right)$$

$$T = \frac{T_{in} + T_{out}}{2}$$

The tubes temperature T_{tube} is supposed to change in the same way as the T_{out}. The procedure is synopsized in the next flow chart:

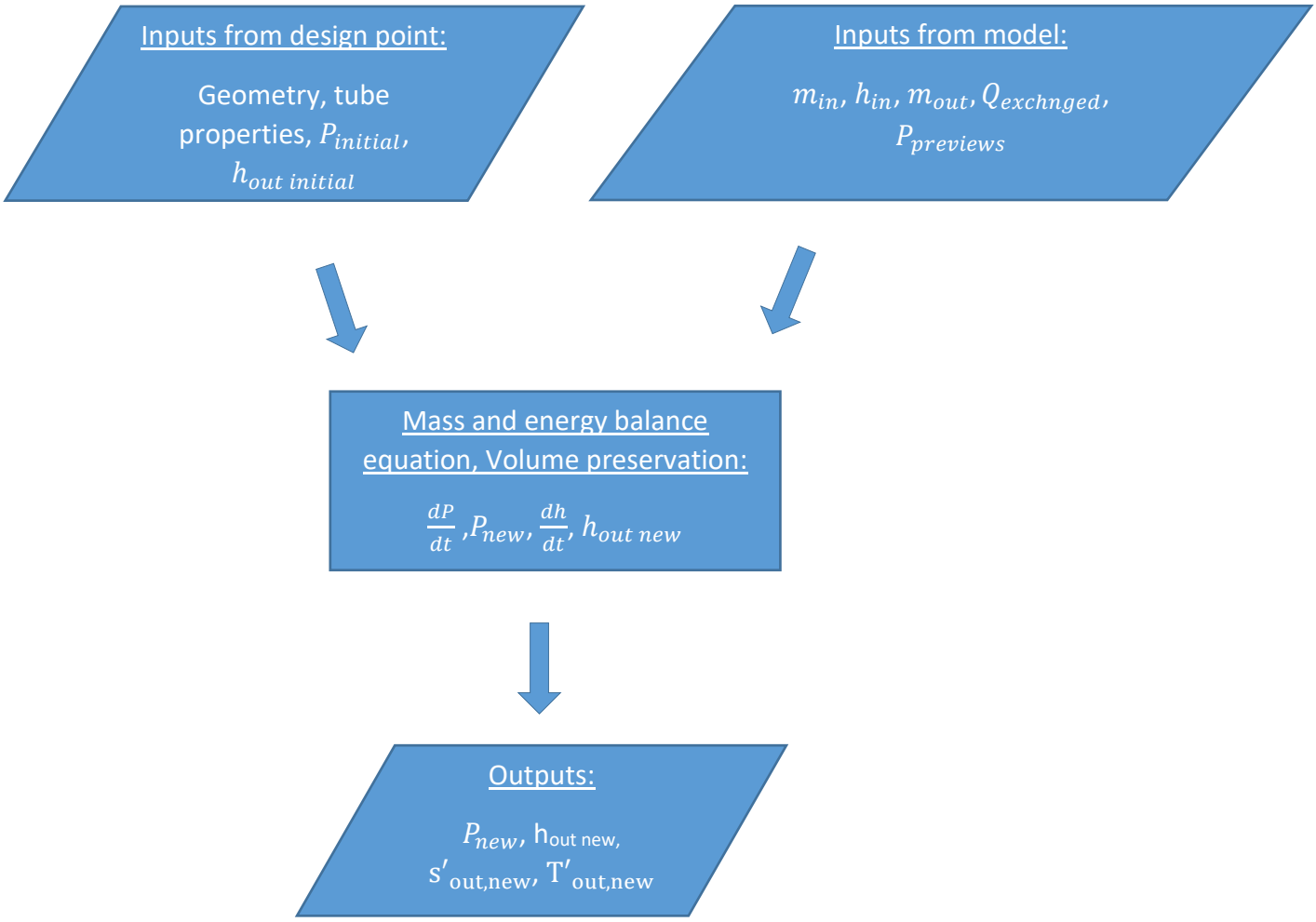

3.5 Conclusions

In this chapter the design point models and the off-design dynamic models are explained, for all three cases that are studied. The design point models construct the ORC cycle that produces the maximum power in the specific conditions and with the assumption that are done. What is more, they calculate essential data for the dynamic models such as the Stodola coefficient K_s and the number of tubes that the heat exchangers have N_t. The off-design dynamic models are realized by the proper connection of individual blocks. The blocks are used to simulate the behavior of the cycle components in dynamic changes. The approach proposed by Vaja is followed in the current study. The heat exchanger is modeled with a moving boundary model, which is not very accurate but it is simple, fast and is preferable when it comes to control design. It is known that the dynamic models contain errors due to the assumptions that are made, but the overall approach is sufficient. Unfortunately, there is no real system in order to be used to check the accuracy of the models. Additionally, no experimental data were found in the literature, describing precisely all the parameters of an ORC in transient conditions. Although the accuracy of the models is unknown, the flexibility is achieved in both the design point and dynamic models. The initial parameters, which are defined by the user, make the design models easy to apply in every hot source stream. The dynamic models are flexible also as they are formed by discrete blocks. These blocks can be easily altered to simulate an existing system, if the equations proposed in this study are not valid for a specific application or better fitting equations are known. In conclusion, the goal of flexibility is achieved.

4. Modeling tools

In this chapter the modeling tools that were used are presented. The tools are used to realize the modelling approach that is been developed. This involves the MATLAB® programming language and its modelling tool, Simulink®.

4.1 MATLAB®

MATLAB® is a high-performance language for technical computing. It integrates computation, visualization, and programming in an easy-to-use environment where problems and solutions are expressed in familiar mathematical notation. Common uses are:

- Mathematics and computation
- Algorithm Development
- Modeling, simulation, and prototyping
- Data analysis, exploration, and visualization
- Scientific and engineering graphics
- Application development, including Graphical User Interface building

MATLAB® is an interactive system whose basic data element is an array that does not require dimensioning. This allows the solving of many technical computing problems, especially those with matrix and vector formulations, in a fraction of the time it would take to write a program in a scalar non interactive language. The name MATLAB® stands for matrix laboratory. MATLAB® was originally written to provide easy access to matrix software developed by the LINPACK and EISPACK projects, which together represent the state-of-the-art in software for matrix computation.

MATLAB® has evolved over a period of years with input from many users. In university environments, it is the standard instructional tool for introductory and advanced courses in mathematics, engineering, and science. In industry, MATLAB® is the tool of choice for high-productivity research, development, and analysis. MATLAB® features a family of application-specific solutions called toolboxes. Very important to most users of MATLAB®, toolboxes allow the learning and applying specialized technology. Toolboxes are comprehensive collections of MATLAB® functions (M-files) that extend the MATLAB® environment to solve particular classes of problems. Areas in which toolboxes are available include signal processing, control systems, neural networks, fuzzy logic, wavelets, simulation, and many others.

4.2 Simulink®

Simulink®® is a block diagram environment for multi-domain simulation and Model-Based Design. It supports system-level design, simulation, automatic code generation, and continuous test and verification of embedded systems. Simulink® provides a graphical editor, customizable block libraries, and solvers for modeling and simulating dynamic systems. It is integrated with MATLAB®®, enabling the incorporation with MATLAB® algorithms into models and exporting simulation results to MATLAB® for further analysis.

Key Features

- Graphical editor for building and managing hierarchical block diagrams
- Libraries of predefined blocks for modeling continuous-time and discrete-time systems
- Simulation engine with fixed-step and variable-step ODE solvers
- Scopes and data displays for viewing simulation results
- Project and data management tools for managing model files and data
- Model analysis tools for refining model architecture and increasing simulation speed
- MATLAB® Function block for importing MATLAB® algorithms into models
- Legacy Code Tool for importing C and C++ code into models

4.3 REFPROP®

REFPROP® is an acronym for REFerence fluid PROPerties. This program, developed by the National Institute of Standards and Technology (NIST), provides tables and plots of the thermodynamic and transport properties of industrially important fluids and their mixtures with an emphasis on refrigerants and hydrocarbons, especially natural gas systems.

REFPROP® is based on accurate pure fluid and mixture models. It implements three models for the thermodynamic properties of pure fluids: equations of state explicit in Helmholtz energy, the modified Benedict-Webb-Rubin equation of state, and an extended corresponding states (ECS) model. Mixture calculations employ a model that applies mixing rules to the Helmholtz energy of the mixture components; it uses a departure function to account for the departure from ideal mixing. Viscosity and thermal conductivity are modeled with either fluid-specific correlations, an ECS method, or in some cases the friction theory method.

5.Results and Simulations

In this chapter the results of the simulation are presented and remarks are made upon them. The modeling approach that is presented in chapter 3 is followed in order to create the models. In the begging, the design point of each case is calculated. This includes a comparison study between different organic fluids as working mediums in order to determine the one that maximizes the power output. After this, basic parameters of the components are calculated by the design point model, such as the Stodola coefficient of the turbines and the length of the shell-n-tube heat exchangers. In this way, all the essential parameters for the dynamic simulations are obtained. Dynamic simulations are done for a load increase of the engines, from 85% to 100% within 50 seconds. The results show that the system, of each of the cases studied, is operating safely and that the control strategy proposed is acceptable, reaching its goals. What is more the results are smooth and without oscillations, which is a common problem in dynamic models. The overall behavior of the system is the expected one.

The cases which are studied are presented:

1) Only jacket water's heat is utilized, one subcritical pressure level
2) Both jacket water's and supercharged air heat are utilized by using two subcritical pressure levels
3) Both jacket water's and supercharged air heat are utilized by using one subcritical and one supercritical pressure level

5.1 First case

The one hot source-one pressure level model is applied for the first case for several working fluids in order to find the one that maximizes the power output. The working fluids that are thought to be suitable for the application are the following: R-134a, R-125, R-245ca, R-245fa, R-227ea, RC-318. The results are summarized in the next table

Table 5.1 First case design point for various working fluids

	R-245ca	R-134a	R-125	R-227ea	R-245fa	RC-318
P_{evap} (kPa)	355,34	1799,89	3368,92	1256,93	500,52	898,8
P_{cond} (kPa)	120,99	766,88	1562,54	526,09	176,84	363,88
T_{evap} (°C)	62,94	63,04	62,93	62,93	62,94	62,93
T_{cond} (°C)	30	30	30	30	30	30
ΔT_{sup} (°C)	5	5	5	5	5	5
ΔT_{sub} (°C)	5	5	5	5	5	5
T''_{out} (°C)	76,3	76,3	76,3	76,3	76,3	76,3
$\eta_{is,turb}$	0,61	0,74	0,76	0,73	0,65	0,72
$\eta_{is,pump}$	0,7	0,7	0,7	0,7	0,7	0,7
m_{ORC} (kg/s)	27,62	32,84	54,56	47,33	29,28	49,13
m_{cold} (kg/s)	169,05	176,79	182,52	162,08	169,54	157,78
W_{turb} (kW)	344,06	423,67	440,63	394,69	366,99	377,1
W_{pump} (kW)	6,67	40,05	117,23	35,53	10,11	25,02
W_{net} (kW)	337,39	383,61	323,4	359,16	356,88	352,08
ϕ (%)	9,56	9,56	9,56	9,56	9,56	9,56
$\eta_{thermal}$ (%)	5,17	5,88	4,96	5,5	5,47	5,4
η_{total} (%)	0,49	0,56	0,47	0,53	0,52	0,52

The optimum scenario as it can be seen is usage of R134a as working fluid. For this, the T-s diagram is constructed:

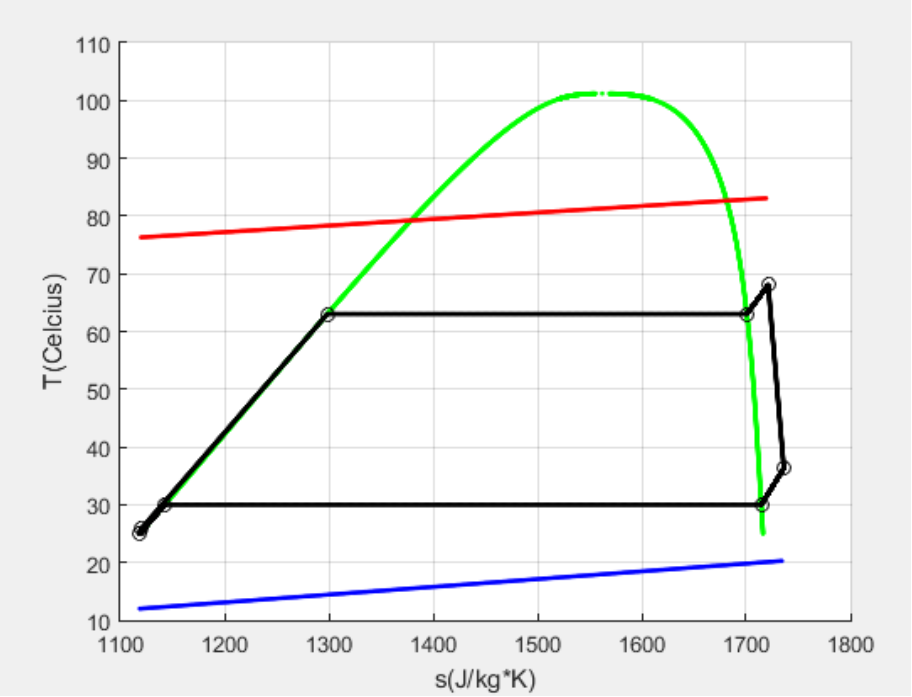

Fig 5.1 First case T-s diagram

For the optimum scenario, the shell-n-tube heat exchangers are designed and their mean features are shown in the table below:

Table 5.2 First case, characteristics of shell-n-tubes

	Evap	Cond
d_{in} (mm)	14	14
d_{out} (mm)	16,8	16,8
Nt	1513	1628
p_t (mm)	23,52	23,52
B_s	1,4	1,4
D_s (m)	1,09	1,13
De (mm)	19,51	19,51
Re''	30049,76	6165,66
α'' (kW/m^2*K)	4,62	2,69
Re'_L	10002,91	9999,15
α_{pre}(kW/m^2*K)	0,31	0,32
$\alpha_{evap}/\alpha_{cond}$ (kW/m^2*K)	1,66	1,74
$\alpha_{sup}/\alpha_{sub}$ (kW/m^2*K)	0,42	0,33
L (m)	6,64	6,97

The dynamic behavior of the system can be studied at this point. The case is the increase of the engines load from 85% to 100% within 50 seconds. This results in a change both in the of jacket's water temperature and mass flow rate. The temperature is increasing 1.62 K and the mass flow rate decreasing 33.4 kg/s during the transient period.

The system starts from the design point of 85% load as stated before and remains as it is for 50 secs in order to assure it starts from a stable condition. Then from 50 secs till 100 secs the load change takes place and from 100 secs till 250 secs the system reaches steady state conditions again, with superheating and subcooling returning to their nominal values. The results are presented below in the form of diagrams:

Inputs:

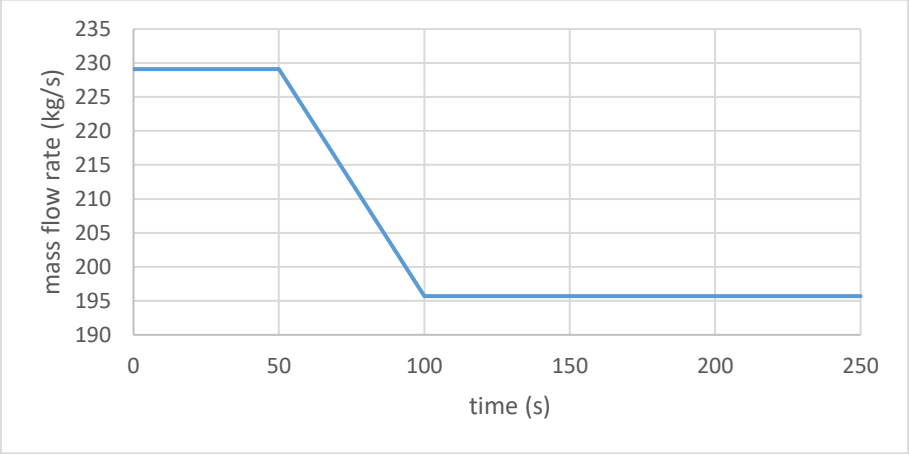

Fig 5.2 First case, jacket water mass flow rate

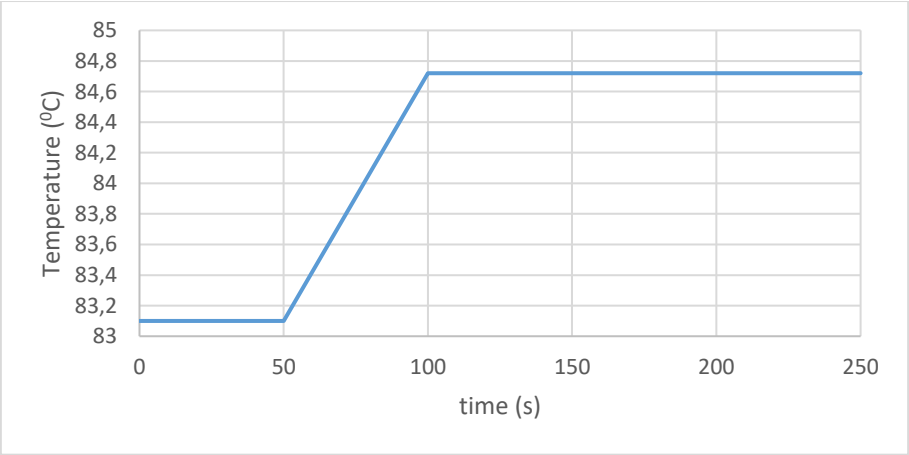

Fig 5.3 First case, jacket water temperature

Outputs:

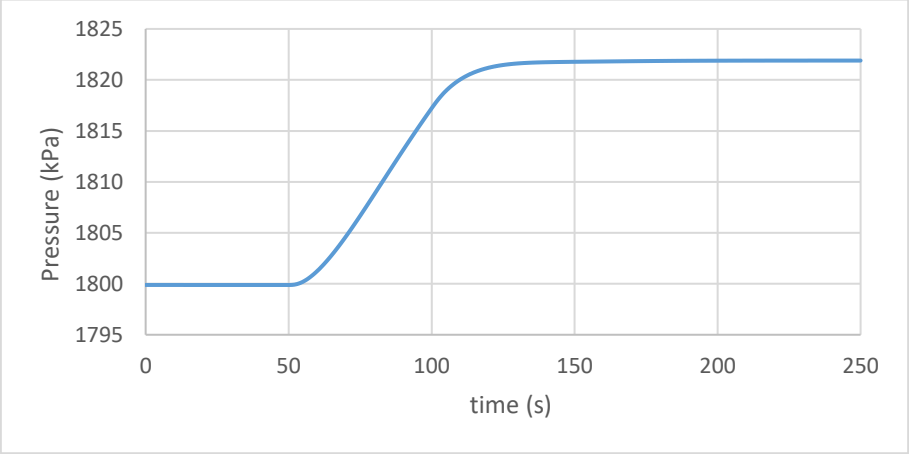

Fig 5.4 First case, evaporation pressure

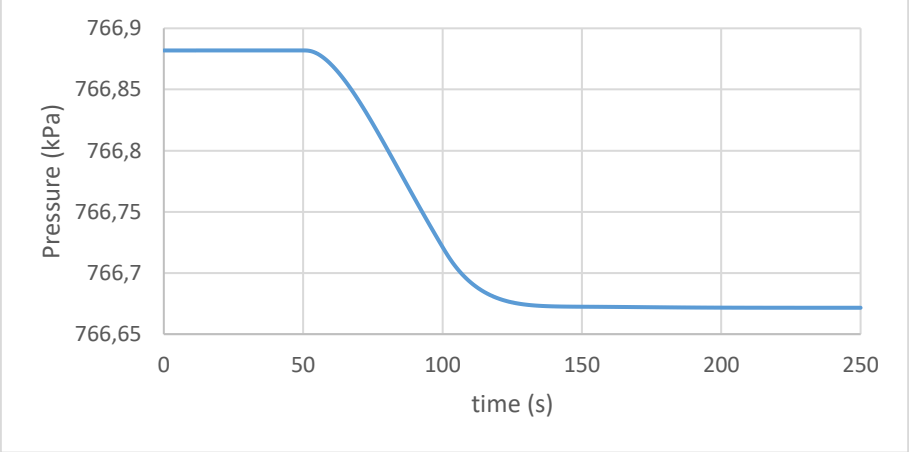

Fig 5.5 First case, condensation pressure

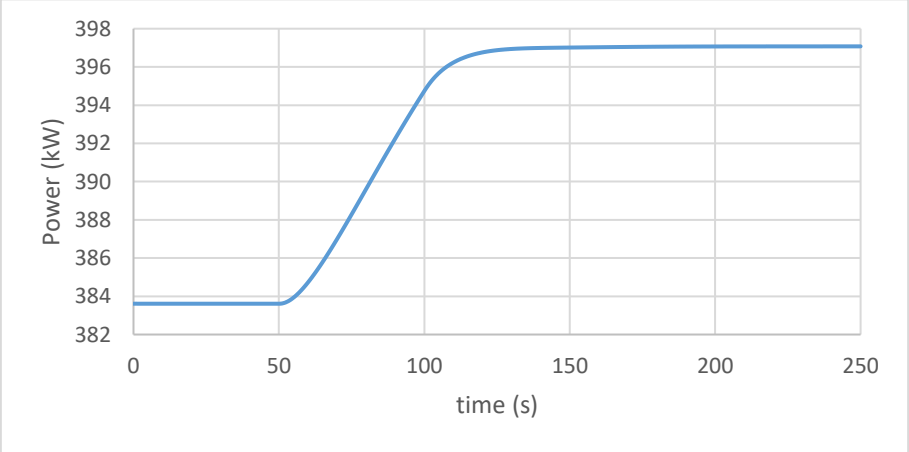

Fig 5.6 First case, net power

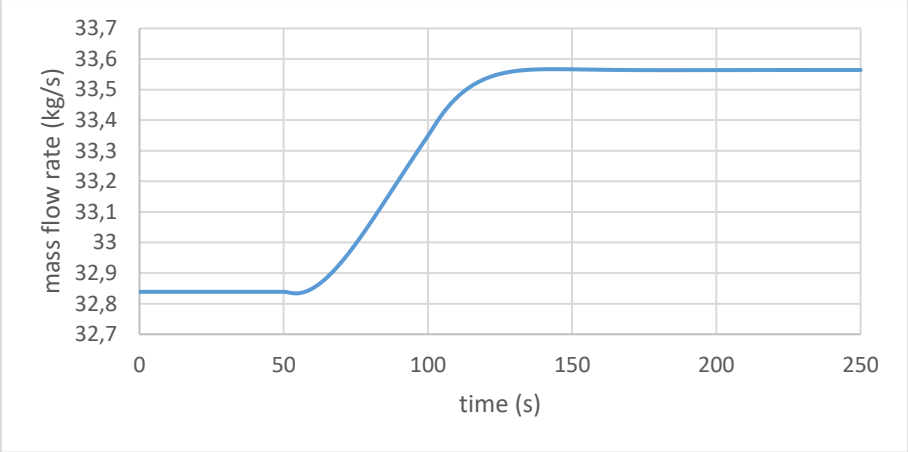

Fig 5.7 First case, turbine mass flow rate

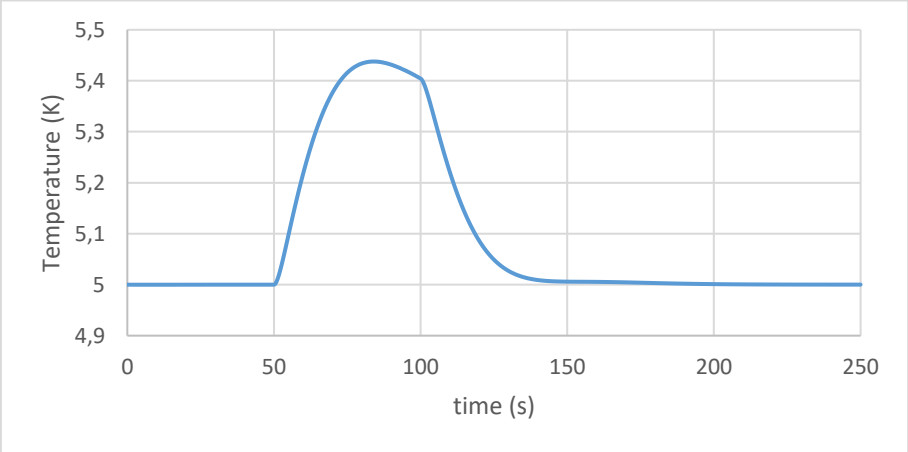

Fig 5.8 First case, superheating

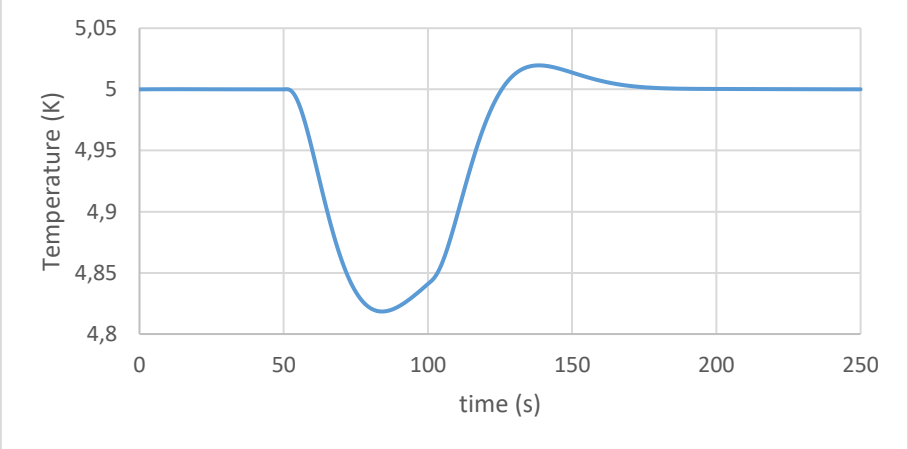

Fig 5.9 First case, subcooling

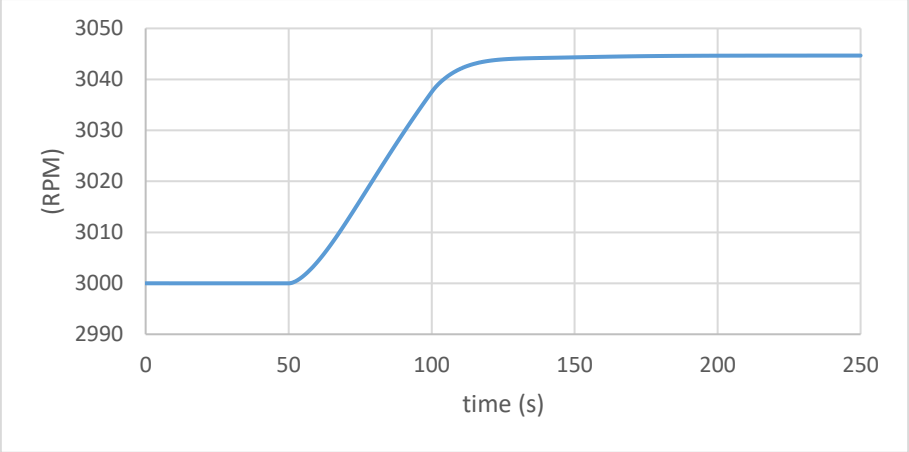

Fig 5.10 First case, pump rotational speed

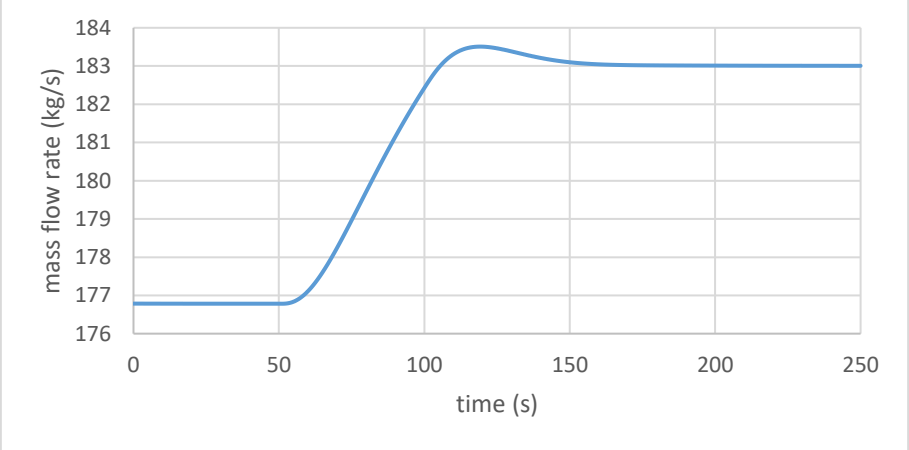

Fig 5.11 First case, cold source mass flow rate

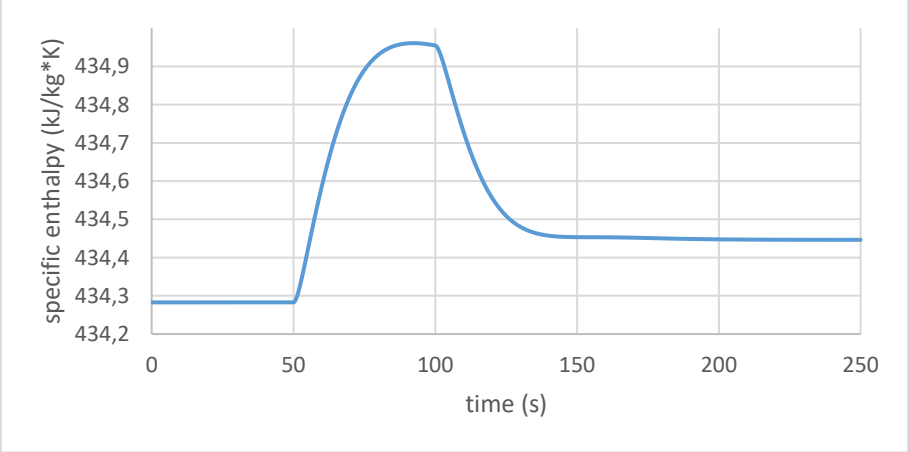

Fig 5.12 First case, turbine inlet enthalpy

Remarks:

1) The superheating is increasing as the ships load is increasing and the temperature of the hot source is increasing as well
2) The control system starts to increase he RPM of the pump as a response to the rise of the superheating. This results in bigger mass flow rate passing through the pump and so the pressure in the evaporator is rising
3) The power produced by the ORC is increasing as the load of the ship changes. This is done because both bigger mass flow rate of organic fluid runs through the system and the specific work of the turbine and is increasing
4) An increasing cooling power is demanded from the condenser, throughout the transient period, while the control system tries to maintain subcooling at the nominal value. This happens because both the mass flow rate of the ORC and superheating are increasing
5) Through various simulations it was found that superheating has a dominant impact in the condenser. As vapor has much lower a' than liquid, an increase in superheating means that there is much less available surface in the heat exchanger to cool the liquid in the desired conditions
6) The pressure of the condenser is relatively constant, only a small change is happening. The pressure is relatively constant because the condenser contains mainly low density compressible vapor and because the temperature of the cold source remains constant
7) Finally, the control strategy proposed is able to maintain the cycle under safe conditions in the transient period and reach steady conditions after, without oscillations and overshoots

5.2 Second case

The two hot sources-two subcritical pressure levels model is applied for several working fluids in order to find the one that maximizes the power output. The working fluids that have been thought to be suitable for the application are the following: R-134a, R-125, R-245ca, R-245fa, R-227ea, RC-318. The results are summarized in the next table

Table 5.3 Second case design point for various working fluids

	R-245ca	R-134a	R-125	R-227ea	R-245fa	RC-318
$P_{evap,LP}$ (kPa)	319,8	1653,99	3121,74	994,65	452,12	705,61
$P_{evap,HP}$ (kPa)	885,16	2164,24	2313,46	1684,67	1284,76	1632,41
P_{cond} (kPa)	120,99	766,88	1562,54	526,09	176,84	363,88
$T_{evap,LP}$ (°C)	59,35	59,45	59,45	53,37	59,35	53,37
$T_{evap,HP}$ (°C)	98,1	71,14	46,14	75,68	100,86	89,12
T_{cond} (°C)	30	30	30	30	30	30
$\Delta T_{sup,LP}$ (°C)	5	5	5	5	5	5
$\Delta T_{sup,HP}$ (°C)	5	5	5	5	5	5
ΔT_{sub} (°C)	5	5	5	5	5	5
$T''_{out,LP}$ (°C)	76,3	76,3	76,3	76,3	76,3	76,3
$T''_{out,HP}$ (°C)	79,8	46,12	44,15	44,15	77,91	44,15
$\eta_{is,turb,LP}$	0,63	0,74	0,77	0,76	0,67	0,75
$\eta_{is,turb,HP}$	0,75	0,75	0,75	0,75	0,75	0,75
$\eta_{is,pump}$	0,7	0,7	0,7	0,7	0,7	0,7
$m_{ORC,LP}$ (kg/s)	13,16	15,53	25,49	23,1	13,94	24,19
$m_{ORC,HP}$ (kg/s)	16,05	28,34	47,69	40,17	17,35	39,26
m_{cold} (kg/s)	178,72	236,2	244,8	216,68	181,2	203,75
$W_{turb,LP}$ (kW)	152,69	182,42	190,51	145,84	161,01	140,82
$W_{pump,LP}$ (kW)	2,69	16,27	47,31	11,12	4,09	7,87
$W_{net,LP}$ (kW)	150	166,14	143,2	134,71	156,92	132,95
φ_{LP} (%)	4,74	4,74	4,74	4,74	4,74	4,74
$\eta_{thermal,LP}$ (%)	4,88	5,41	4,66	4,39	5,11	4,33
$\eta_{total,LP}$ (%)	0,23	0,26	0,22	0,21	0,24	0,21
$W_{turb,HP}$ (kW)	468,72	446,05	211,21	455,5	489,18	525,44
$W_{pump,HP}$ (kW)	12,62	46,74	42,76	47,76	20,49	47,35
$W_{net,HP}$ (kW)	456,1	399,31	168,45	407,74	468,69	478,09
φ_{HP} (%)	58,91	79,32	80,52	80,52	60,05	80,52
$\eta_{thermal,HP}$ (%)	10,81	7,03	2,92	7,07	10,89	8,29
$\eta_{total,HP}$ (%)	6,37	5,57	2,35	5,69	6,54	6,67
$W_{net,tot}$ (kW)	606,09	565,46	311,65	542,45	625,61	611,04

The optimum scenario as it can be seen is usage of R245fa as working fluid. For this, the T-s diagram is constructed:

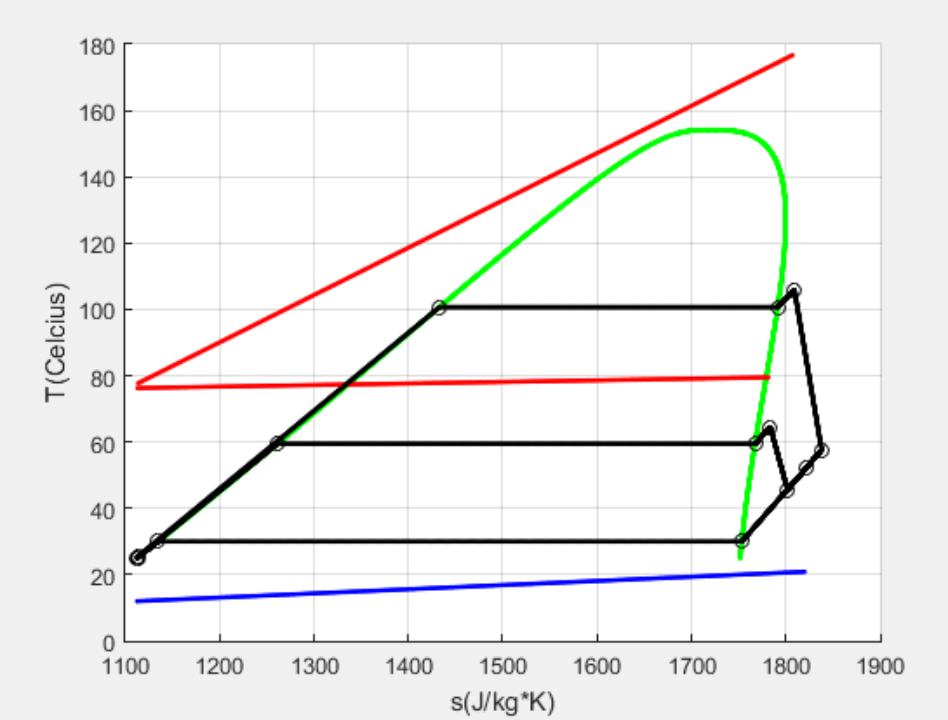

Fig 5.13 Second case T-s diagram

For the optimum scenario the shell-n-tube heat exchangers are designed and their mean features are shown in the table below:

Table 5.4 Second case, characteristics of shell-n-tubes

	Evap HP	Evap LP	Cond
d_{in} (mm)	5	10	10
d_{out} (mm)	6	12	12
Nt	1076	434	1041
p_t (mm)	9,6	16,8	16,8
B_s	1,51	1,09	1,09
D_s (m)	0,37	0,42	0,64
De (mm)	10,94	13,94	13,94
Re''	8541,77	69062,76	14771,81
α'' (kW/m^2*K)	0,34	10,35	5,55
Re'_L	9995,75	9992,49	10001,68
α_{pre}(kW/m^2*K)	1,11	0,55	0,83
$\alpha_{evap}/\alpha_{cond}$ (kW/m^2*K)	6,84	6,57	5,32
$\alpha_{sup}/\alpha_{sub}$ (kW/m^2*K)	2,19	0,93	0,54
L (m)	12,59	5,25	6,52

The dynamic behavior of the system during an increase of ships load from 85% to 100% within 50 seconds is being studied here. This results in a change of both jacket water temperature and mass flow rate. The temperature is increasing 1.62 K and the mass flow rate decreasing 33.4 kg/s during the transient period.

The system starts from the design point of 85% load as stated before and remains as it is for 50 secs in order to assure it starts from a stable condition. Then from 50 secs till 100 secs the load change takes place and from 100 secs till 250 secs the system reaches steady state conditions again, with superheating and subcooling returning to their nominal values. The results are presented below in the form of diagrams:

Inputs:

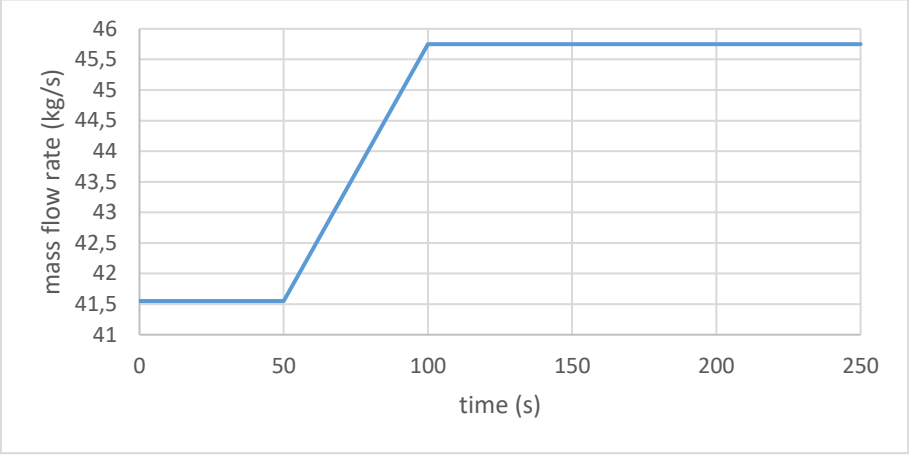

Fig 5.14 Second case, supercharge air mass flow rate

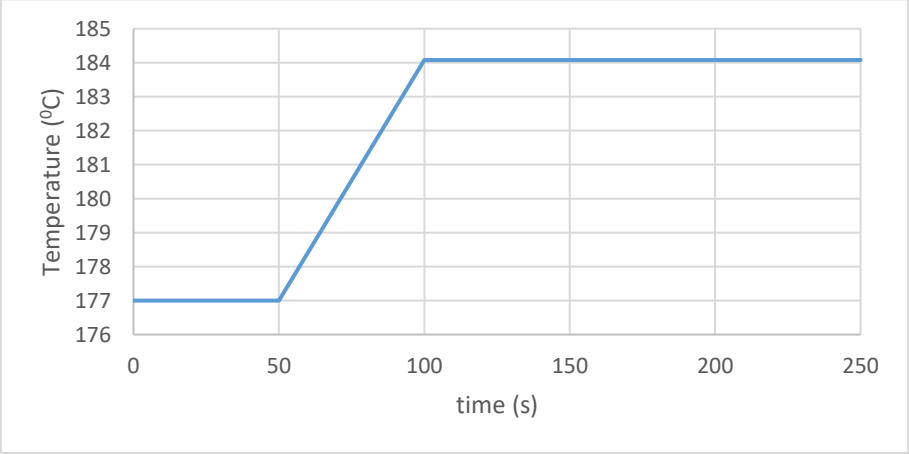

Fig 5.15 Second case, supercharge air temperature

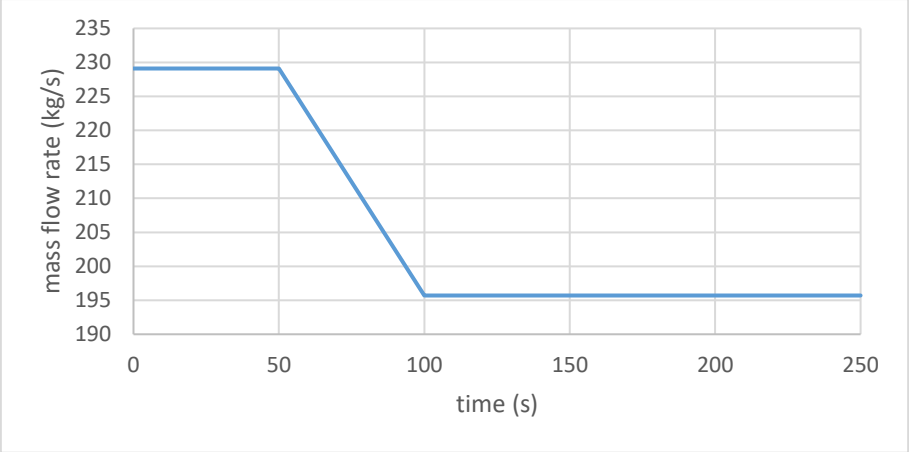

Fig 5.16 Second case, jacket water mass flow rate

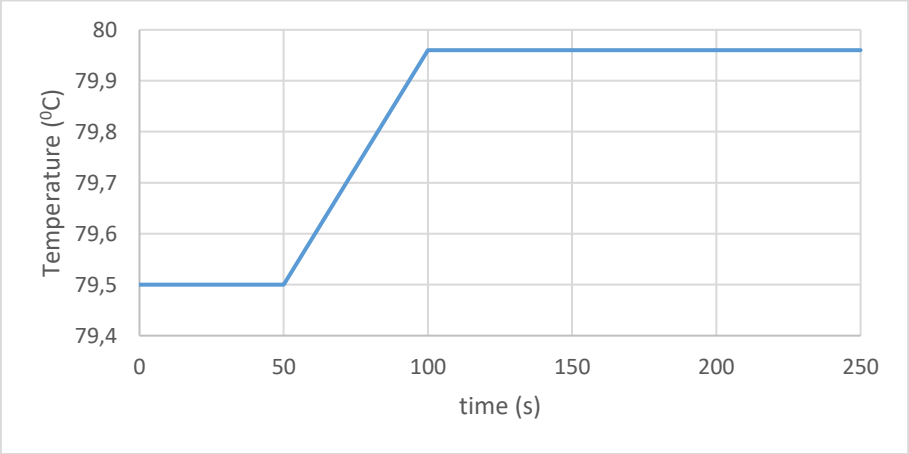

Fig 5.17 Second case, jacket water temperature

Outputs:

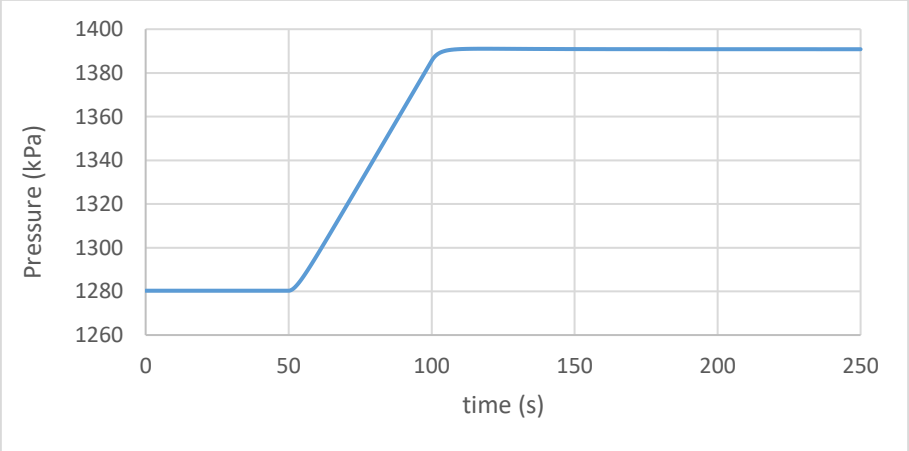

Fig 5.18 Second case, high evaporation pressure

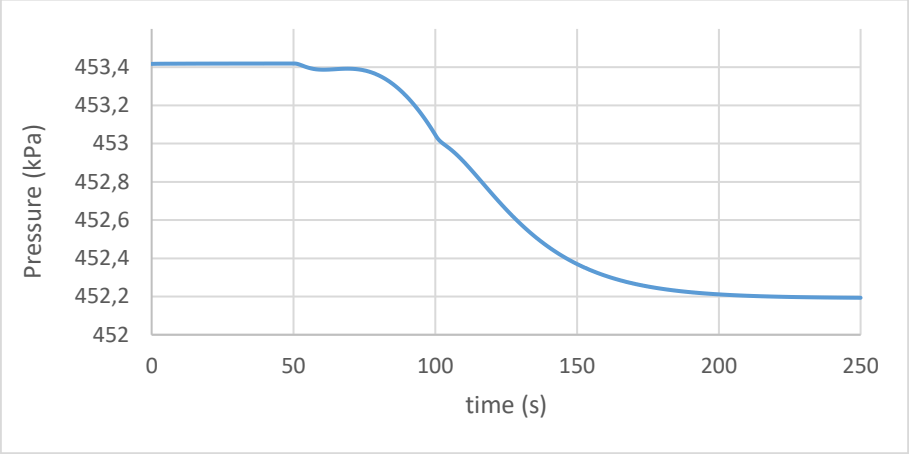

Fig 5.19 Second case, low evaporation pressure

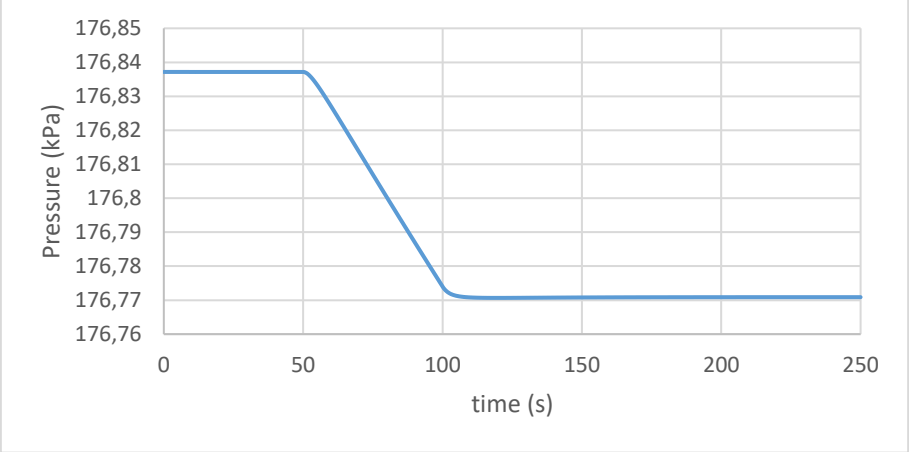

Fig 5.20 Second case, condensation pressure

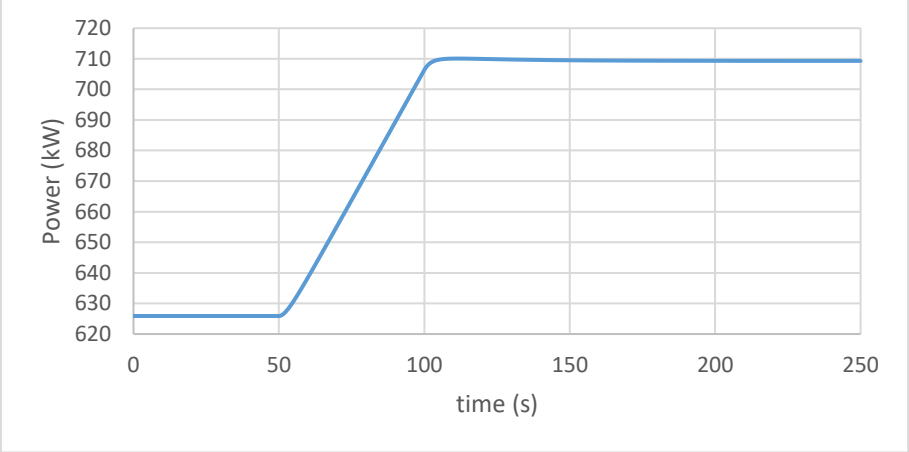

Fig 5.21 Second case, net power

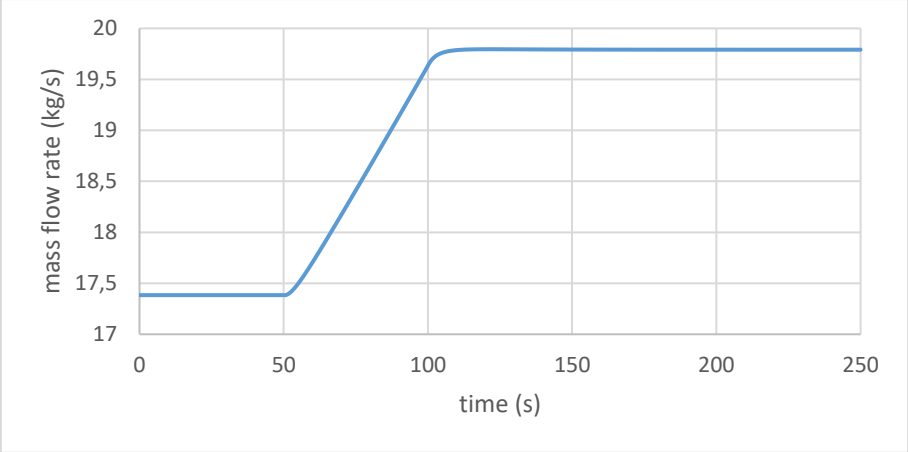

Fig 5.22 Second case, high pressure turbine mass flow rate

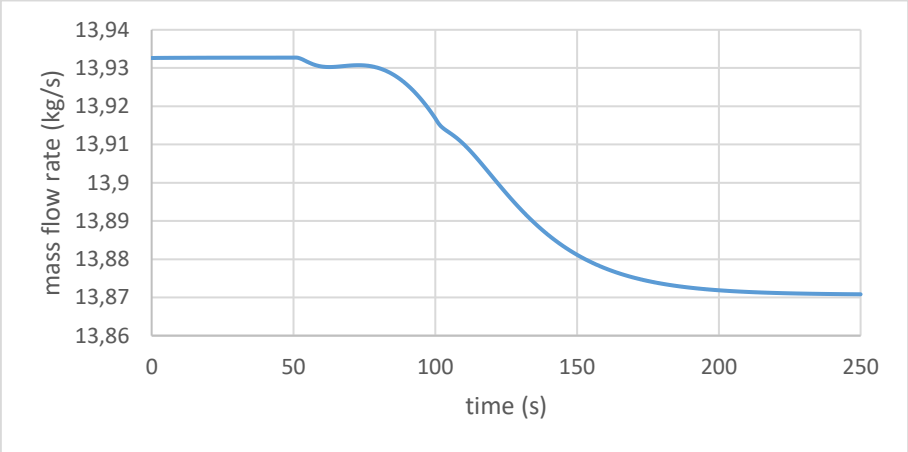

Fig 5.23 Second case, low pressure turbine mass flow rate

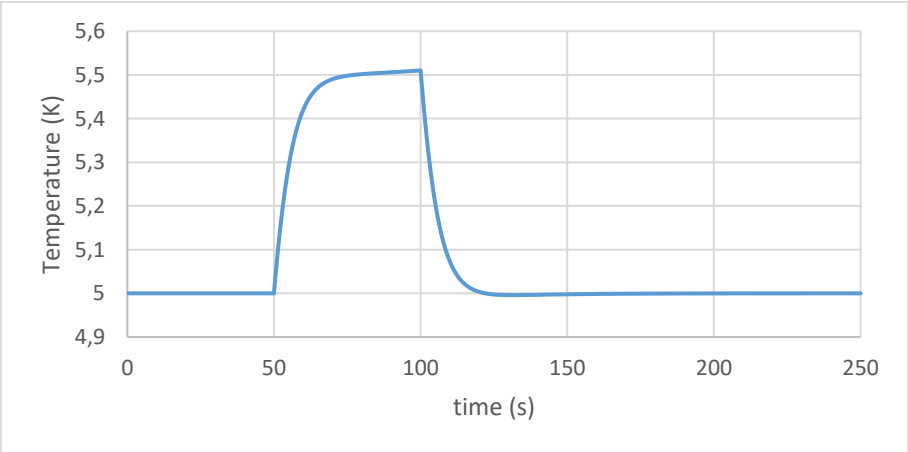

Fig 5.24 Second case, high pressure level superheating

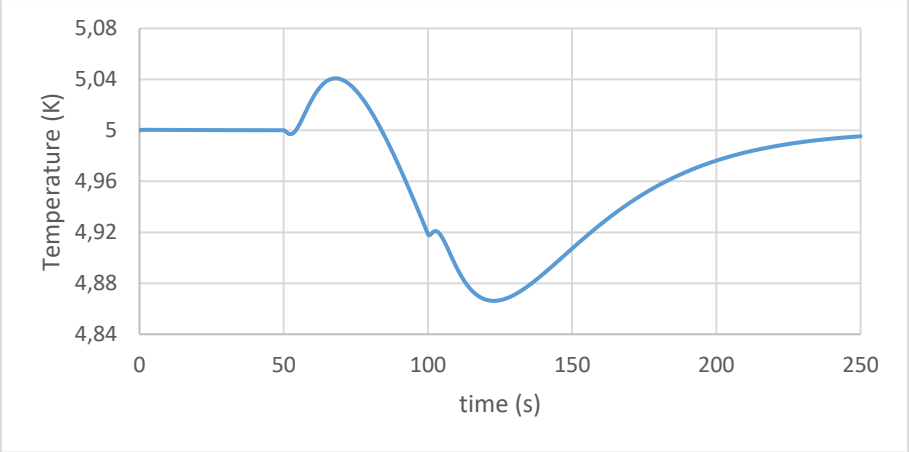

Fig 5.25 Second case, low pressure level superheating

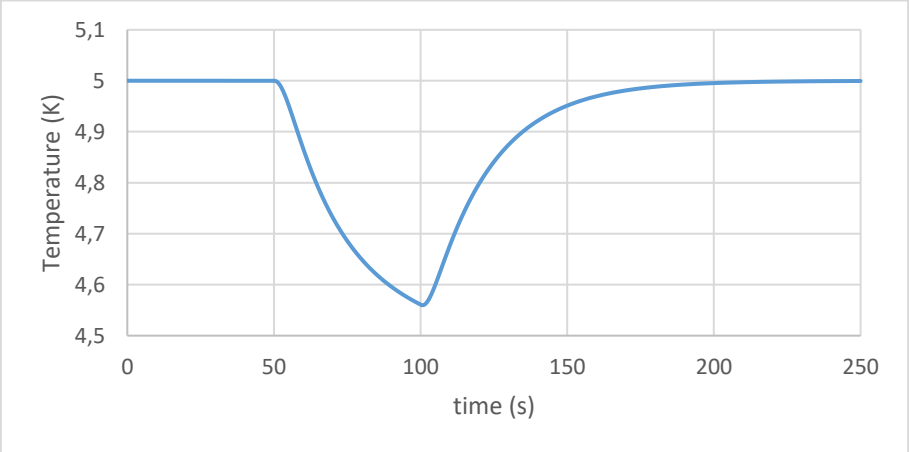

Fig 5.26 Second case, subcooling

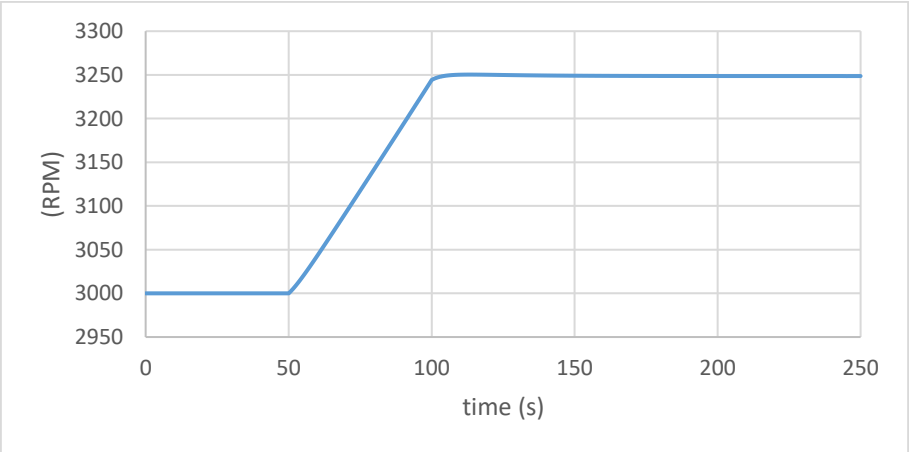

Fig 5.27 Second case, high pressure pump rotational speed

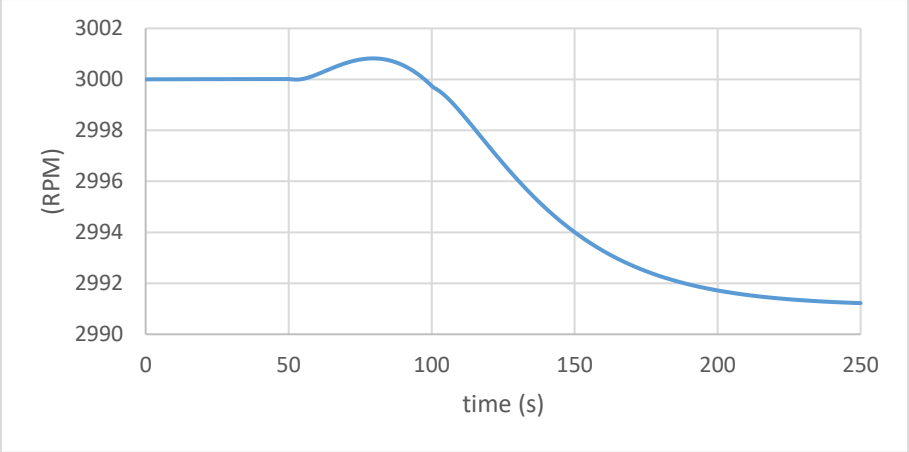

Fig 5.28 Second case, low pressure pump rotational speed

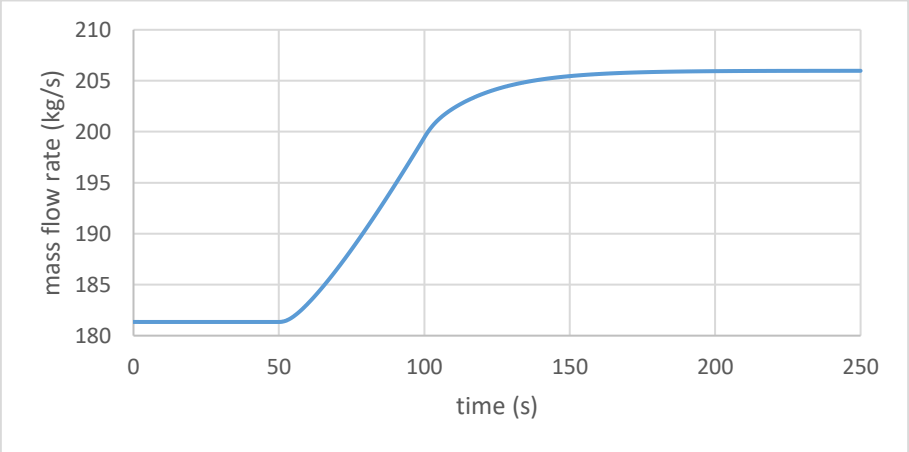

Fig 5.29 Second case, cold source mass flow rate

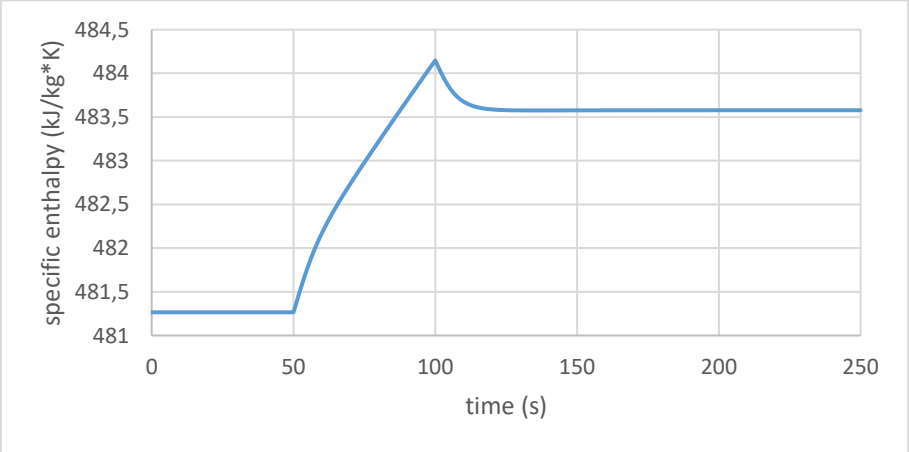

Fig 5.30 Second case, high pressure turbine inlet enthalpy

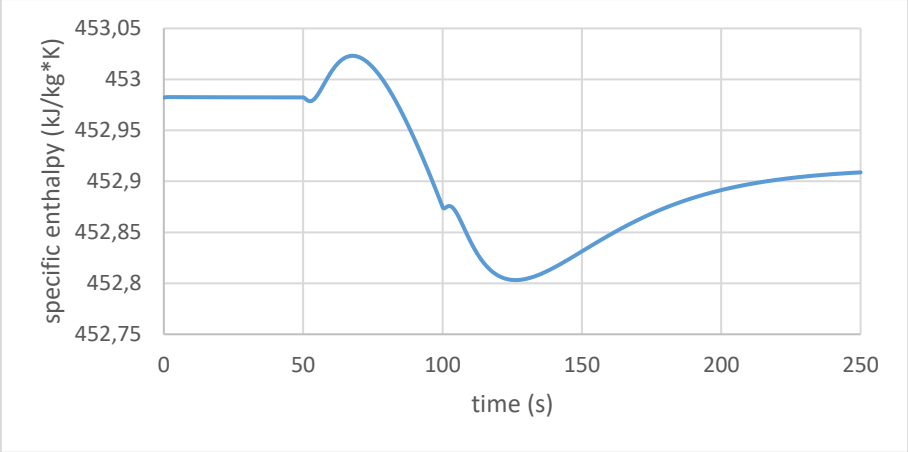

Fig 5.31 Second case, low pressure turbine inlet enthalpy

Remarks:

1) The superheating of the high pressure level is increasing as the ships load is increasing and the temperature of the supercharge air is increasing as well
2) The subcooling is decreasing as it is expected, because the mass flow rate running through the condenser is increasing and also the superheating of the high pressure level is increasing. The air temperature and mass flow rate change much more than the water ones, demanding an increasing cooling power from the condenser in order to maintain subcooling at the nominal value
3) The control system starts to increase he RPM of the high pressure pump. This results in bigger mass flow rate passing through the pump and so the pressure in the high pressure evaporator in rising
4) Because the subcooling is decreasing, in the begging the superheating of the low pressure level is increasing although the mass flow rate of the water is decreasing. After 25 seconds it starts decreasing for 50 seconds, obtaining value lesser than 5 ^{o}C, and by the end of the simulation it reaches the nominal value of 5 ^{o}C again.
5) The high pressure evaporator pressure is increasing 120 kPa while the low pressure is decreasing 1,2 kPa. This is done because the thermodynamic characteristics of the supercharge air change much more than the ones of the jacket water and the control system of each evaporator reacts separately. The final pressure is formed by the Stodola coefficient K_t, as it connects the pressure levels with the mass flow rate passing through the turbine

6) The pressure of the condenser is relatively constant, as the one of the high pressure evaporator is increasing and the one of the low pressure evaporator is decreasing. Also it contains mainly low density compressible vapor and the temperature of the cold source remains constant.
7) The power produced by the ORC is increasing significantly as the load of the ship changes. This is done because both bigger mass flow rate runs through the high pressure turbine and also the its specific power is greater. On the other hand, in the magnitudes which are connected to the jacket water happens the opposite, but the increase of the HP magnitudes is much greater
8) Finally, the control strategy proposed is able to maintain the cycle under safe conditions through the transient period and reach steady conditions after, without oscillations and overshoots in most of the magnitudes

5.3 Third case

The two hot sources-two pressure levels model, one subcritical and one supercritical, is applied for several working fluids in order to find the one that maximizes the power output. The working fluids that have been thought to be suitable for the application are the following: R-134a, R-125, R-227ea, RC-318. The results are summarized in the next table

Table 5.5 Third case design point for various working fluids

	R-134a	R-125	R-227ea	RC-318
$P_{evap,LP}$ (kPa)	1620,5	2642,27	1132,28	807
$P_{evap,HP}$ (kPa)	6279,25	8257,65	5708,83	4514,25
P_{cond} (kPa)	766,88	1562,54	526,09	363,88
$T_{evap,LP}$ (ºC)	58,59	51,95	58,59	58,6
$T_{evap,HP}$ (ºC)	138,53	123,57	143,73	141,71
T_{cond} (ºC)	30	30	30	30
$\Delta T_{sup,LP}$ (ºC)	5	5	5	5
ΔT_{sub} (ºC)	5	5	5	5
$s_{turb,in}$ (kJ/kg·K)	1,72	1,53	1,56	1,52
$T''_{out,LP}$ (ºC)	76,3	76,3	76,3	76,3
$T''_{out,HP}$ (ºC)	59,83	48,17	52,51	49,96
$\eta_{is,turb,LP}$	0,74	0,78	0,74	0,73
$\eta_{is,turb,HP}$	0,75	0,75	0,75	0,75
$\eta_{is,pump}$	0,7	0,7	0,7	0,7
$m_{ORC,LP}$ (kg/s)	15,55	25,33	22,63	23,59
$m_{ORC,HP}$ (kg/s)	23,6	39	33,1	36,2
m_{cold} (kg/s)	210,78	215,22	190,84	191,99
$W_{turb,LP}$ (kW)	178,66	153,04	168	161,33
$W_{pump,LP}$ (kW)	15,68	32,62	14,1	9,95
$W_{net,LP}$ (kW)	162,98	120,42	153,9	151,38
φ_{LP} (%)	4,74	4,74	4,74	4,74
$\eta_{thermal,LP}$ (%)	5,31	3,92	5,01	4,93
$\eta_{total,LP}$ (%)	0,25	0,19	0,24	0,23
$W_{turb,HP}$ (kW)	709,77	738,78	721,89	705,4
$W_{pump,HP}$ (kW)	152,59	305,98	174,73	142,18
$W_{net,HP}$ (kW)	557,18	432,8	547,16	563,22
φ_{HP} (%)	71,01	78,08	75,45	77
$\eta_{thermal,HP}$ (%)	10,95	7,74	10,12	10,21
$\eta_{total,HP}$ (%)	7,78	6,04	7,64	7,86
$W_{net,tot}$ (kW)	720,16	553,22	701,07	714,6

The optimum scenario as it can be seen is usage of R134a as working fluid. For this, the T-s diagram is constructed:

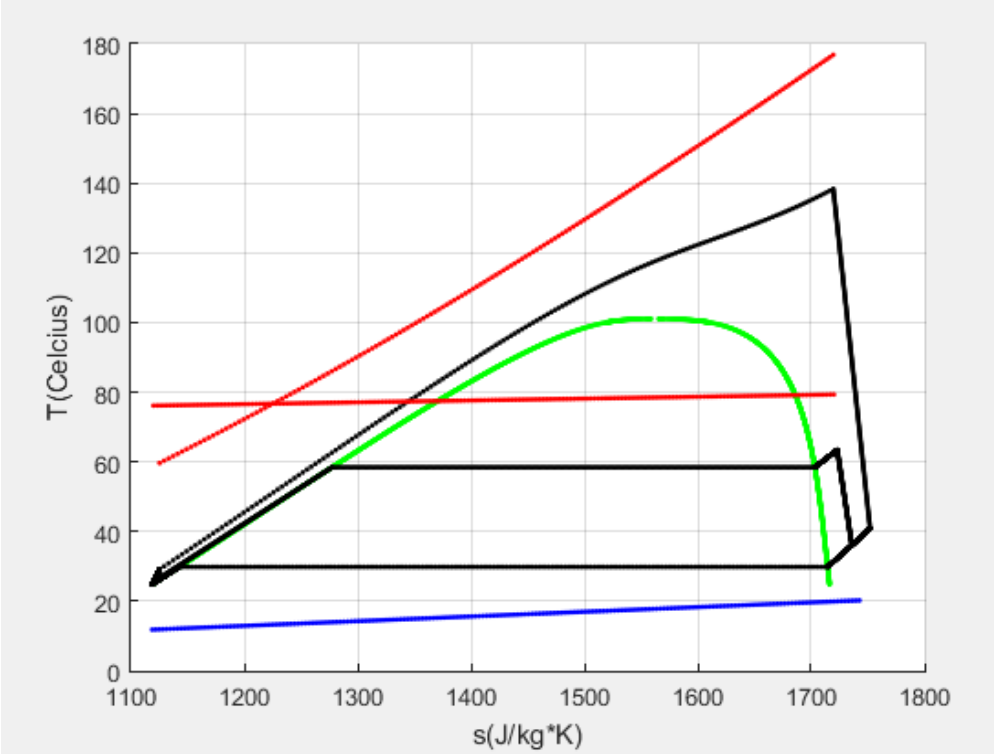

Fig 5.32 Third case T-s diagram

For the optimum scenario the shell-n-tube heat exchangers are designed and their mean features are shown in the table below:

Table 5.6 Third case, characteristics of shell-n-tubes

	Evap HP	Evap LP	Cond
d_{in} (mm)	6	14	14
d_{out} (mm)	7,2	16,8	16,8
Nt	2449	718	1941
p_t (mm)	11,52	23,52	23,52
B_s	1,73	1,4	1,4
D_s (m)	0,68	0,75	1,23
De (mm)	13,12	19,51	19,51
Re''	4938,26	41718,68	9769,76

α'' (kW/m^2*K)	0,21	5,6	3,16
Re'_L	10001,57	9998,62	9999,54
α_{pre}(kW/m^2*K)	0	0,31	0,16
$\alpha_{evap}/\alpha_{cond}$ (kW/m^2*K)	0	0,4	0,3
$\alpha_{sup}/\alpha_{sub}$ (kW/m^2*K)	0	1,73	1,74
$\alpha_{supercrit}$(kW/m^2*K)	0,63	0	0
L (m)	12,11	5,56	7,5

The dynamic behavior of the system is being studied now. The case that is studied is the increase of ships load from 85% to 100% within 50 seconds. This results in a change both in the of jacket's water temperature and mass flow rate. The temperature is increasing 1.62 K and the mass flow rate decreasing 33.4 kg/s during the transient period.

The system starts from the design point of 85% load as stated before and remains as it is for 50 secs in order to assure it starts from a stable condition. Then from 50 secs till 100 secs the load change takes place and from 100 secs till 300 secs the system reaches steady state conditions again, with superheating and subcooling returning to their nominal values. The results are presented below in the form of diagrams:

Inputs:

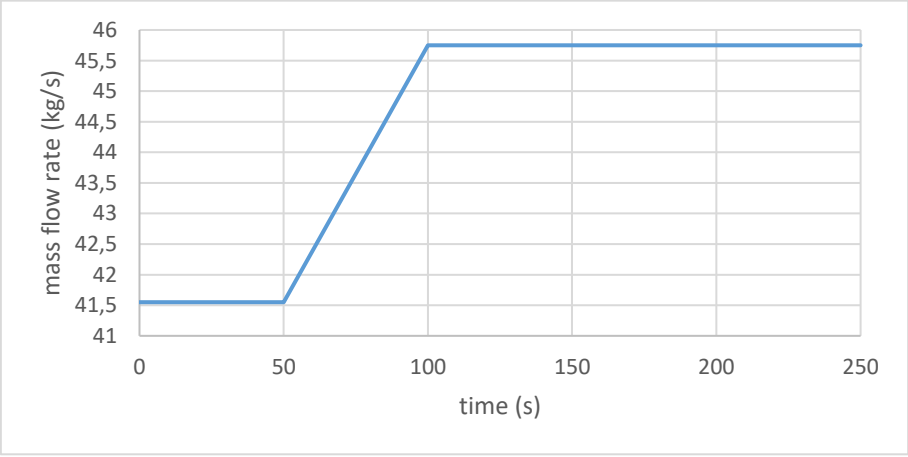

Fig 5.33 Third case, supercharge air mass flow rate

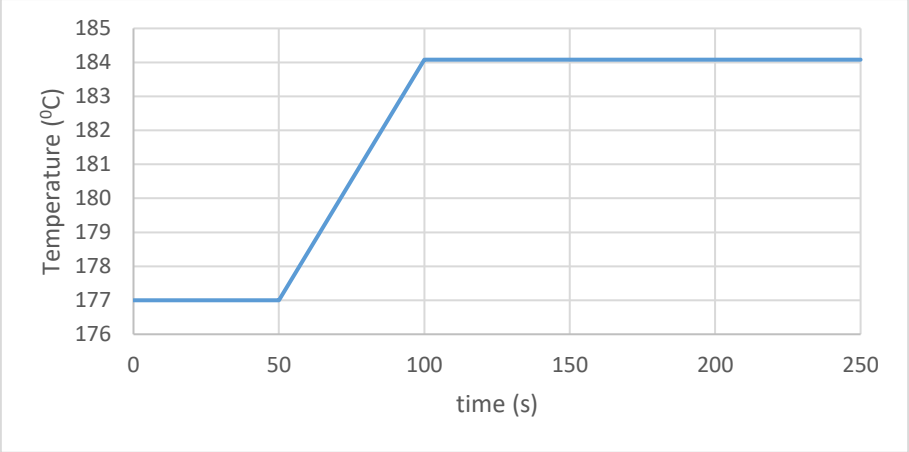

Fig 5.34 Third case, supercharge air temperature

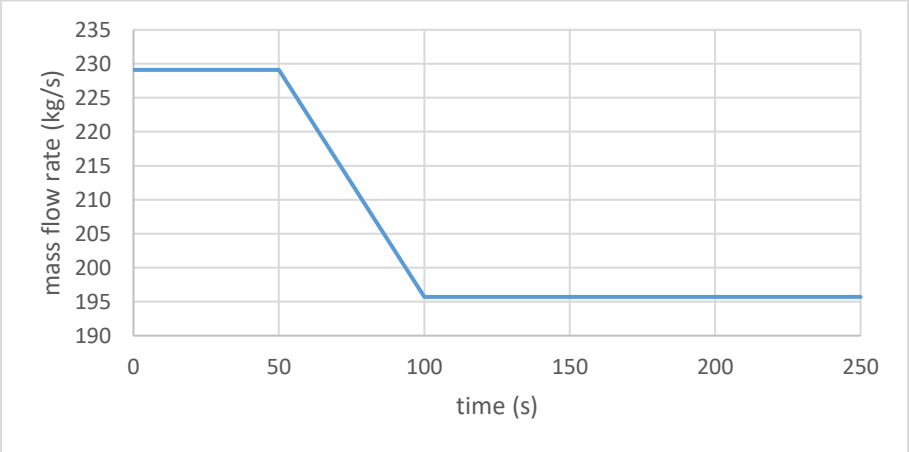

Fig 5.35 Third case, jacket water mass flow rate

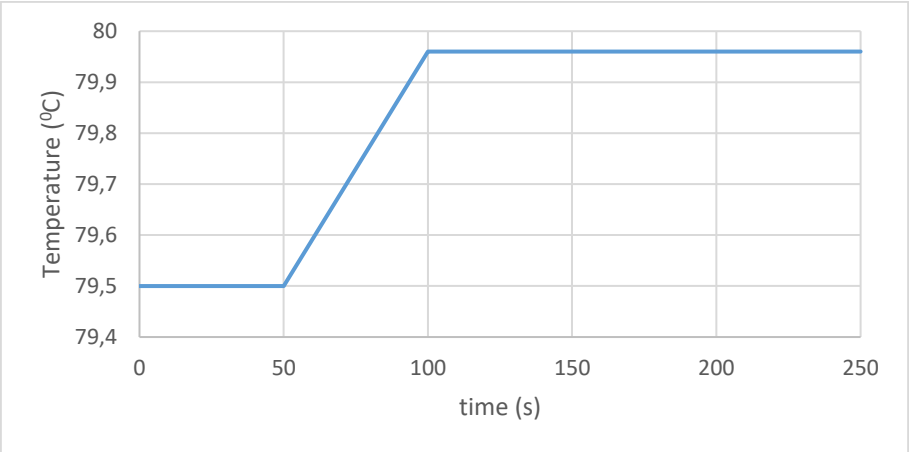

Fig 5.36 Third case, jacket water temperature

Outputs:

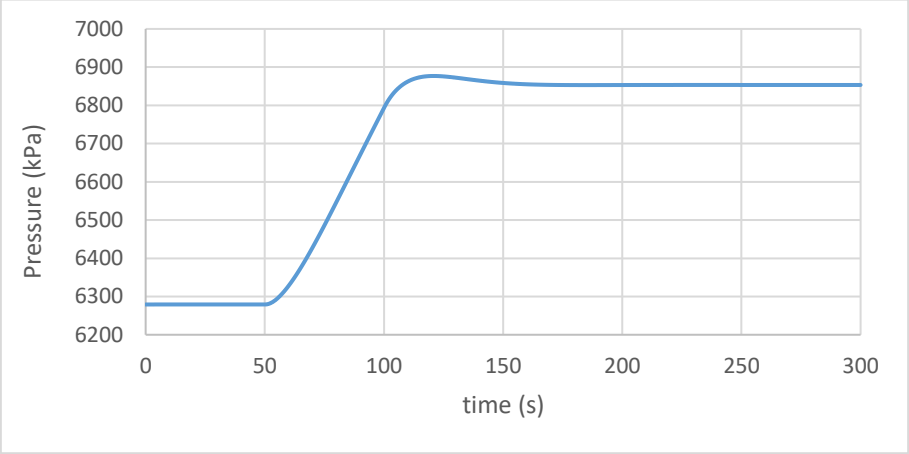

Fig 5.37 Third case, high evaporation pressure

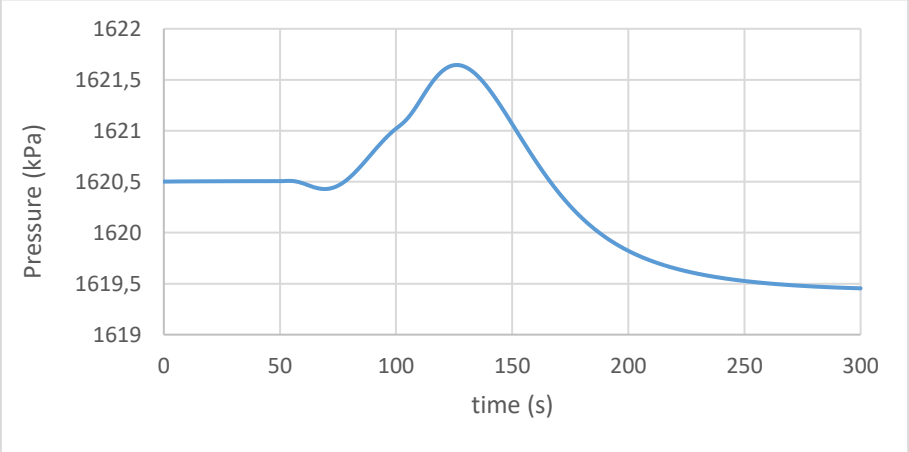

Fig 5.38 Third case, low evaporation pressure

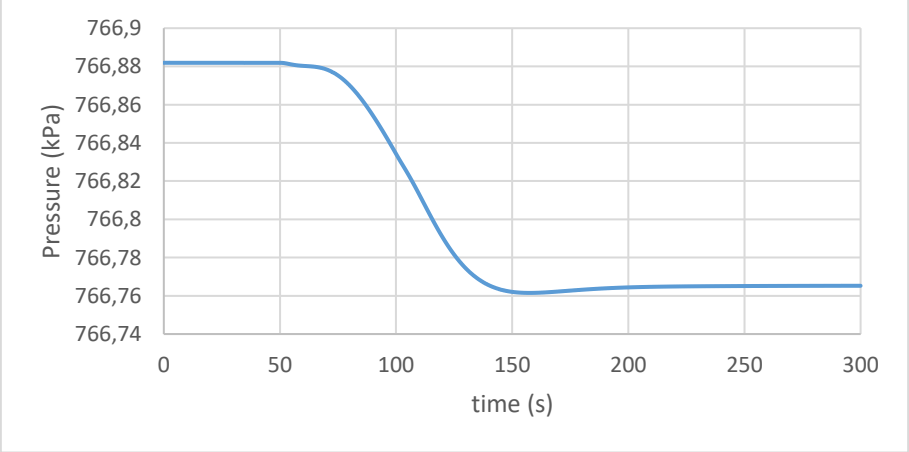

Fig 5.39 Third case, condensation pressure

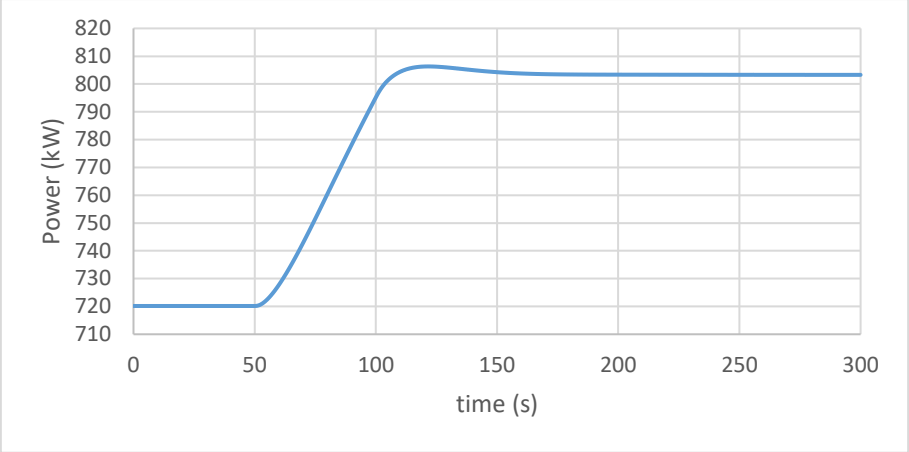

Fig 5.40 Third case, net power

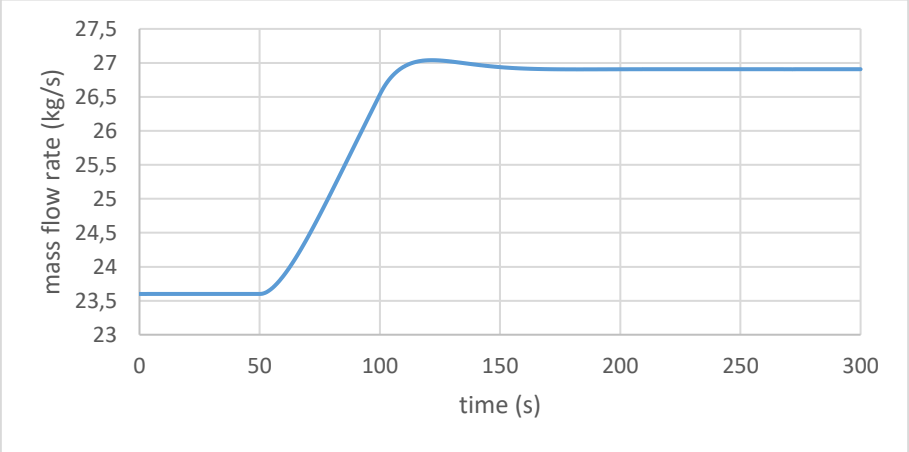

Fig 5.41 Third case, high pressure turbine mass flow rate

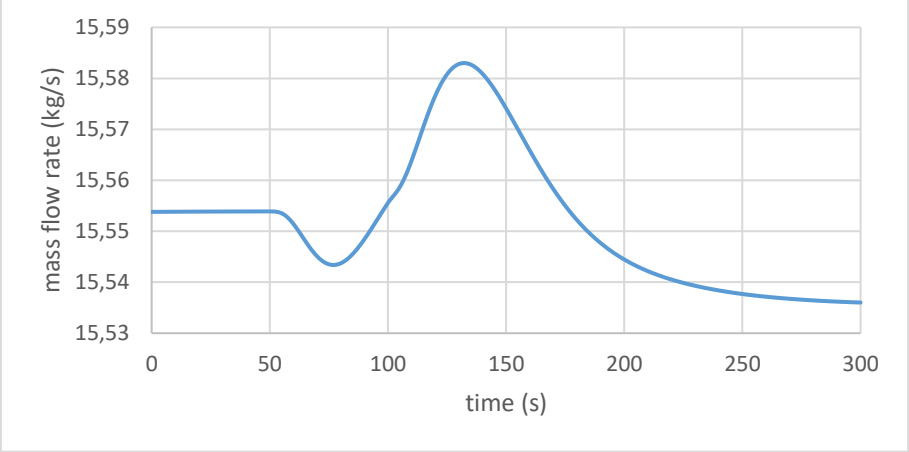

Fig 5.42 Third case, low pressure turbine mass flow rate

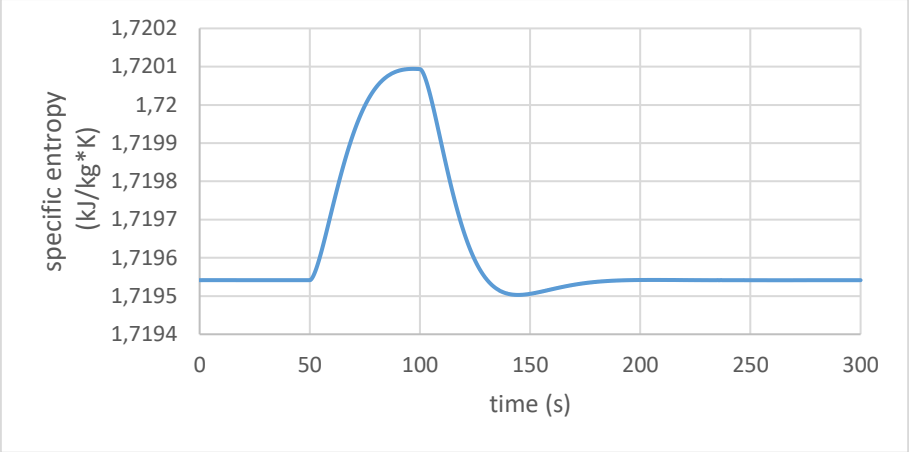

Fig 5.43 Third case, high pressure turbine inlet specific entropy

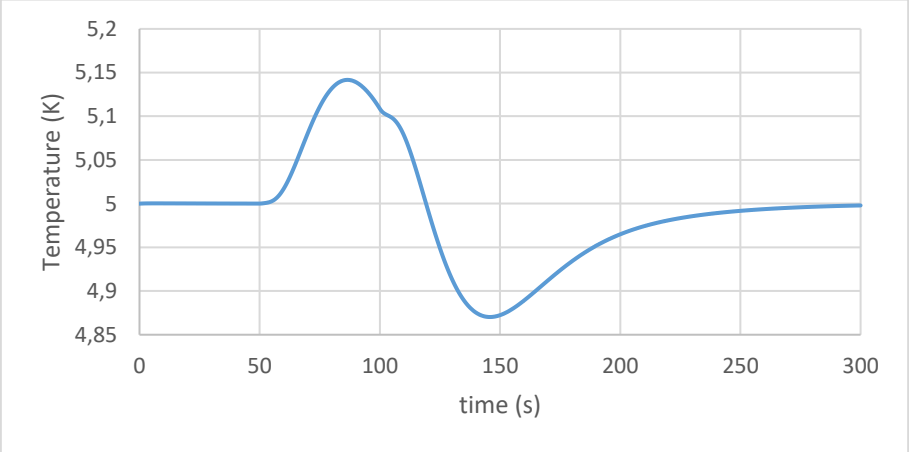

Fig 5.44 Third case, low pressure level superheating

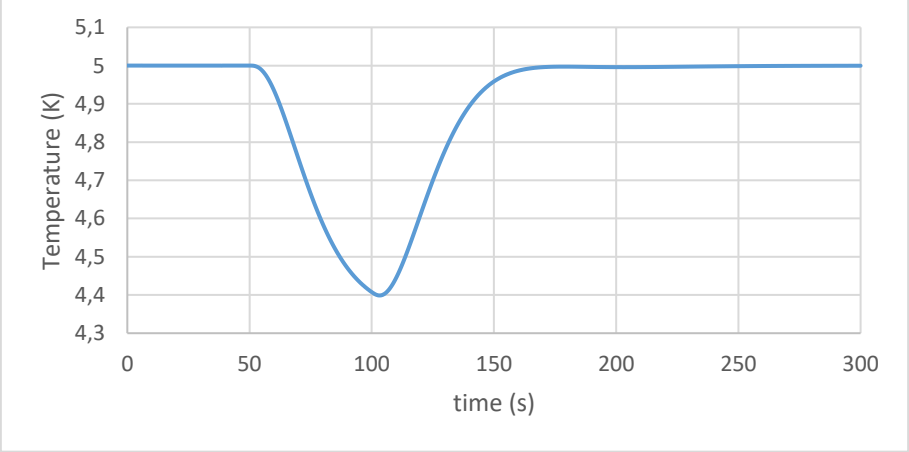

Fig 5.45 Third case, subcooling

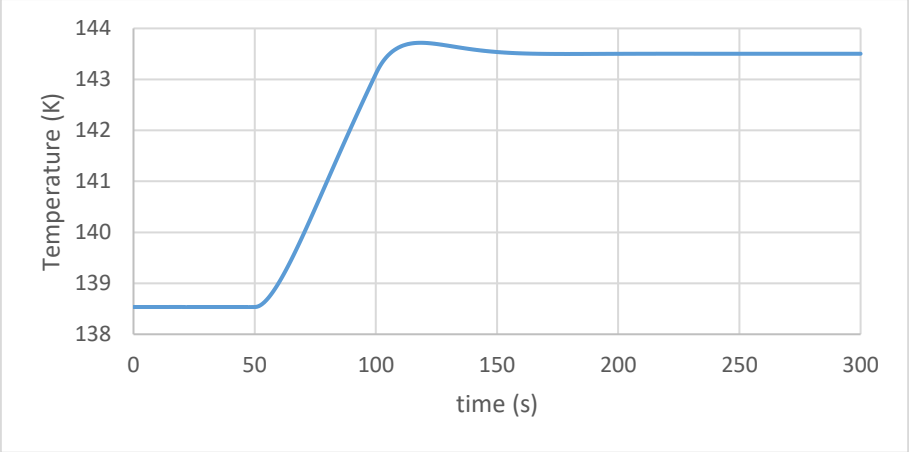

Fig 5.46 Third case, high pressure turbine inlet temperature

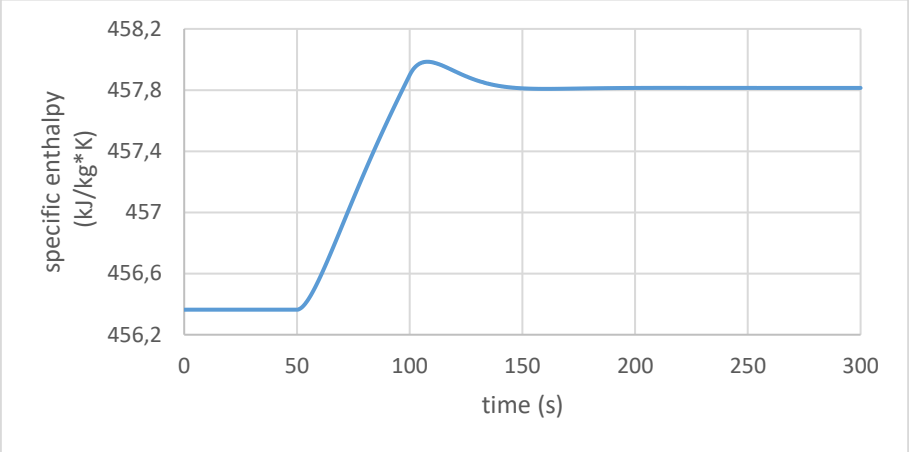

Fig 5.47 Third case, high pressure turbine inlet specific enthalpy

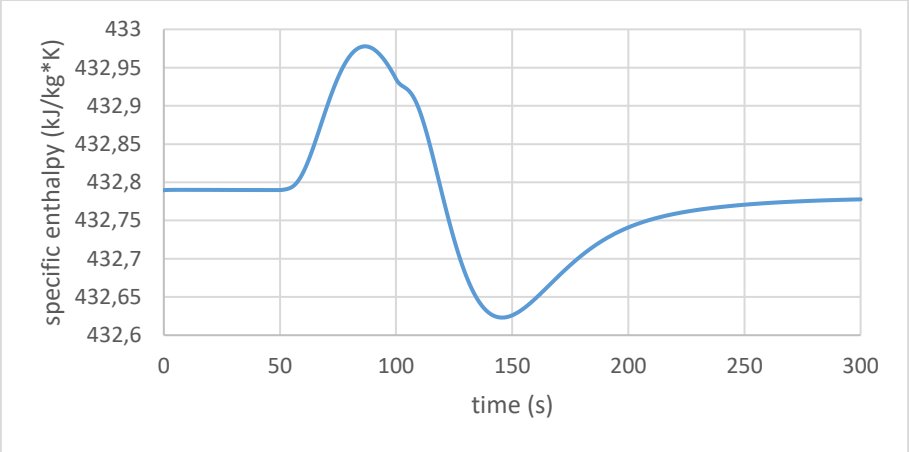

Fig 5.48 Third case, low pressure turbine inlet specific enthalpy

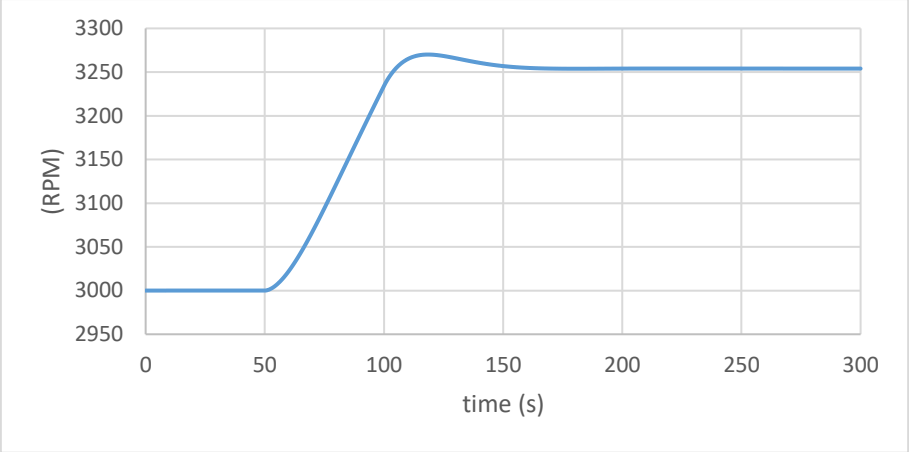

Fig 5.49 Third case, high pressure pump rotational speed

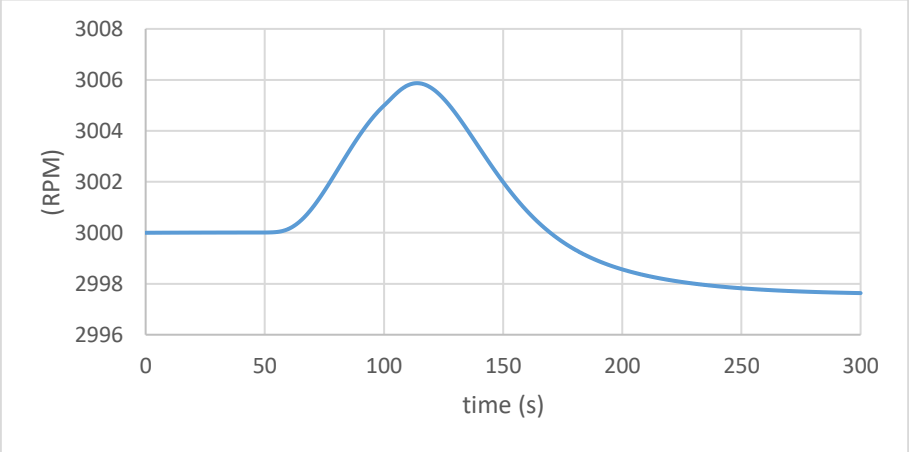

Fig 5.50 Third case, low pressure pump rotational speed

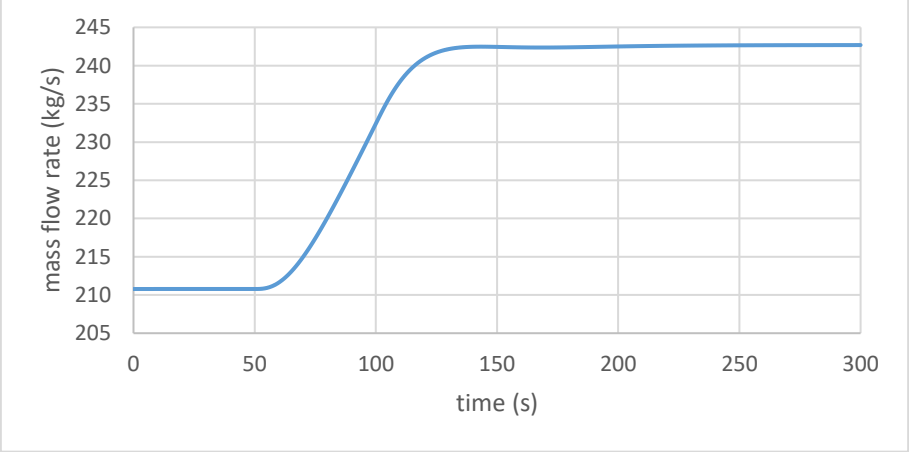

Fig 5.51 Third case, cold source mass flow rate

Remarks:

1) The $T_{turb,in,HP}$ and $s_{\mathrm{turb,in}}$ are increasing as the ships load is increasing and the temperature of the supercharge air is increasing as well
2) ΔT_{sub} is decreasing as it is expected, because the $\dot{m}_{wf,HP}$ increases and also the temperature of the HP is increasing. The air temperature and mass flow rate change much more than the water ones, demanding an increasing cooling power from the condenser in order to maintain ΔT_{sub} at the nominal value
3) The control system starts to increase he RPM of the HP pump. This results in bigger mass flow rate passing through the pump and so the pressure in the high pressure evaporator in rising
4) The high pressure evaporator pressure is increasing 700 kPa while the low pressure is decreasing 1 kPa totally in the end of the simulation. This is done because the thermodynamic characteristics of the supercharge air change much more than the ones of the jacket water and the control system of each evaporator reacts separately. What is more, the supercritical evaporator is containing incompressible working fluid, meaning that its pressure changes drastically with small variations between inlet and outlet mass flow rate. The final pressure is formed by the Stodola coefficient K_t, as it connects the pressure levels with the $\dot{m}_{wf}$
5) The pressure of the condenser is relatively constant, as the one of the high pressure evaporator is increasing and the one of the low pressure evaporator is decreasing. Also the temperature of the cold source remains constant. What is more, the condenser contains mainly compressible vapor.
6) The power produced by the ORC is increasing significantly as the load of the ship changes. This is done because both bigger $\dot{m}_{wf,HP}$ runs through the system and the $\Delta h_{turb,HP}$ is increasing significantly. On the other hand, $\dot{m}_{wf,LP}$ and $\Delta h_{turb,LP}$, which are connected to the jacket water, are slightly degreasing, but the increase of the HP magnitudes is much greater
7) Because ΔT_{sub} is decreasing, in the begging the $\Delta T_{sup,LP}$ is increasing although the mass flow rate of the water is decreasing. After 25 seconds it starts decreasing for 50 seconds, obtaining value lesser than 5 ^{o}C, and by the end of the simulation it reaches the nominal value of 5 ^{o}C again. This behavior is similar to the one that is seen in the second case
8) Finally, the control strategy proposed is able to maintain the cycle under safe conditions through the transient period and reach steady conditions after, without oscillations and overshoots in most of the magnitudes

5.4 Conclusions

In this chapter the results are presented for all three cases that are studied. A comparison study between different fluids is done in case in order to find the one that maximizes the power output. For the first and third layout R134a has the best performance and for the second R245fa. After the definition of the design point the basic parameters of components like heat exchangers where calculated. Dynamic simulations are presented, in order to prove the safety of the ORC unit. In all three cases the system operates steadily and was able to reach equilibrium conditions shortly after the end of the hot sources characteristic variation. It is reminded that the PI control system of each case is tuned separately in order to provide optimum results. Specific comments about each case are done separately after the demonstration of the results.

6.Conclusions

The aim of this work is to create flexible design and dynamic models of single and dual pressure ORC and apply them to the ICE of a LNG carrier for waste heat recovery. The design point models are created using the Matlab® programming language and dynamic off-design point models by using both Matlab® and Simulink®. The objective function for the design point models is the maximization of the power output. The approach for the dynamic model is the one proposed by Vaja [13]. The data for the LNG carrier are obtained from the diploma thesis [29] and the publication [7] of Soffiato et. al. The design point that is chosen is the same point that Soffiato chose (85% load of three engines), while the transient input for the dynamic model is the increase of engines load from 85% to 100%, assuming a linear increase within 50 seconds.

Three different layouts for the ICEs-ORC combined cycle have been proposed, based on a single-stage, a two-stage subcritical and a two-stage supercritical ORC. Off-design dynamic models have been developed for each solution. The design point models have general characteristics and can be applied to many cases for obtaining the optimum design point. They are easy to adjust because important parameters such as working fluid and ΔT_{pp} are inputs. For the development of the dynamic model, the calculation of some components critical characteristics is done. For the pump, the operation map is designed by correlations proposed by Vaja and the affinity laws, while for the turbine the operation curve is calculated by correlations proposed by Vaja and Stodola law. The heat exchangers are type E counter flow shell-n-tube and their basic parameters are calculated using the Kern method and proper correlations proposed in the literature. The off-design dynamic models approach is similar to the one proposed by Vaja, realized by separated blocks and splitting the heat transfer and storage problem into two different blocks. This modular approach offers flexibility to the models, as it is possible to change any block and obtain again a properly working system model without needing to affect the rest of the code. This characteristic makes the model user friendly and easy to change. It is considered a big advantage as it offers the opportunity to simulate the behavior of systems before their construction and existing systems also, after proper tuning. Finally, a control system is designed for each case, to keep the operation under safe conditions. The usage of PI controllers is found to be sufficient through literature review and result analysis.

The results of both the design and dynamic models are found satisfactory. For the one pressure level ORC the maximum power outcome is 383,61 kW, while for the two subcritical pressure levels is 625,61kW. The supercritical cycle in found to produce 720,16kW, making it the most productive cycle. The input for the transient simulations is the increase of the engines load from 85%, that is the design point, to 100% within 50 seconds. In all transient simulations the system operates safely and reaches steady state conditions within 100 seconds after the end of the transient input. The superheating and subcooling are always at a safe level in all cases studied. This

indicates that the control strategy proposed is acceptable. As an outcome can be said that the transient phenomena of the ICE of a ship do not prevent the installation of an ORC for WHR on-board. The oscillations of the vessel during voyages are not modeled in this study. It is considered that they will affect the real system as the continuous altering of gravity force will affect the heat exchange where two phase area exists. The existing layout, having the organic medium inside the tubes, is considered to be the best scenario, as there is less space for oscillations than all the other possible layouts.

It is known that the approach that has been followed in the dynamic models has simplifications of the real problem. The main one is the split of the dynamic model of the heat exchanger in two blocks. The literature is found insufficient in this aspect, as there are only few models proposed and also there is not enough information on how to realize them. Although there are simplifications, the results are good and are considered to simulate the phenomena in a correct way. There are no oscillations in any physical magnitude, which is a common problem in dynamic models. For further validation of the models experimental data are need, which do not exist. The models can be changed in future work, following different approaches, in order to estimate the effect that they have on the final results.

Future work proposed to continue this study:

1) The study can be repeated with finned tubes instead of smooth ones in order to reduce the size of the shell-n-tube heat exchangers
2) The type E heat exchangers could be replaced by type F or J to compare the difference in the system size and dynamic response
3) A fixed boundary model can replace the current one for the evaporators and the condenser
4) A variable rotational speed turbine can be added so as to keep the pressure levels steady
5) An interesting topic is a techno-economic study as to find out the most profitable configuration and the most profitable working fluid.
6) An economic evaluation of the current system could be done, calculating the annual earning using the results of the dynamic model for partial loads

7.Appendix

The equations that were used to solve the heat transfer problem and were found in the Edwards book for designing heat exchangers [25] and Kern's book for process heat transfer [27]. There the following are proposed:

$$\text{for triangular pitch of 45 degrees a usual value is } P_t = 1.4 d_{out}$$

$$B_{s\,max} = 70 {d_{out}}^{0.75}, \text{here a value of } B_s = 30 {d_{out}}^{0.75} \text{ is chosen}$$

$$D_s = P_t \left(\frac{4Nt}{0.9\pi}\right)^{0.5}$$

$$A_s = \frac{D_s \cdot B_s \cdot (P_t - d_{out})}{P_t}$$

$$D_e = 8 \frac{\sqrt{3}\left(\frac{P_t}{2}\right)^2 - \frac{\pi}{8}(d_{out})^2}{\pi \cdot d_{out}}$$

8.References

[1] Quoilin, S.; Aumann, R. Dynamic modeling and optimal control strategy of waste heat recovery Organic Rankine Cycles. Appl. Energy 2011, 88, 2183–2190

[2] Kern, D.Q., Process Heat Transfer, McGraw-Hill, New York, 1950.

[3] Low grade waste heat recovery with subcritical and supercritical Organic Rankine Cycle based on natural refrigerants and their binary mixtures K. Braimakis, M. Preißinger, D. Brüggemann, S. Karellas, K. Panopoulos, Energy 88, 80-92

[4] Predicting the optimum design of single stage axial expanders in ORC systems: Is there a single efficiency map for different working fluids? Da Lio L., G. Manente, A. Lazzaretto. Applied Energy, 2016, vol. 167, (C), p. 44-58

[5] Sprouse, C., Depcik, C., 2013, Review of organic Rankine cycles for internal combustion engine exhaust waste heat recovery, Applied Thermal Engineering, vol. 51, p. 711-722.

[6] Shu G., Liang Y., Wei H., Tian H., Zhao., Liu L. (2013),'A review of waste heat recovery on two stroke IC-engine aboard ships', Renewable and Sustainable Energy Reviews, 19, pp. 385-401

[7] Soffiato, M., Frangopoulos, C. A., Manente, G., Rech S., Lazzaretto A., 2015, Design Optimization of ORC Systems for Waste Heat Recovery onboard an LNG Carrier, Energy Conversion and Management, vol. 92, p. 523-534.

[8] Wei, D., Lu, X., Lu, Z., and Gu, J. (2008). "Dynamic modeling and simulation of an Organic Rankine Cycle (ORC) system for waste heat recovery." Applied Thermal Engineering, 28(10), 1216-1224.

[9] Bamgbopa, M.O.; Uzgoren, E. Quasi-dynamic model for an Organic Rankine Cycle. Energy Convers. Manag.
2013, 72, 117–124

[10] Quoilin, S.; Aumann, R. Dynamic modeling and optimal control strategy of waste heat recovery Organic Rankine Cycles. Appl. Energy 2011, 88, 2183–2190

[11] Willatzen, M., Pettit, N.B.O.L., Ploug-Sørensen, L., 1998. A general dynamic simulation model for evaporators and condenser in refrigeration. Part I: moving boundary formulation of two phase flows with heat exchange.Int. J. Refrigeration 21 (5), 398–403.

[12] Mazzi, N.; Rech, S.; Lazzaretto, A. Off-design dynamic model of a real Organic Rankine Cycle system fueled by exhaust gases from industrial processes. Energy 2015, 90, 537–551

[13] I. Vaja, Definition of an Object Oriented Library for the Dynamic Simulation of Advanced Energy Systems: Methodologies, Tools and Application to Combined ICE-ORC Power Plants, PhD Thesis, Industrial Engineering Department, University of Parma, Italy, 2009

[14] Z. Liu, R.H.S. Winterton A general correlation for saturated and subcooled flow boiling in tube and annuli Int. J. Heat Mass Transfer, 34 (1991), pp. 2759–2766

[15] Vélez F, Segovia J, Martín MC, Antolín G, Chejne F, Quijano A. Comparative study of working fluids for a Rankine cycle operating at low temperature. In: Proceedings of the 4th international congress on energy and environment engineering and management. 2011.

[16] U Larsen, L Pierobon, F Haglind, C Gabrielii. Design and optimization of organic Rankine cycles for waste heat recovery in marine applications using the principles of natural selection. Energy 55, 803-812

[17] He S., Chang H., Zhang X. et.al.. Working fluid selection for an Organic Rankine Cycle utilizing high and low temperature energy of an LNG engine Applied Thermal Engineering 90 (2015) 579e589

[18] E.H. Wang, H.G. Zhang, Y. Zhao, B.Y. Fan, Y.T. Wua, Q.H. Muc. Performance analysis of a novel system combining a dual loop organic Rankine cycle (ORC) with a gasoline engine. Energy 43 (2012) 385e395

[19] Jian Song, Chun-wei Gu. Parametric analysis of a dual loop Organic Rankine Cycle (ORC) system for engine waste heat recovery. Energy Conversion and Management 105 (2015) 995–1005

[20] Guopeng Yu, Gequn Shu*, Hua Tian, Haiqiao Wei, Lina Liu. Simulation and thermodynamic analysis of a bottoming Organic Rankine Cycle (ORC) of diesel engine (DE). Energy 51 (2013) 281e290

[21] Uusitalo A., Honkatukia J., Backman J. et. al. Experimental study on charge air heat utilization of large-scale reciprocating engines by means of Organic Rankine Cycle. Applied Thermal Engineering 89 (2015) 209e219

[22] Lecompte S., Huisseune H., Broek M., Vanslambrouck B., De Paepe M. Review of organic Rankine cycle (ORC) architectures for waste heat recovery Renewable and Sustainable Energy Reviews 47 (2015) 448–461.

[23] Da Lio, L.; Manente, G.; Lazzaretto, A. New efficiency charts for the optimum design of axial flow turbines for organic Rankine cycles. Energy 2014, 77, 447–459.

[24] K.E. Gungor, R.H.S. Winterton A general correlation for flow boiling in tubes and annuli Int. J. Heat Mass Transfer, 29 (1986), pp. 351–358

[25] John E. Edwards Design and rating of shell and tube heat exchangers. P and I Design Ltd, Teesside

[26] Karellas, S. Schuster, A. Leontaritis, A.D. Influence of supercritical ORC parameters on plate heat exchanger design. Appl. Therm. Eng. 2012, 33–34, 70–76.

[27] D. Butterworth. A comparison of some void-fraction relationships for co-current gas-liquid flow. Int. J. Multiphase Flow, Vol. 1, pp. 845-850. Pergamon/Elsevier, 1975

[28] K.J. Astrom, R.D. Bell. Drum-boiler dynamics. Automatica 36 (2000) 363-378

[29] Marco Soffiato, Thesis, Industrial Engineering Department, University of Padova, Italy, 2014

[30] Cavallini, Zecchin High Velocity Condensation of Organic Refrigerants Inside Tubes, 8th International Congress of Refrigeration, Vol. 2, Washington DC, 1971, pp. 193-200

[31] Cavallini, Zecchin: A Dimensionless Correlation for Heat Transfer in Forced Convection Condensation. 6th Int. Heat Transfer Conf. Tokyo, 1974, pp. 309-313

[32] George Dimopoulos, Nikolaos Kakalis. 'Next Generation Energy Management' , DNVGL, page 8, 2014

[33] G. Manente, A. Toffolo, A. Lazzaretto, M. Paci, An Organic Rankine Cycle off-design model for the search of the optimal control strategy, Energy, Vol. 58, pp. 97-106, 2013.

[34] J.D. Jackson, W.B. Hall, Forced convection heat transfer. in: S. Kakac, D.B. Spalding (Eds.), Turbulent Forced Convection in Channels and Bundles, vol. 2, 1979, p. 563

[35] J.D. Jackson, W.B. Hall, Influences of buoyancy on heat transfer to fluids flowing in vertical tubes under turbulent conditions. in: S. Kakac, D.B. Spalding (Eds.), Turbulent Forced Convection in Channels and Bundles, vol. 2, 1979, p. 640.

Ελληνικό τμήμα

Πλαγιανός Γεώργιος Παναγιώτης

Ευέλικτα μοντέλα για τον σχεδιασμό και δυναμική λειτουργία Οργανικών Κύκλων Rankine, μονής και διπλής πίεσης: εφαρμογή σε ένα πλοίο μεταφοράς LNG

Εισαγωγή

Οι θερμικές μηχανές λειτουργούν μεταξύ δύο θερμοκρασιών προς παραγωγή μηχανικού έργου. Απορροφούν θερμότητα από την πηγή υψηλής θερμοκρασίας και μετά την παραγωγή έργου απορρύπτουν την υπολειπόμενη θερμότητα σε δοχεία χαμηλότερης θερμοκρασίας. Η διαδικασία αξιοποίησης απορρυπτόμενης θερμότητας εκμεταλλεύεται την υπολειπόμενη αυτή θερμότητα προς παραγωγή επιπλέον έργου και στην συνέχεια απορρύπτει θερμότητα σε ακόμα χαμηλότερη θερμοκρασία. Ο Οργανικός Κύκλος Rankine (ORC) διαθέτει την ικανότητα να λειτουργήσει με θερμή πηγή σχετικά χαμηλής θερμοκρασίας και ικανοποιητική απόδοση σε αντίθεση με τον κανονικό Κύκλο Rankine. Τυπικές τιμές του βαθμού απόδοσης είναι από 5% μέχρι 23%, ανάλογα με την θερμή πηγή και το οργανικό μέσο.

Η σωστή επιλογή του σημείου σχεδίασης του ORC είναι κρίσιμη, καθώς καθορίζει την συνολική απόδοση του συστήματος τόσο στο ίδιο το σημείο όσο και εκτός αυτού. Ένα ακόμα σημαντικό θέμα είναι η εξασφάλιση της ασφαλής και αποδοτικής λειτουργίας του συστήματος στις συνθήκες εκτός του σημείου σχεδίασης. Τα δυναμικά μοντέλα είναι ικανά να προβλέψουν τόσο τα μεταβατικά φαινόμενα κάτω από μεταβαλλόμενες εξωτερικές συνθήκες όσο και τις συνθήκες λειτουργίας εκτός σημείου σχεδίασης. Έτσι, βοηθούν στην δημιουργία ασφαλών συνθηκών λειτουργίας και στην ανάπτυξη σωστού συστήματος ελέγχου.

Η επιλογή του οργανικού μέσου χρήζει ιδιαίτερης προσοχής αφού έχει καθοριστική επίδραση στον θερμικό και συνολικό βαθμό απόδοσης. Στην βιβλιογραφία παρατηρείται από τον Καρέλλα [3] ότι για τις ίδιες συνθήκες αξιοποίησης θερμότητας χαμηλής θερμοκρασίας, διαφορετικά οργανικά μέσα μπορούν να έχουν μέχρι και 7% απόκλιση στον βαθμό απόδοσης. Παρόλου που ο αριθμός των οργανικών μέσων είναι τεράστιος, δίνονται κατευθυντήριες γραμμές στην βιβλιογραφία από ερευνητές όπως οι Vivian et. al. [4], για την σωστή επιλογή, βάσει χαρακτηριστικών όπως η κρίσιμη θερμοκρασία.

Ένα εξαιρετικά ενδιαφέρον πεδίο εφαρμογής των ORC είναι η αξιοποίηση απορρυπτόμενης θερμότητας. Τα πλοία απορρύπτουν τεράστια ποσά λόγω της χρήσης μηχανών εσωτερικής καύσης (ΜΕΚ) όπως δείχνει η μελέτη των Spouse et. al. [5]. Οι Shu et. al. [6] ανάλυσαν την εκμετάλλευση θερμότητας από έναν δίχρονο ναυτικό κινητήρα και κατέληξαν στο συμπέρασμα πως ο ORC είναι το βέλτιστο σύστημα. Οι Soffiato et. al. [7] ανάλυσαν τα εν δυνάμει εκμεταλλεύσιμα από ORC θερμά ρεύματα στην ΜΕΚ ενός LNG carrier. Πρέπει να τονιστεί στο σημείο αυτό πως στις ναυτικές εφαρμογές η ασφάλεια αποτελεί την προτεραιότητα, έτσι προτού εφαρμοστεί ένα καινούργιο σύστημα θα πρέπει να έχει αποδείξει την αξιοπιστία του εκ προοιμίου.

Τα δυναμικά μοντέλα είναι ένας βολικός τρόπος να ελεγχθεί η συμπεριφορά συστημάτων στα μερικά φορτία και χρησιμοποιούνται επίσης στην ανάπτυξη συστημάτων ελέγχου. Οι Wei et. al. [8] πραγματοποίησαν μία ανάλυση πάνω στα διαφορετικά δυναμικά μοντέλα ORC, δείχνοντας ότι υπάρχουν μεγάλες διαφορές τόσο στην ακρίβεια όσο και στον υπολογιστικό χρόνο που απαιτούν. Ο Vaja [13] παρουσιάζει αναλυτικά την κατασκευή ενός απλού και ευέλικτου μοντέλου ORC, αποτελούμενου από μεμονωμένα μπλοκ. Η προσέγγιση του ακολουθείται στην εργασία αυτή λόγω της απλότητάς της. Οι Quoilin et. al. [10] κατασκεύασαν ένα δυναμικό μοντέλο ORC και στην συνέχεια το χρησιμοποίησαν για την κατασκευή συστήματος ελέγχου, δείχνοντας έτσι την μεγάλη χρησιμότητα τους.

Ο σκοπός αυτής της διπλωματικής εργασίας είναι να κατασκευάσει ευέλικτα, γενικής χρήσης μοντέλα για τον καθορισμό του σημείου σχεδιασμού τριών διαφορετικών κύκλων ORC, καθώς και ευέλικτα δυναμικά μοντέλα με σκοπό να τα προσομοιώσει και να τα ελέγξει. Οι τρεις διαφορετικοί κύκλοι που μελετώνται είναι με μία υποκρίσιμη πίεση ατμοποίησης, δύο υποκρίσιμες πιέσεις ατμοποίησης και δύο πιέσεις ατμοποίησης εκ των οποίων η μία είναι υπερκρίσιμη. Τα μοντέλα εφαρμόστηκαν σε ένα LNG carrier για εκμετάλλευση απορρυπτόμενης θερμότητας από την ΜΕΚ. Για το σκοπό αυτό τα μοντέλα του σημείου σχεδίασης εφαρμόστηκαν προς εύρεση του βέλτιστου και διαστασιολογήθηκαν κύρια εξαρτήματα του κύκλου, όπως το μήκος των εναλλακτών θερμότητας. Στην συνέχεια εφαρμόστηκαν τα δυναμικά μοντέλα για τα μερικά φορτία της μηχανής και αναπτύχθηκαν συστήματα ελέγχου για να διασφαλίσουν την σταθερότητα και ασφάλεια του συστήματος.

9.Πρώτη περίπτωση και παρατηρήσεις

Στο παρόν κεφάλαιο, τα αποτελέσματα της πρώτης από τις τρεις περιπτώσεις που μελετηθήκαν παρουσιάζονται και γίνονται παρατηρήσεις επ'αυτών. Αρχικά, το σημείο σχεδιασμού της εξεταζόμενης περίπτωσης υπολογίζεται. Αυτό περιλαμβάνει μία συγκριτική μελέτη μεταξύ διάφορων οργανικών υγρών προς εύρεση του εργαζόμενου μέσου που μεγιστοποιεί την παραγόμενη ισχύ. Ύστερα, βασικές παράμετροι των εξαρτημάτων υπολογίζονται από τα μοντέλα του σημείου σχεδίασης, όπως η σταθερά του Stodola για τους στροβίλους και ο αριθμός των σωλήνων για τους εναλλάκτες. Κατά αυτό τον τρόπο, όλες οι απαραίτητες παράμετροι για τις δυναμικές προσομοιώσεις αποκτώνται. Η δυναμική προσομοίωσης γίνεται για αύξηση του φορτίου των ΜΕΚ από 85% σε 100% μέσα σε 50 δευτερόλεπτα. Τα αποτελέσματα δείχνουν ότι το σύστημα λειτουργεί ασφαλώς και η στρατηγική ελέγχου που προτείνεται είναι αποδεκτή, πετυχαίνοντας τον στόχο της.

Οι μελετηθείσες περιπτώσεις είναι τρεις:

1) Μόνο το νερό του χιτωνίου χρησιμοποιείται, με μια πίεσης ατμοποίησης
2) Χρησιμοποιούνται το νερό του χιτωνίου και ο αέρας της υπερπλήρωσης, με δύο υποκρίσιμες πιέσεις ατμοποίησης
3) Χρησιμοποιούνται το νερό του χιτωνίου και ο αέρας της υπερπλήρωσης, με μια υποκρίσιμη και μία υπερκρίσιμη πίεση ατμοποίησης

Πρώτη περίπτωση

Το μοντέλα μίας θερμής πηγής-μιας πίεσης ατμοποίησης εφαρμόζεται στην πρώτη περίπτωση για διάφορα οργανικά ρευστά για εύρεση αυτού που μεγιστοποιεί την παραγόμενη ισχύ. Τα μέσα που θεωρούνται κατάλληλα είναι τα ακόλουθα: R-134a, R-125, R-245ca, R-245fa, R-227ea, RC-318. Τα αποτελέσματα συνοψίζονται στον ακόλουθο πίνακα.

Πίνακας 9.1 Σημείο σχεδιασμού πρώτης περίπτωσης για διάφορα μέσα

	R-245ca	R-134a	R-125	R-227ea	R-245fa	RC-318
P_{evap} (kPa)	355,34	1799,89	3368,92	1256,93	500,52	898,8
P_{cond} (kPa)	120,99	766,88	1562,54	526,09	176,84	363,88
T_{evap} (°C)	62,94	63,04	62,93	62,93	62,94	62,93
T_{cond} (°C)	30	30	30	30	30	30

ΔT_{sup} (°C)	5	5	5	5	5	5
ΔT_{sub} (°C)	5	5	5	5	5	5
T''_{out} (°C)	76,3	76,3	76,3	76,3	76,3	76,3
$\eta_{is,turb}$	0,61	0,74	0,76	0,73	0,65	0,72
$\eta_{is,pump}$	0,7	0,7	0,7	0,7	0,7	0,7
m_{ORC} (kg/s)	27,62	32,84	54,56	47,33	29,28	49,13
m_{cold} (kg/s)	169,05	176,79	182,52	162,08	169,54	157,78
W_{turb} (kW)	344,06	423,67	440,63	394,69	366,99	377,1
W_{pump} (kW)	6,67	40,05	117,23	35,53	10,11	25,02
W_{net} (kW)	337,39	383,61	323,4	359,16	356,88	352,08
ϕ (%)	9,56	9,56	9,56	9,56	9,56	9,56
$\eta_{thermal}$ (%)	5,17	5,88	4,96	5,5	5,47	5,4
η_{total} (%)	0,49	0,56	0,47	0,53	0,52	0,52

Το βέλτιστο σενάριο όπως φαίνεται είναι η χρήση του R-134a για εργαζόμενο μέσο. Κατασκευάζεται το διάγραμμα T-s.

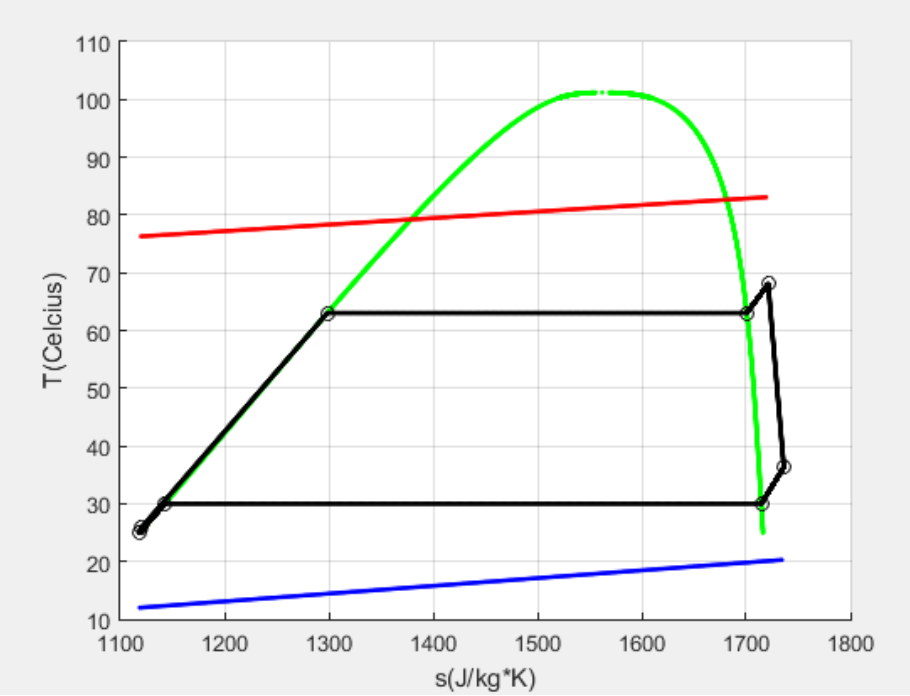

Εικόνα 9.1 T-s διάγραμμα πρώτης περίπτωσης

Για το βέλτιστο σενάριο, οι εναλλάκτες τύπου αυλών-κελύφους διαστασιολογούνται και τα κύρια χαρακτηριστικά τους παρουσιάζονται στον κάτωθι πίνακα:

Πίνακας 9.2 Πρώτη περίπτωση, χαρακτηριστικά των εναλλακτών

	Evap	Cond

d_{in} (mm)	14	14
d_{out} (mm)	16,8	16,8
Nt	1513	1628
p_t (mm)	23,52	23,52
B_s	1,4	1,4
D_s (m)	1,09	1,13
De (mm)	19,51	19,51
Re''	30049,76	6165,66
α'' (kW/m^2*K)	4,62	2,69
Re'_L	10002,91	9999,15
α_{pre}(kW/m^2*K)	0,31	0,32
$\alpha_{evap}/\alpha_{cond}$ (kW/m^2*K)	1,66	1,74
$\alpha_{sup}/\alpha_{sub}$ (kW/m^2*K)	0,42	0,33
L (m)	6,64	6,97

Η δυναμική συμπεριφορά του συστήματος δύναται να μελετηθεί στο σημείο αυτό. Η μελετηθείσα περίπτωση είναι η αύξηση του φορτίου των μηχανών από 85% σε 100% μέσα σε 50 δευτερόλεπτα. Αυτό έχει επίπτωση τόσο στην παροχή νερού από το χιτώνιο όσο και στην θερμοκρασία αυτού. Η θερμοκρασία ανεβαίνει 1.62K κι η παροχή μειώνεται 33.4 kg/s κατά την μεταβατική περίοδο.

Το σύστημα ξεκινάει από το σημείο σχεδιασμού, δηλαδή 85% φορτίο και παραμένει εκεί για 50 δευτερόλεπτα προκειμένου να διασφαλιστεί ότι ξεκινάει από συνθήκες ηρεμίας. Τότε, από τα 50 μέχρι τα 100 δευτερόλεπτα συμβαίνει η μεταβολή του φορτίου ων μηχανών και από τα 100 μέχρι τα 250 δευτερόλεπτα το σύστημα φτάνει συνθήκες ηρεμίας ξανά, με την υπερθέρμανση και την υπόψυξη να λαμβάνουν τις ονομαστικές τιμές τους. Τα αποτελέσματα παρουσιάζονται στα διαγράμματα που ακολουθούν:

Είσοδοι:

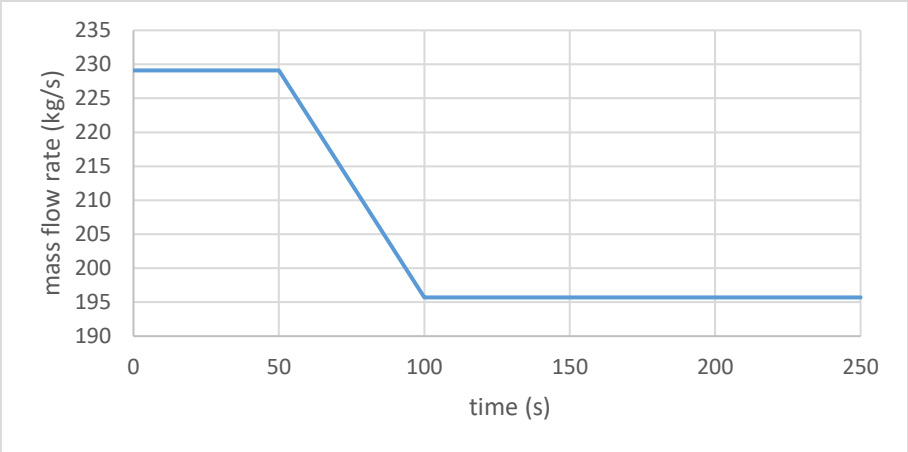

Εικόνα 9.2 Πρώτη περίπτωση, παροχή μάζας νερού χιτωνίου

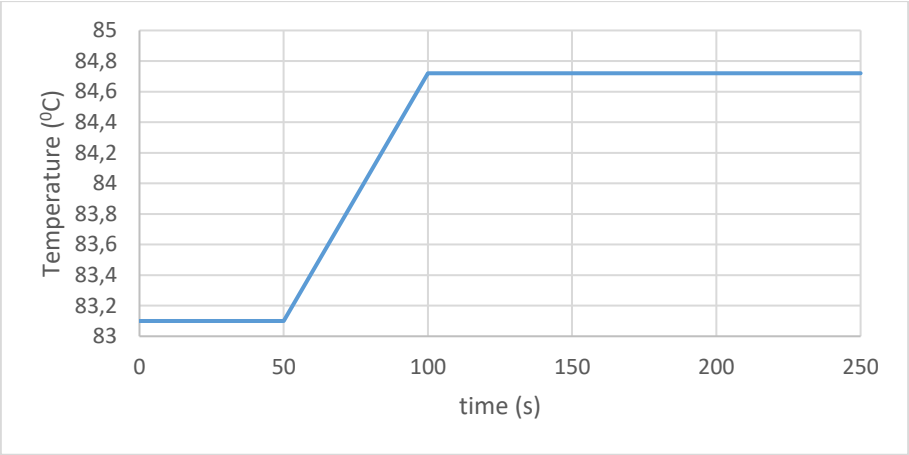

Εικόνα 9.3 Πρώτη περίπτωση, θερμοκρασία νερού χιτωνίου

Έξοδοι:

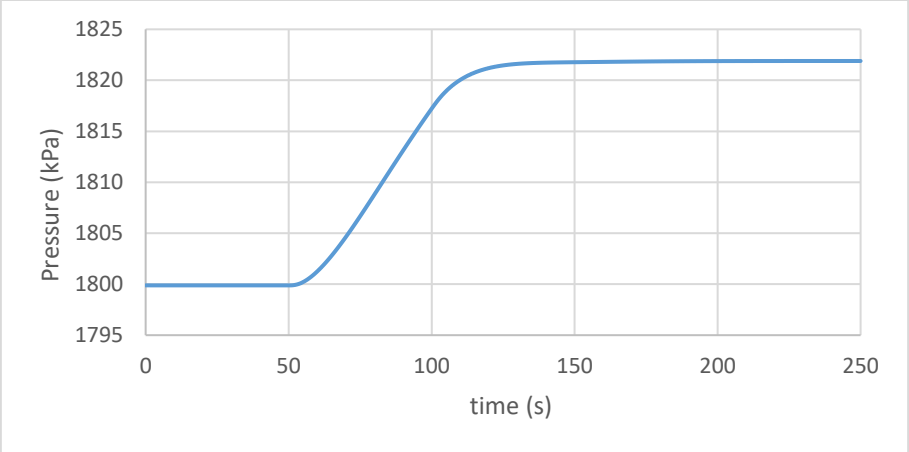

Εικόνα 9.4 Πρώτη περίπτωση, πίεση ατμοποίησης

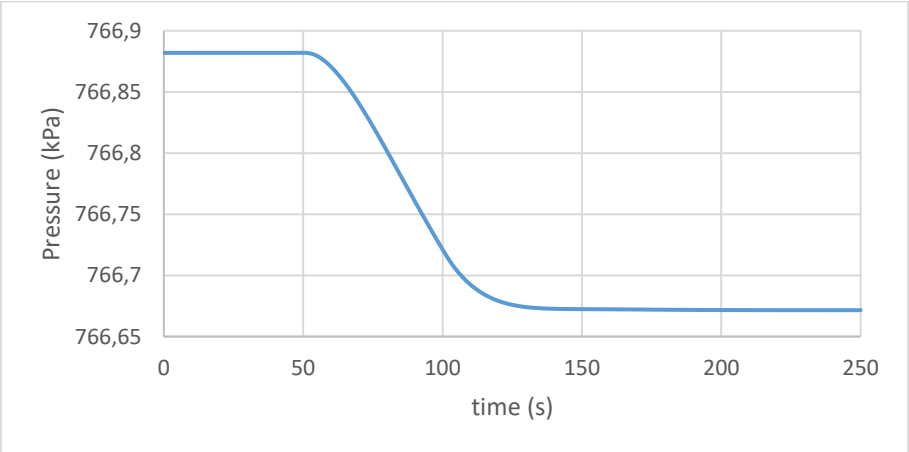

Εικόνα 9.5 Πρώτη περίπτωση, πίεση συμπύκνωσης

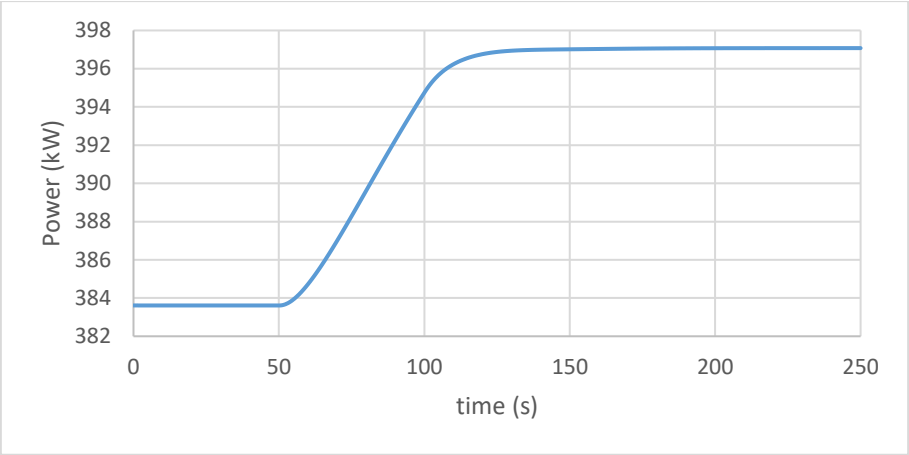

Εικόνα 9.6 Πρώτη περίπτωση, ωφέλιμη ισχύς

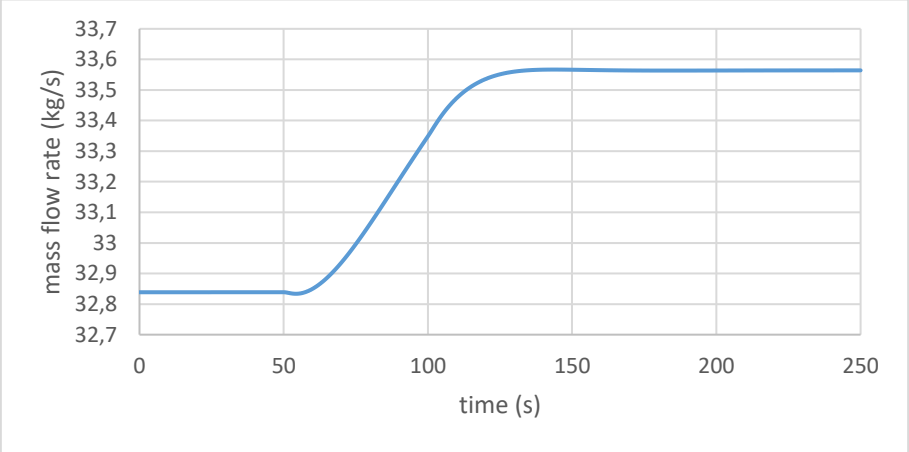

Εικόνα 9.7 Πρώτη περίπτωση, παροχή μάζας στροβίλου

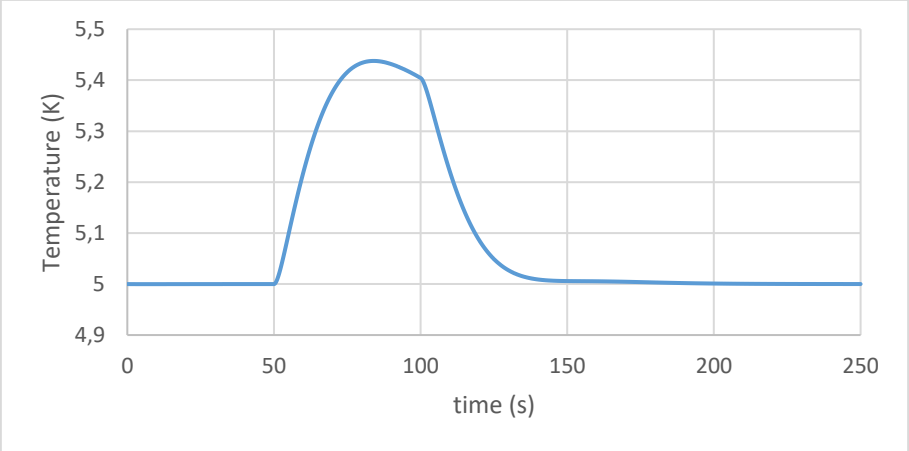

Εικόνα 9.8 Πρώτη περίπτωση, υπερθέρμανση

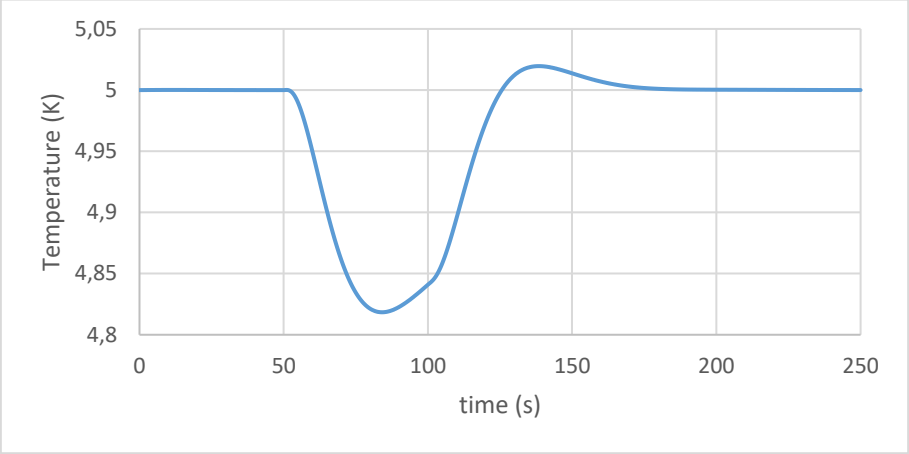

Εικόνα 9.8 Πρώτη περίπτωση, υπόψυξη

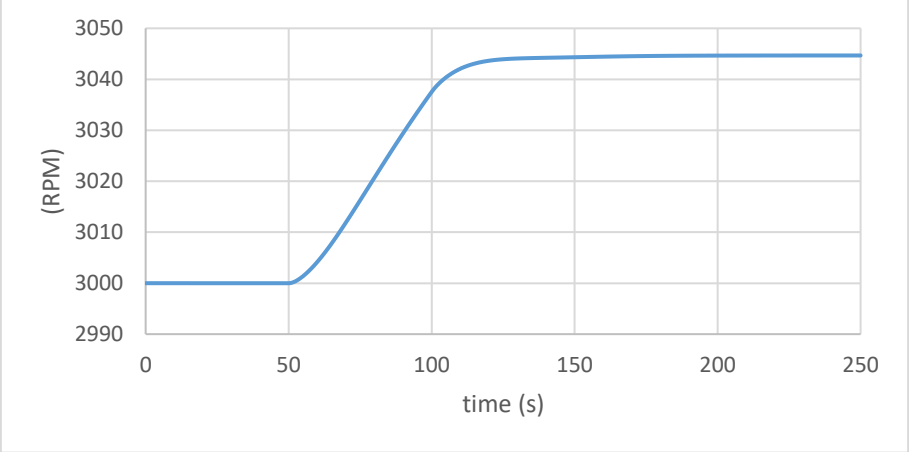

Εικόνα 9.10 Πρώτη περίπτωση, στροφές αντλίας

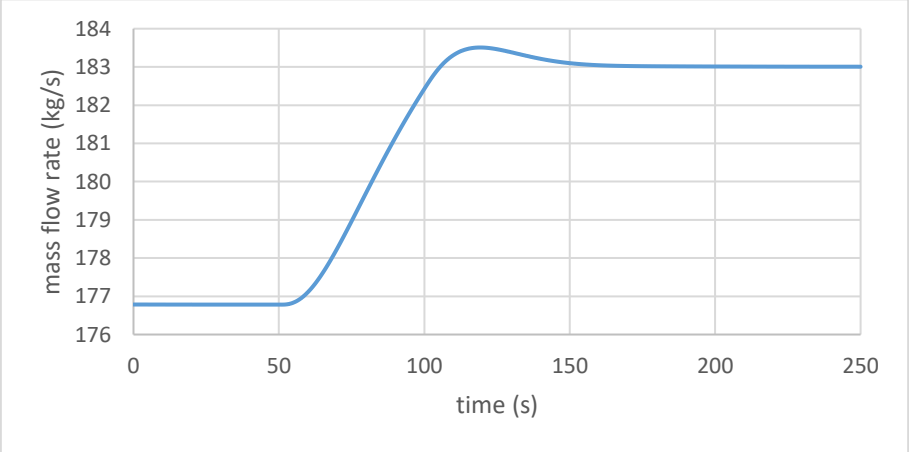

Εικόνα 9.11 Πρώτη περίπτωση, παροχή μάζας ψυχρού ρεύματος

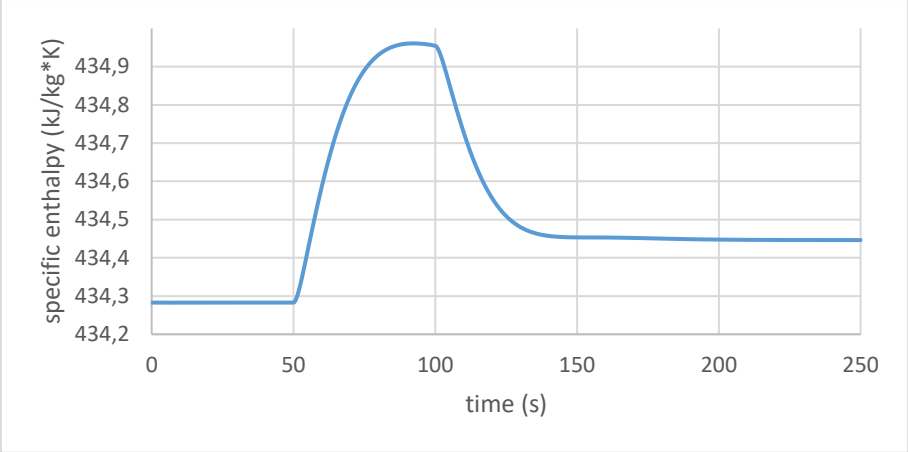

Εικόνα 9.12 Πρώτη περίπτωση, ειδική ενθαλπία εισόδου στροβίλου

Παρατηρήσεις:

1) Η υπερθέρμανση αυξάνεται καθώς το φορτίο του πλοίου αυξάνεται, οδηγώντας έτσι σε αύξηση της θερμοκρασίας και της παροχής μάζας της θερμής πηγής.
2) Το σύστημα ελέγχου αρχίζει να αυξάνει τις στροφές τις αντλίας, αντιδρώντας στην αύξηση του υπερθέρμανση. Αυτό έχει σαν αποτέλεσμα μεγαλύτερη παροχή μάζας να διατρέχει την αντλία και ταυτόχρονα να ανεβαίνει η πίεση στον ατμοποιητή
3) Η παραγόμενη ισχύς από τον ORC αυξάνεται καθώς το φορτίο του πλοίου ανεβαίνει. Αυτό συμβαίνει γιατί μεγαλύτερη παροχή μάζας του οργανικού υγρού περνάει από το σύστημα και γιατί το ειδικό έργο του στροβίλου αυξάνει
4) Μια αυξανόμενη ψυκτική ισχύς απαιτείται από τον συμπυκνωτή κατά την μεταβατική περίοδο, καθώς το σύστημα ελέγχου προσπαθεί να διατηρήσει την υπόψυξη στην ονομαστική της τιμή. Αυτό συμβαίνει γιατί παροχή μάζας του οργανικού κύκλου και η υπερθέρμανση αυξάνονται.
5) Μέσα από προσομοιώσεις βρέθηκε ότι η υπερθέρμανση υπερθέρμανση έχει καθοριστική επίδραση στον συμπυκνωτή. Επειδή ο ατμός έχει χαμηλότερη συναγωγιμότητα από το υγρό, μία αύξηση στην υπερθέρμανση σημαίνει ότι υπάρχει αρκετά λιγότερη διαθέσιμη επιφάνεια στον συμπυκνωτή για να ψύξει το υγρό στις επιθυμητές συνθήκες
6) Η πίεση στον συμπυκνωτή είναι σχετικά σταθερή, με μία μικρή αλλαγή μόνο να πραγματοποιείται. Αυτό συμβαίνει γιατί ο συμπυκνωτής περιέχει κυρίως χαμηλής πυκνότητας ασυμπίεστο ατμό και επειδή η θερμοκρασία της ψυχρής πηγής παραμένει σταθερή

7) Τέλος, η στρατηγική ελέγχου που προτάθηκε είναι ικανή να διατηρήσει τον κύκλο κάτω από ασφαλείς συνθήκες λειτουργείας σε όλη την μεταβατική περίοδο και να φτάσει σε σταθερές συνθήκες ύστερα, χωρίς ταλαντώσεις και υπερακοντίσεις

Συμπεράσματα

Ο σκοπός αυτής της παρούσας διπλωματικής είναι να κατασκευάσει ευέλικτα μοντέλα για το σχεδιασμό και την δυναμική μοντελοποίηση ενός και δύο επιπέδων ατμοποίησης ORC και να τα εφαρμόσει σε ένα LNG carrier για εκμετάλλευση απορρυπτόμενης θερμότητας. Τα μοντέλα σημείου σχεδιασμού κατασκευάστηκαν στο προγραμματιστικό περιβάλλον της Matlab® ενώ τα δυναμικά μοντέλα στο περιβάλλον του Simulink® με ταυτόχρονη χρήση κώδικα Matlab®. Η αντικειμενική συνάρτηση που ικανοποιούν τα μοντέλα σχεδιασμού είναι η μεγιστοποίηση της παραγόμενης ισχύος. Η προσέγγιση που ακολουθήθηκε στα δυναμικά μοντέλα είναι αυτή που προτείνεται από τον Vaja [13]. Τα δεδομένα για την μηχανή του πλοίου πάρθηκαν από την διπλωματική θέση [29] και την δημοσίευση [7] των Soffiato et. al. Σαν σημείο σχεδιασμού επιλέχθηκε το ίδιο σημείο που είχαν διαλέξει και οι Soffiato et. Al. (85% φορτίο σε τρεις μηχανές), ενώ σαν μεταβατική είσοδος για το δυναμικό μοντέλο χρησιμοποιήθηκε μία αύξηση του φορτίου των μηχανών από 85% σε 100% μέσα σε 50 δευτερότατα, υποθέτοντας γραμμική αλλαγή.

Τρεις διαφορετικοί κύκλοι ORC προτείνονται, βασισμένοι στον απλό, στον διπλό και στον διπλό υπερκρίσιμο ORC. Δυναμικά μοντέλα αναπτύχθηκαν για κάθε διαφορετικό κύκλο. Τα μοντέλα σχεδιασμού του σημείου λειτουργίας έχουν γενικό χαρακτήρα και μπορούν να εφαρμοστούν σε διαφορετικές περιπτώσεις, βρίσκοντας σε κάθε περίπτωση το βέλτιστο σημείο. Είναι εύκολα προσαρμόσιμα γιατί οι σημαντικές παράμετροι λειτουργίας όπως το εργαζόμενο μέσω και το pinch point είναι παράμετροι εισόδου καθοριζόμενοι από τον χρήστη. Για την ανάπτυξη του δυναμικού μοντέλου γίνεται εκ των προτέρων διαστασιολόγηση βασικών εξαρτημάτων από τα μοντέλα σχεδιασμού. Για την αντλία, κατασκευάζεται ο χάρτης λειτουργίας σύμφωνα με τους νόμους ομοιότητάς και μια σχέση προτεινόμενη από τον Vaja, για τον στρόβιλο η καμπύλη λειτουργίας σύμφωνα με τον νόμο του Stodola και μία σχέση προτεινόμενη από τον Vaja. Οι εναλλάκτες θερμότητας είναι shell-n-tube τύπου E, λειτουργούν κατά αντιρροή και ο σχεδιασμός τους έγινε ακολουθώντας την μέθοδο του Kern. Η προσέγγιση που ακολουθήθηκε στο κομμάτι της δυναμικής μοντελοποίησης είναι η προτεινόμενη από τον Vaja. Τα διάφορα εξαρτήματα του κύκλου μοντελοποιήθηκαν με ξεχωριστά μπλοκ. Η μεταφορά θερμότητας και η αποθήκευση μάζας και ενέργειας που συμβαίνει στους εναλλάκτες υπολογίζονται

από δύο διαφορετικά μπλοκ. Αυτή η προσέγγιση του προβλήματος προσφέρει ευελιξία, καθώς δίνει την δυνατότητα να αντικατασταθεί το οποιοδήποτε μπλοκ με άλλο και στο τέλος να προκύψει ένα νέο μοντέλο, χωρίς να χρειαστεί η αλληλεπίδραση με τα υπόλοιπα κομμάτια του κώδικα. Το χαρακτηριστικό αυτό κάνει το μοντέλο φιλικό στο χρήστη και εύκολο στην αναπροσαρμογή. Θεωρείται σημαντικό πλεονέκτημα καθώς δίνει την ευκαιρία προσομοίωσης τόσο συστημάτων πριν την κατασκευή τους όσο και υπαρχόντων μετά από κατάλληλη προσαρμογή. Η χρήση PI ελεγκτών βρέθηκε να είναι ικανοποιητική τόσο μέσα στην βιβλιογραφία όσο και από την ανάλυση των αποτελεσμάτων.

Τα αποτελέσματα τόσων μοντέλων σχεδιασμού όσο και των δυναμικών βρίσκονται ικανοποιητικά. Για τον απλό κύκλο η μέγιστη παραγόμενη ισχύ είναι 383,61 kW ενώ για τον διπλό υποκρίσιμο είναι 625,61kW. Ο υπεκρίσιμος βρέθηκε να παράγει 720,16kW, γεγονός που τον καθιστά τον πιο αποδοτικό. Η είσοδος για την μοντελοποίηση των μεταβατικών φαινομένων είναι η αύξηση του φορτίου των μηχανών από 85% σε 100% μέσα σε 50 δευτερόλεπτα. Όλες οι μεταβατικές αποκρίσεις δείχνουν ότι τα συστήματα λειτουργούν ασφαλώς και φτάνουν στην μόνιμη κατάσταση μέσα σε 100 δευτερόλεπτα μετά το τέλος της μεταβολής της εισόδου. Η υπερθέρμανση και η υπόψυξη διατηρούνται πάντοτε σε ασφαλή επίπεδα, σε όλες τις περιπτώσεις που μελετήθηκαν. Αυτό υποδηλώνει ότι η στρατηγική ελέγχου που προτείνεται είναι αποδεκτή. Σαν γενικότερο συμπέρασμα μπορεί να λεχθεί ότι τα μεταβατικά φαινόμενα των ΜΕΚ ενός πλοίου δεν εμποδίζουν την εγκατάσταση ORC για ανάκτηση θερμότητας. Οι ταλαντώσεις του πλοίου δεν έχουν μοντελοποιηθεί σε αυτή τη μελέτη. Θεωρείται ότι επηρεάζουν την λειτουργεία του πραγματικού συστήματος, καθώς οι εναλλασσόμενες βαρύτικες δυνάμεις θα επηρεάσουν την μεταφορά θερμότητας στις περιοχές που υπάρχουν δύο φάσεις. Η παρούσα διάταξη, με το οργανικό μέσο στο εσωτερικό των σωλήνων, θεωρείται η καλύτερη δυνατή αφού έχει το λιγότερο χώρο για ταλάντωση από όλες τις άλλες διατάξεις.

Είναι γνωστό ότι η προσέγγιση που ακολουθήθηκε περιέχει απλοποιήσεις του πραγματικού προβλήματος. Η κυριότερη είναι ο διαχωρισμός του δυναμικού μοντέλου του εναλλάκτη σε δύο μπλοκ. Η βιβλιογραφία βρέθηκε ελλιπής στον συγκεκριμένο τομέα καθώς υπάρχουν λίγα προτεινόμενα μοντέλα, τα οποία όμως δεν εξηγούνται αρκετά αναλυτικά ώστε να αναπαραχθούν. Παρόλο που υπάρχουν απλοποιήσεις τα αποτελέσματα είναι καλά και θεωρείται ότι μοντελοποιούν τα υπάρχουσα φαινόμενα κατά σωστό τρόπο. Δεν υπάρχουν ταλαντώσεις σε κανένα φυσικό μέγεθος, το οποίο αποτελεί ένα σύνηθες πρόβλημα στα δυναμικά μοντέλα. Για επιπλέον διακρίβωση των μοντέλων χρειάζονται πειραματικά δεδομένα, τα οποία δεν υπάρχουν. Τα μοντέλα μπορούν να αλλάξουν σε μελλοντική δουλειά, ακολουθώντας διαφορετικές προσεγγίσεις, προς διαπίστωση των επιπτώσεων που έχουν στα τελικά αποτελέσματα.

Μελλοντική δουλειά που προτείνεται πάνω στην παρούσα εργασία είναι:

1) Η μελέτη μπορεί να επαναληφθεί με σωλήνες με περίγεια αντί λείων, με σκοπό την μείωση του μεγέθους των εναλλακτών.
2) Οι τύπου Ε εναλλάκτες μπορούν να αντικατασταθούν με τύπου F ή J, και να συγκριθούν οι διαφορές το μέγεθος του συστήματος κι την μεταβατική απόκριση.
3) Ένα μοντέλο fixed boundary μπορεί να αντικαταστήσει το τωρινό για τους ατμοποιητες και τους συμπυκνωτές.
4) Μπορεί να εισαχθεί μία τουρμπίνα μεταβλητών στροφών, έτσι ώστε να κρατήσει σταθερές τις πιέσεις.
5) Ενδιαφέρον θέμα αποτελεί μία τεχνο-οικονομική μελέτη για να βρεθεί η πιο συμφέρουσα διάταξη καθώς και το πιο συμφέρουσο οργανικό μέσο.
6) Μία οικονομική εκτίμηση των παρόντων συστημάτων μπορεί να γίνει, υπολογίζοντας τα ετήσια κέρδη χρησιμοποιώντας τα δυναμικά μοντέλα για να υπολογίσει την παραγωγή ισχύς στα μερικά φορτία.